Flame Retardancy of Polymer Nanocomposites based on Layered Aluminum Phosphate and Computational Study of Intercalation of Amines into α-Zirconium Phosphate and Adsorption of a Model Organic Pollutant

Ning Wang 1982-
Marquette University

FLAME RETARDANCY OF POLYMER NANOCOMPOSITES BASED ON LAYERED ALUMINUM PHOSPHATE AND COMPUTATIONAL STUDY OF INTERCALATION OF AMINES INTO α-ZIRCONIUM PHOSPHATE AND ADSORPTION OF A MODEL ORGANIC POLLUTANT

By

Ning Wang, M. S.

A Thesis submitted to the Faculty of the Graduate School,
Marquette University,
in Partial Fulfillment of the Requirements for
the Degree of Master of Science

December 2011
Milwaukee, Wisconsin

ABSTRACT

FLAME RETARDANCY OF POLYMER NANOCOMPOSITES BASED ON TARANAKITE AND COMPUTATIONAL STUDY OF INTERCALATION OF AMINES INTO α-ZIRCONIUM PHOSPHATE AND ADSORPTION OF A MODEL ORGANIC POLLUTANT

Ning Wang, M.S.

Marquette University, 2011

Layered metal materials, such as layered metal hydroxides, hydroxy double salts, and layered metal phosphates can be used for applications such as fire retardancy, ion exchangers, or removal of pollutants. Optimization of materials for these applications requires an understanding of their physical and chemical properties.

Part A: Flame retardancy of polymer nanocomposites based on taranakite

Taranakite with tunable interlayer spacing has been prepared and modified by sodium dodecyl sulfate (AL-SDS). The layered materials are used as the additive to study the fire retardancy of polymers, including polystyrene (PS), polypropylene (PP), and polyvinyl alcohol (PVA). The dispersion of taranakite was characterized by X-ray diffraction. The thermal stability of taranakite and polymer composites was assessed by thermogravimetric analysis, and the results obtained suggest that the presence of taranakite improved the thermal stability of the polymer composites. The onset degradation temperature and mid-point temperature increased with increasing loading of taranakite in PS, PP and PVA. An understanding of the degradation mechanism of the polymer/taranakite composites allows us to explore the potential role of this layered material in enhancing polymer fire retardancy. The fire retardancy properties of the polymer composites were evaluated by cone calorimeter (PS, PP) or by use of a micro cone calorimeter (PVA). Polymer composites containing taranakite have been shown to exhibit lower peak heat released rate (PHRR) compared with the virgin polymers, especially for PVA. The source of the reduction in peak heat release rate for non-polar polymers, such as PS and PP, is hypothesized to be due to the formation of char that slows down the burning process and the formation of ester groups during decomposition of the polymers. For a polar polymer, such as PVA, hydrogen bonding of the phosphate ion and polymer molecule at the first degradation step is likely to contribute to the improved thermal stability.

Part B: Computational study of intercalation of amines into α-Zirconium phosphate and adsorption of a model organic pollutant

α -Zirconium Phosphate (α-ZrP) is an example of a layered material that can be used as an ion exchanger. The intercalation of amines into the interlayer of α-ZrP, and the adsorption of chlorophenol by the modified α-ZrP, was investigated. The intercalated α-0ZrP can be used to remove the organic pollutants from aqueous solution. Density functional theory using the B3LYP functional with a 6-311G* basis set was used to explain the previous experimental results.

Previous experimental work in our laboratory has focused on the adsorption of 4-chlorophenol by ZrP-DHDA, XRD and FTIR data suggest that chlorophenol and DHDA were co-intercalated in the d-space of α-ZrP. Density functional theory calculations were carried out in this work using phosphoric acid as simple model systems. Based on the computational results reported here, the driving force for the adsorption was found to be hydrogen bonding between the phosphate and chlorophenol.

PREFACE

Layered metal materials are a family of 2-dimensional nano or micro-scale solids containing several layers stacked with interlayer galleries. While there are numerous examples of these compounds, only select examples, such as layered double hydroxides (LDHs), layered metal phosphates and layered double salts, have been tested for applications such as catalysis, drug delivery, anion separation, fire retardancy, and environmental water decontamination. These materials are promising targets for their applications since they have structural properties that can be utilized as design parameters to fine tune effectiveness in chosen applications.

The goals of this work are to synthesis and characterize layered metal phosphates with specific metal cations (aluminum and zirconium) and to explore the applications of these compounds in either fire retardancy of polymers or removal of pollutants from aqueous solution.

In Chapter 1, the preparation and characterization of taranakite, and a modification of it by sodium dodecyl sulphate, are described. The fire retardancy and thermal stability of polymer composites with these materials as additives were also investigated. Compared with LDHs and other layered materials, polymers with taranakite showed enhanced fire retardancy with polar and non-polar polymers.

In Chapter 2, density functional theory (B3LYP/6-311G*) calculations were combined with previous experimental results to characterize the intercalation of amines into the α-zirconium phosphate (α-ZrP) and the adsorption of 4-chlorophenol from aqueous solution by the amine-intercalated α-zirconium phosphate. The energies for different possible interactions between the interlayer phosphate, amines and chlorophenol were determined in order to provide an explanation of the co-intercalated arrangement of amines and chlorophenol.

ACKNOWLEDGMENTS

Ning Wang, M.S.

My sincere gratitude goes to my research advisor, Prof. Jeanne M. Hossenlopp for her knowledge, guidance, and support throughout this work, and for the extraordinary amount of personal support and patience, she offered to me throughout my stay at Marquette University. And I would also like to extend my appreciation to Prof. James Gardinier and Prof. Qadir Timerghazin for affording time out of their schedules to serve on my research committee. I am also thankful to Prof. Charles Wilkie and coworkers for the helpful discussions in polymer fire retardancy. Support from the National Science Foundation and National Institute of Standards and Technology is gratefully acknowledged. I am grateful to my group members, Dr. Allen Chaparadza, Dr. Darlington Mlambo, Stephen Majoni and Cleopas Machingauta for help discussions. And lastly, I am thankful to my family for their love and support.

TABLE OF CONTENTS

LIST OF FIGURES

LIST OF TABLES

Part A. Preparation and characterization of layered aluminum phosphate and effects on dispersion and fire retardancy on polymers

Chapter 1 Introduction

The expanding use of polymers in a wide variety of applications results in a continuous demand for improved thermal and mechanical properties to endure increasingly stringent conditions.[3-5] The reduction in the polymers' propensity to ignite and burn efficiently is a critical factor to consider because the polymer/plastic materials comprise a large fraction of the fire loading in houses, commercial environments and transportation. Hence, it is clear that fire retardants are important part of polymer formulations.[6]

The conventional fire retardants are halogen-based compounds that are economical and which can enhance the fire retardancy of polymers without degrading their physical property, such as strength. However, toxic species such as dioxins and furans, which are generated during the combustion of halogen-containing composites, could cause serious environmental contamination.[7-9] Therefore, developing halogen-free, low-smoke, and environmentally-friendly fire retardant composites has become increasingly important in recent years. Inorganic hydroxides, such as aluminum hydroxide or magnesium hydroxide are among the most widely used inorganic fire retardants at the present time due to their non-toxic and environmentally friendly properties.[10-14] However, the high levels of loading (30 wt%-60 wt%) are required, leading to additional costs, processing difficulties and a decrease in physical properties of the polymers. Hence the development of new highly effective, "green" fire retardants has prompted much attention during the last decade.[5,15,16]

Fire retardants with very small particle size appear to offer significant advantages over conventional formulations. Nano-scale layered metal materials, such as clay and layered double hydroxides (LDHs) have been tested as potential fire retardants that could improve the flame retardancy, while improving physical properties (such as the tensile strength, and elongation at break).[17-19] In layered material/polymer systems, concurrent improvements across multiple properties are typically achieved, such as flammability and also the biodegradability behaviors.[20,21] These improvements of polymer nanocomposites usually originate from the change of the polymer nature in the vicinity of the additive and depend strongly on the dispersions of additives in the polymers. [22-24]

1.1 Structure and properties of polymer/layered nanocomposites

The incorporation of layered materials in polymers was first reported in the early 1960's, while the serious investigation of this area began in the 1990's. Two applications are cited as milestones for the revival of interest during the 1990's: (a) the Toyota research group developed the PA-6-clay nanocomposites for large scale industrial application;[25] and (b) Vaia *et al*. found that blending layered materials with polymers in the molten state offers a versatile and environmentally benign approach for synthesizing nanocomposites.[26] This new class of materials is becoming of increasing interest world-wide due to the fact that the addition of a relatively small amount of these materials enhances most of polymers properties, such as mechanical, thermal stability, flame retardancy.[27]

Most of the literature concerning layered materials as additives to polymers has focused on nanocomposites of two types of nanomaterials: (a) montmorillonite (MMT), a cationic clay;[28-30] (b) layered double hydroxides (LDHs), sometimes referred to as hydrotalcite-like anionic

clays.[31-34] Recently, synthetic layered metal phosphates are emerging as a new class of nanofillers for polymers.[35] For example, α-zirconium phosphate has been employed to fabricate polymer nanocomposites with good mechanical properties.[36;37] Because of the weak interactions between α-ZrP nanoplatelets, the intercalation or exfoliation of the nanolayers in polymeric matrix can be achieved via *in situ* polymerization and solution methods.[38;39]

1.1.1 Cationic clays

Cationic clays, also named smectite clays,[40-42] are a family of layered silicate materials known as 2:1 phyllosilicates. Examples include montmorillonite, fluorohectorite, hectorite, saponite, kaolinite and magadiite. The most widely used for polymer nanocomposites is montmorillonite (MMT). The general formula of MMT is (Na, Ca) (Al, $Mg)_6$ $(Si_4O_{10})_3(OH)_6 \cdot n$ H_2O, and the structure of MMT consists of stacked layers made of two silica tetrahedrons fused to an edge-shared octahedral sheet containing metal cations, such as Al^{3+} or Mg^{2+}, hydroxyl groups and oxygen groups.[42] The layer thickness is approximately 1 nm and the length may vary from 30 nm to several microns with an aspect ratio (length/thickness) greater than 1000. The adjacent layers are separated by a regular van der Waals gap, called the interlayer or gallery. Substitution of tetrahedral Si(IV) by M(III) (such as Al^{3+}) within the layers generates a negative charge, which the net charge can be counterbalanced by sodium or calcium ions in the interlayer.

Most cationic clays show a range of useful properties including surface acidity and cationic diffusion which make them a useful as base materials for medicines, catalysts, ion exchangers, corrosion protectors and also as additives for potentially enhancing fire retardancy of polymers.[43-45]

1.1.2 Anionic clays

Synthetic anionic clays,[46-50] are also of great interest due to their potential applications in many different areas. The most popular anionic clays are hydrotalcite - like layered double hydroxides. The general formula for LDHs is $[M^{2+}_{1-x} M^{3+}_{1-x} (OH)_2]^{x+} A^{n-} \cdot nH_2O$, where M^{2+} and M^{3+} are metal cations which occupy the octahedral lattice sites of the brucite – $(Mg(OH)_2)$[51;52] like layers forming positively charged hydroxides sheets, with anions, A^{n-} and H_2O occupying the interlayer space. Partial M^{2+} to M^{3+} substitution induces a positive charge on the layers which balanced by the presence of the interlayer anions. Figure 1.1 is the scheme of the LDH structure and its chemical formula.

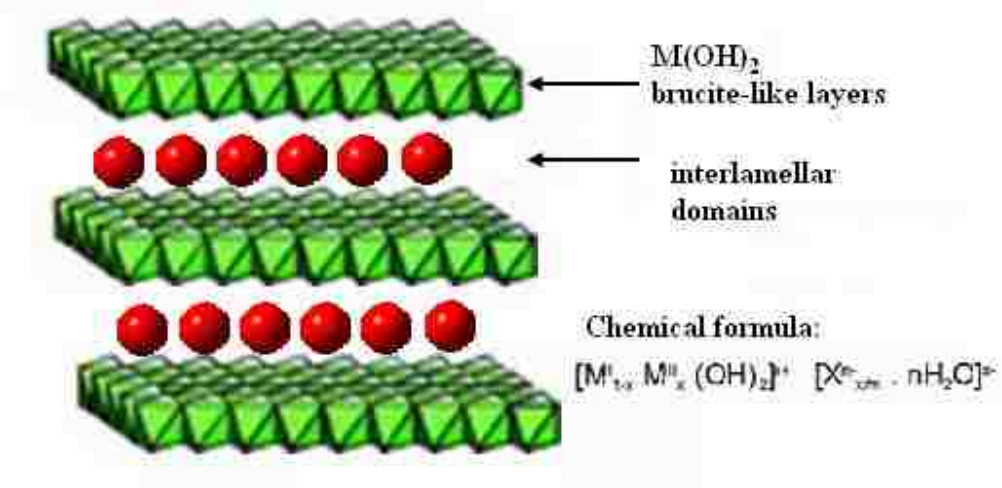

Figure 1.1 The scheme of the LDH structure and chemical formula.

Pinnavaia and coworkers investigated the structure and properties of Mg/Al LDHs.[53] The gallery height of these LDHs with Cl^- as the interlayer anions, is about 2.97Å. The pristine LDHs could not be readily dispersed in the polymer matrix to obtain the polymer nanocomposites because the d-spacing is too small to allow monomers or polymer molecules get into the interlayer spaces, and the hydrophilic surfaces of LDHs layers are not compatible with hydrophobic polymer

molecules. Therefore, substitution-suitable interlayer organic anions are needed to change the polarity of LDHs. There are two methods typically used to modify the LDHs by using organic molecules. One method is direct synthesis of an LDH with organophilic surfactants in its gallery space, while the other method is the synthesis of LDHs with a small inorganic anions followed by an anion exchange reaction to incorporate surfactant anions with long organic chains (shown in Figure 1.2). Pinnavaia and Constantino have studied the properties of LDHs with different exchangeable anions.[53] The intercalation of these long chains anion will result the expansion of the gallery height. Intercalated LDHs are of interest in various aspects of chemistry including catalysis,[54;55] fire retardancy,[56-58] ion mobility,[59] environment protection[20;60] and pharmaceutical applications.[61]

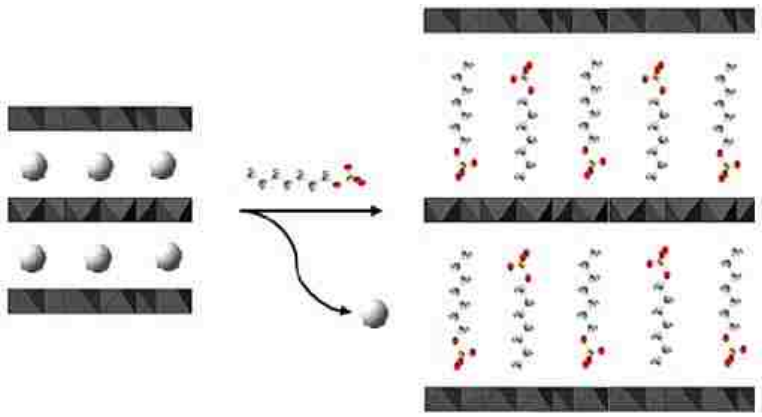

Figure 1.2 Schematic process of intercalation of organic molecules into LDH

In addition to LDHs, there are other types of anionic clays, such as hydroxyl double salts (HDSs), layered hydroxyl salts (LHSs) and layered metal oxides. These materials have the similar structure with LDH, and they also possess the anionic exchange abilities as LDHs. Varying the metal identity and composition in these compounds is expected to generate a wide range of chemical applications.[62-64]

1.1.3 Phosphorus based fire retardants

Phosphorus-containing flame retardants cover a wide range of inorganic and organic compounds and include both reactive products which are chemically bound into the polymer material as well as additive products which are integrated into the material by physical mixing only.[65] They have a broad range of applications, and a good fire safety performance.

1.1.3.1 Organic phosphorus-containing flame retardants

The most important organic phosphorus-containing flame retardants are phosphate esters, phosphonates, and phosphinates.[66] Phosphorus-containing flame retardants are widely used in engineering plastics, polyurethane foams. Phosphate esters are as flame retardant plasticizers in polyvinylchloride (PVC, alkyl/aryl phosphates) and engineering plastics.[67] Phosphates, phosphonates and phosphinates usually work well as reactive phosphorus-containing flame retardants in flexible polyurethane foams for automotive and building applications.[68] Organic phosphinates are a new class of flame retardants for use in engineering plastics, particularly in polyamides.[69] Flame retardant grades based on red phosphorus are mainly used in glass fiber reinforced polyamide 6 and 66.[69] Ammonium polyphosphate (APP) grades are primarily used in intumescent coatings.[66] They are also found in rigid and flexible polyurethane foams and polyolefins in formulations for unsaturated polyesters, phenolics, epoxies, and coatings for textiles.

There are a range of proposed mechanisms organic phosphorus-containing fire retardants.[69] The phosphorus content of the different chemicals varies from as low as 9.5% in case of

Tricresyl Phosphate (TCP) to as high as red phosphorus (100%). In addition, the phosphorus atom is found in oxidation states ranging from 0 to 5. Typically, phosphorus-based flame retardants are designed to develop activity in combination with the starting decomposition of basic polymer. These additives may offer partial gas phase contributions to the flame extinguishing effect which are comparable to halogen-containing flame retardants. However, the main feature is char forming activity sometimes combined with foaming or intumescence, which forms a protective top layer on the surface. This type of solid-phase mechanism provides an advantage of less release of smoke and gases in case of a fire situation.

1.1.3.2 Layered metal phosphates fire retardants

In recent years, increasing attention has been focused on the development of polymeric nanocomposites with an inorganic phase that contains phosphate.[70] α-zirconium phosphate (α-ZrP) is an example of the inorganic layered metal phosphates that show potential application in the fields of fire retardancy.[71] One of the most interesting aspects of these new materials is their capacity to reduce rate of combustion of the polymers, which is similar to that observed with common natural layered nano-fillers such as montmorillonite. However, α-ZrP has a higher ion-exchange capacity and a greater thermal and chemical stability.[71]

1.1.4 Preparation and morphology of the polymer/layered materials composites

There are many methods to incorporate polymers with the galleries of a layered materials, such as exchange,[72] co-precipitation,[73;74] *in situ* polymerization,[74;75] surfactant medicated incorporation,[73] hydrothermal treatment,[74] reconstruction,[76] and restacking.[73] The different pathways of the nanocomposite preparations are shown in Figure 1.3.

Polymer/layered material composites form a variety of structures: Immiscible systems, also known as microcomposites, arise when the polymer is unable to intercalate into the galleries, and a phase-separated composite is formed. In this case, the layered material is not nano-scale dispersed in polymers and is essentially behaving as a micro-scale additive. Intercalated composites, where the extended polymer macromolecules diffuse between unchanged layer sheets, result in a well-ordered multilayer structure of alternating polymeric and inorganic layers with a repeating distance of few nanometers between them. Exfoliated, also known as delaminated nanocomposites, occur when the clay layers are separated and uniformly dispersed, maximizing thus the polymer-layer material interactions.[77-79] Figure 1.4 shows the three polymer/LDH composite structures.

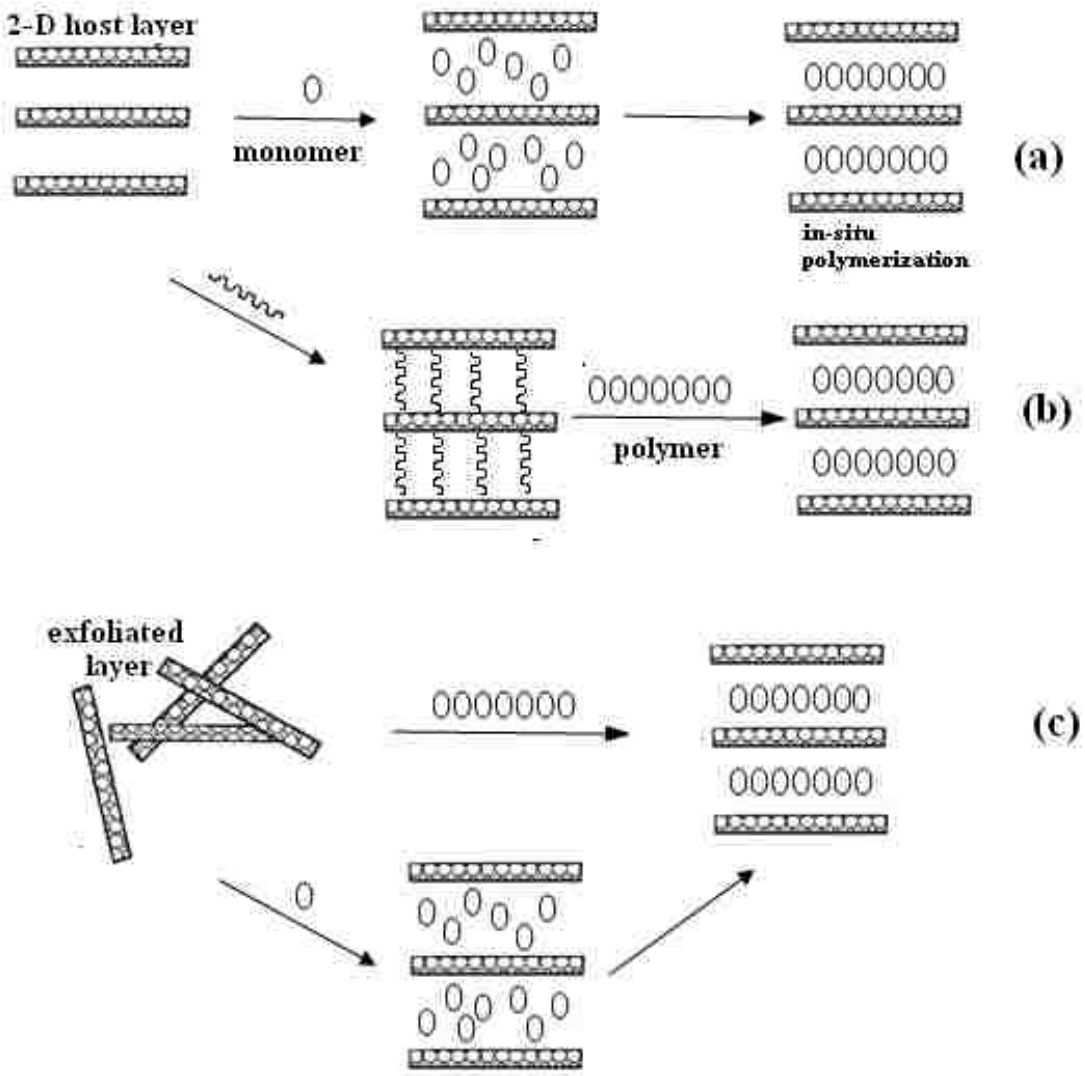

Figure 1.3 Possible pathways for intercalated nanocomposite preparation by (a) monomer exchange and in situ polymerization, (b) direct polymer exchange, and (c) restacking of the exfoliated layers over the polymer (The picture is adapted from ref. 60).

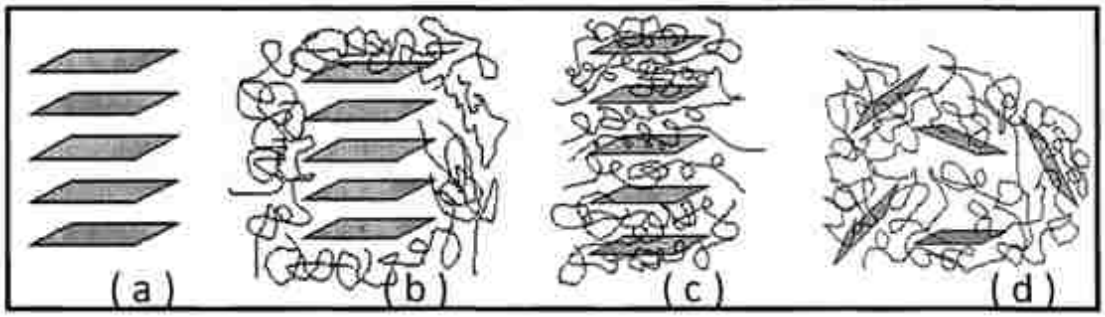

Figure 1.4 Polymer/layered material composite structures. (a) original layered compound, (b) immiscible system (microcomposite), (c) intercalated nanocomposites, (d) exfoliated nanocomposites. (The picture is adapted from ref. 46)

X-ray diffraction (XRD) is the most common method to characterize layered compounds and to identify the dispersion of the polymer matrix into the galleries of the layered materials.[80] XRD is used to probe alterations in the order of layered materials by monitoring the position, shape, and intensity of their basal reflections. Increasing interlayer spacing is identified by a shift of the diffraction peak to lower angles, according to Bragg's law, leading eventually to featureless patterns (such as those exhibited by exfoliated structures or non-crystalline materials). Three typical polymer/ layered materials composites structures may be identified by XRD data. Figure1.5 shows sample XRD patterns of the initial layered materials and what would be expected in the three different models of dispersion. In an immiscible system or a microcomposite, the polymer does not enter into the gallery space of the layered material, so the XRD data of this system is consistent with the original layered materials. An intercalated nanocomposite is obtained when the polymer enters the gallery space and the registry between the layers is maintained but expanded. In this case, the first peak of XRD shifts to the lower angle. In an exfoliated system, also referred to as a delaminated system, an excellent nano-dispersion of the layered material into the polymer matrix is accompanied with a loss of the registry between the layers, and the XRD loses all the peaks. However, there are some

limitations in using the XRD data alone to identify the nanocomposites. For example, when the layered compounds and the polymer are incompatible with each other, aggregation of the layered materials may lead to incoclusive information from the XRD data. A sample containing a largement of aggregrated additive will show all the peaks of original layered materials, while the other areas without the crystals will show the no peaks. Transmission electron microscopy (TEM) is utilized as an effective means of developing insights into the internal structure and spatial distribution of the various dispersions, through direct visualization.[81;82]

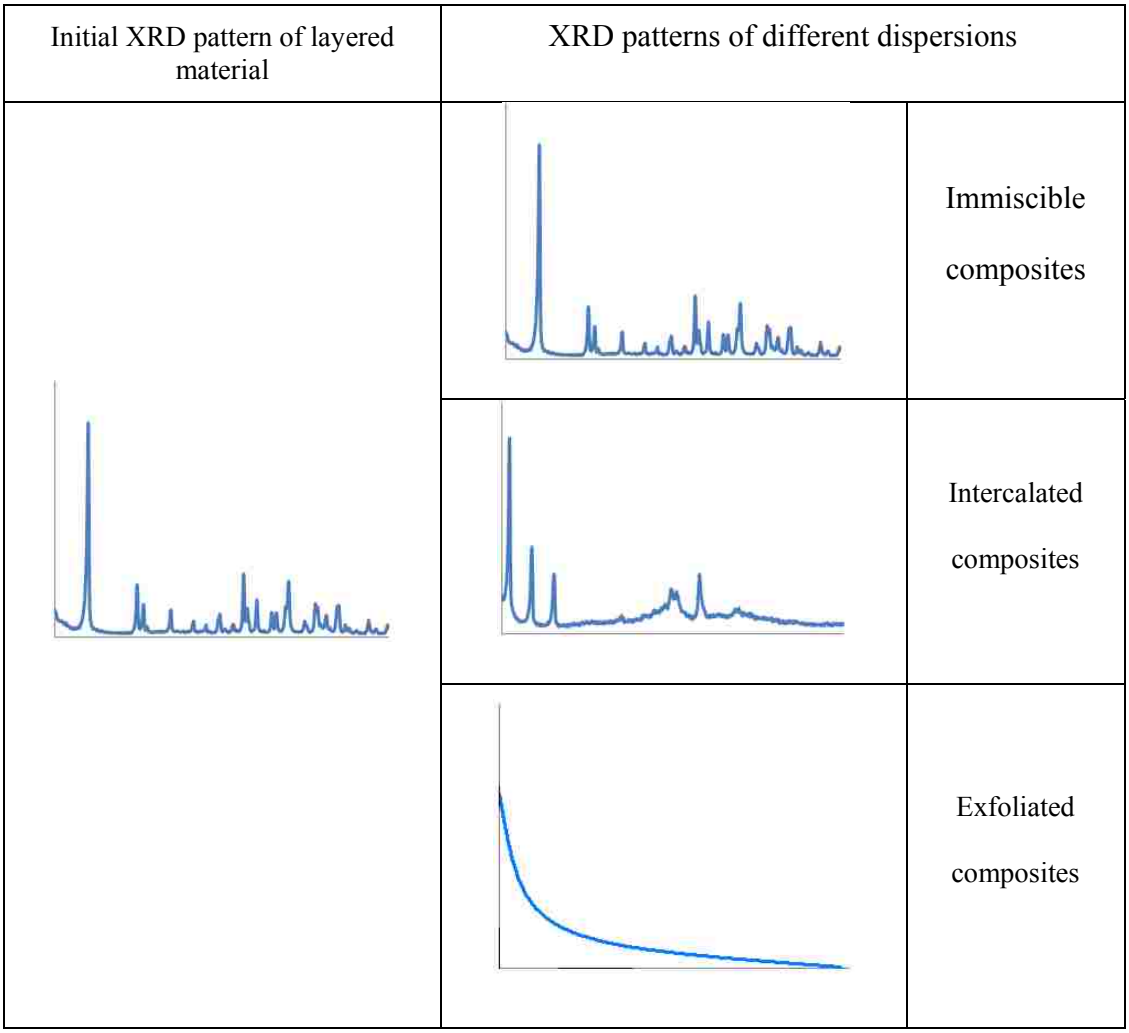

Figure 1.5 XRD patterns of initial layered materials and the three different dispersions

1.1.5 Fire retardancy of polymer/layered nanocomposites

One mechanism proposed to explain the effects of layered materials on polymer combustion is the formation of a multilayered carbonaceous-layered structure on the surface of nanocomposites during the combustion.[83;84] The carbonaceous char may be reinforced by crystalline layers, creating an excellent physical barrier which protects the substrate from heat and oxygen, and slows down the escape of flammable volatiles generated during polymer degradation. Lewin *et al*. proposed another mechanism,[85;86] suggesting that the accumulation of layered compounds on the surface results from the migration of layers driven by their lower surface free energy compared with carbon-based polymers, and this accumulation results the prevention of the polymer degradation.

1.1.6 Methods for evaluating the flammability of polymer/clay composites

Several methods have been used to evaluate nanocomposite flammability and thermal stability:

Thermogravimetric analysis

Thermogravimetric analysis (TGA), is a typical method to determine the thermal properties of polymeric materials. The method measures the changes in sample mass with temperature, under a N_2 atmosphere. The result is a graph plotted with percent mass loss as a function of temperature. The important information includes the degradation onset temperature (10 wt% loss of polymer), the midpoint degradation temperature (50 wt% loss of polymer), and the weight of the char material (usually the weight of nonvolatile material after 600 °C).

Cone Calorimeter

The cone calorimeter (Figure 1.6) has become one of the most important instruments to study the fire retardancy of polymer materials.[87] The heat release rate is obtained. The instrument is constructed using the oxygen consumption principle to determine the rate of heat release.[87]It is a small-scale test, the results of which are applied to large-scale fire situation. This method provides the following important information on heat release rate (HRR) and, especially its peak value (PHRR), total heat released (THR), mass loss rate (MLR) and its average value (AMLR), time to ignition (t_{ig}), and average specific extinction area (ASEA) which is a measure related to smoke production. Ideally, a decrease in PHRR, THR, AMLR, and ASEA with an increase in t_{ig} is desired. The PHRR from burning combustibles is considered to be the most important parameter in predicting the course of the fire and its effect.[88]

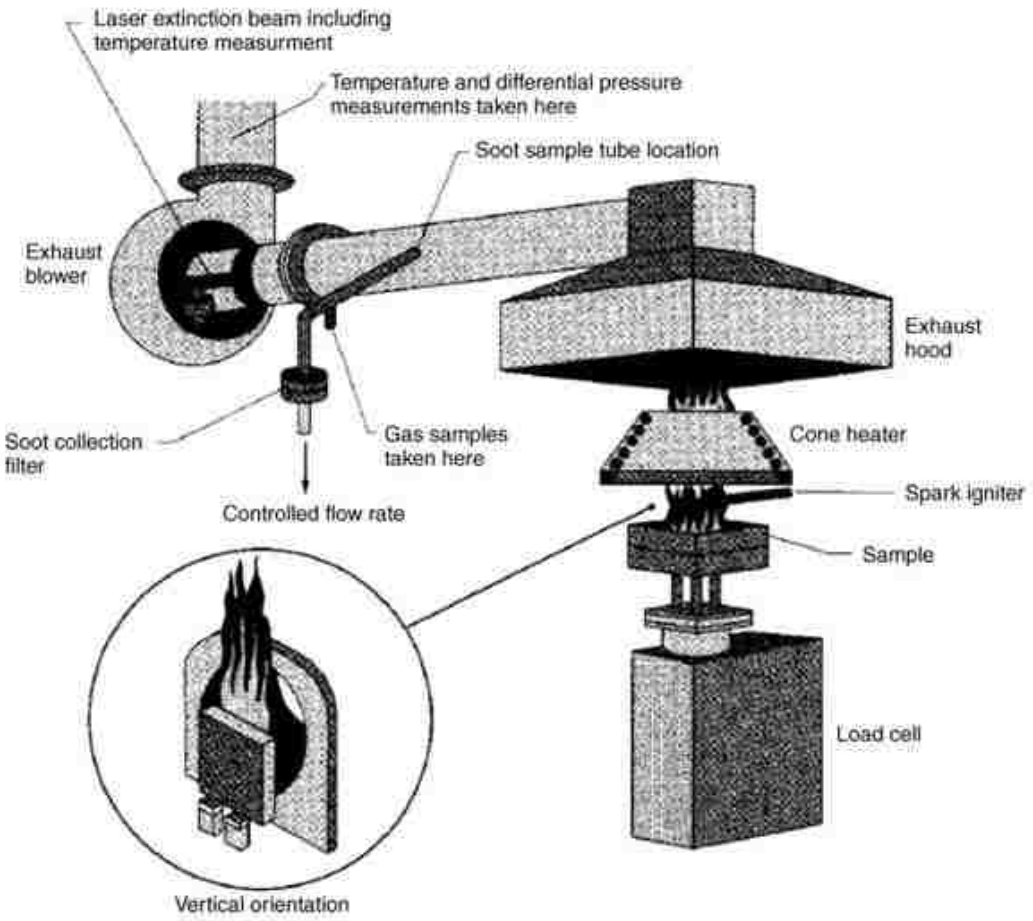

Figure 1.6 Schematic view of the cone calorimeter[89]

The key cone parameters and their units are:

PHRR: peak heat release rate (kW/m^2)

THR: total heat released (MJ/m^2)

AMLR: average mass loss rate ($g/s \cdot m^2$)

ASEA: average specific extinction area (m^2/kg). The ASEA is the parameter related to the smoke. It is the product of two fundamental smoke parameters, specific extinction area and smoke mass fraction of the fuel mass loss.

t_{ig}: time to ignition (second)

t_p: time to peak heat release (second)

Microscale combustion calorimeter (MCC)

A micro-scale combustion calorimetric method has been developed to measure flammability parameters of milligram sample combustion.[90] Compared with a cone calorimeter, the MCC only requires a small amount of sample (1-10 mg). It utilizes a fast high heating rate (1°C/s), and high heating temperature (up to 900°C), so that the pyrolysis and combustion of the sample are complete.[91] Figure 1.7 shows the schematic process of the sample combustion in the MCC. There are two types of gases that pass through the sample holder, nitrogen or oxygen. N_2 leads to the complete pyrolysis, and O_2 leads to combustion. When the pyrolysis occurs in the polymers, the fragments from the cleavage of the polymers can be collected and analyzed by mass spectrometry (MC), infrared Spectrometry (IR) or other analytical methods. In the combustion portion of the experiment, the MCC collects quantitative information of heat release rate, mass flow rate, total heat released and char yield. Unlike the traditional cone calorimeter test, smoke information such as ASEA is not collected.

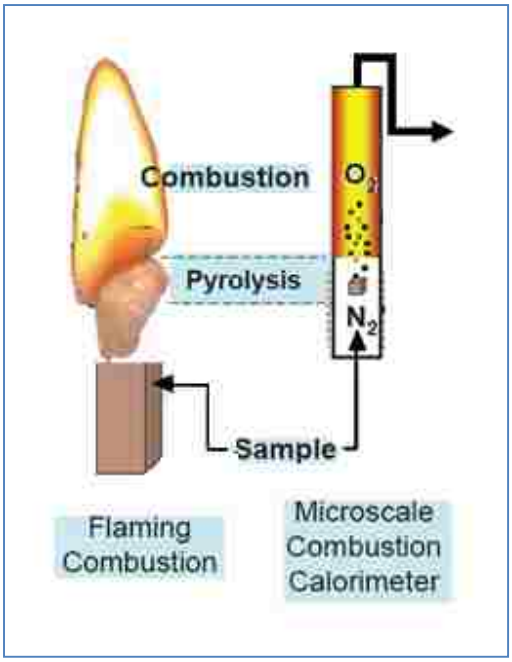

Figure 1.7 Schematic process of combustion of the sample in MCC

1.1.7 Motivation for study

A key property possessed by layered materials is their ability to incorporate large molecules such as polymers into their gallery spaces. The resulting strength and fire properties may vary depending on the morphology of these polymer/clay composites. Therefore, matching a given polymer with optimized layered compounds is important to enhance the desired properties. The ultimate long-term goal of this research is to be able to prepare various layered materials that could be more compatible with polymers, and then to use layered nanomaterials with selected polymers for the production of new fire retarded polymeric systems. In our laboratory, we synthesize many different types of layered nanomaterials, modify them, and study the applications of these materials, including the fire retardancy, as well as organic pollutant removal

from water. In the case of fire retardancy applications, our goal is to optimize materials for improved polymer dispersion and to enhance their thermal properties.

Chapter 2 Experimental

2.1 Materials

Polystyrene (M_W ca. 230000, M_n ca. 140000) , polypropylene (isotactic melt index 230 °C), poly vinyl alcohol (M_W ca. 146000 87% - 89% hydrate), ethylene vinyl acetate (18% vinyl acetate), butanol, and butylamine, were acquired from the Sigma-Aldrich Chemical Co. Aluminum isopropoxide, phosphoric acid (85% w/w), phosphate monobasic potassium (97%), potassium hydroxide, aluminum nitride nonahydrate (97%), sodium dodecyl sulfate (SDS), were obtained from TCI America. All materials were used as obtained from the manufacturers.

2.2 Preparation of layered aluminum phosphate

There are two common methods to synthesize layered aluminum phosphate: hydrothermal and co precipitation methods. Particular compositions and architectures (1-dimension, 2-dimension and 3-dimension) of layered aluminum phosphate crystals can be obtained using different methods.

A literature method for synthesis by co-precipitation was utilized.[92] The ALP synthesized using this method was assigned as taranakite. A solution of $Al(NO_3)_3 \cdot 9H_2O$ (0.12 mol) in deionized and decarbonated (heat the water to 100 °C for 2 hours to release the CO_2 in the water) water (120 mL) was added dropwise to a solution of KOH (0.24 mol for Al/P molar ratio 1:2 or 0.18 mol for Al/P molar ratio 2:3) and KH_2PO_4 (0.24 mol for 1:2 or 0.18 mol for 2:4) in

deionized water (180 mL) with vigorous stirring. The pH was about 4 ~ 5. The resulting slurry was aged at room temperature for 24 hours with stirring, and then washed with deionized and decarbonated water before drying it in air at room temperature.

The hydrothermal synthesis was performed using Chippindale's method.[93] Aluminum isopropoxide (3 g) and phosphoric acid (1.9 mL for 1:2 or 2.4 mL for 2:3) were added to butanol (23.7 mL). The mixture was stirred until homogeneous and the butylamine (7.5 mL) added. The gel was heated to 150°C, and then transferred into a preheated (150°C) Teflon-lined autoclave for 24 hrs. The solid precipitation was collected by filtration, washed with distilled water and briefly dried in air at 80°C.

2.3 Modification of taranakite

The sodium dodecyl sulfate (SDS) modified aluminum phosphate (AL-SDS) was prepared by following a procedure similar to the preparation of magnesium aluminum undecenoate layered double hydroxide.[94] A solution of 72 g SDS (0.4 mol), 10.08 g KOH (0.12 mol) and 16.32 g KH_2PO_4 (0.12 mol) were dissolved in deionized water (500 mL) and heated to 50 °C. Then a solution of 45 g $Al(NO_3)_3 \cdot 9H_2O$ (0.12 mol) in water (120 mL) was added dropwise to SDS solution with vigorous stirring. The resulting colloidal precipitate was aged for 48 hours at 50 °C, and then repeatedly filtered and washed with deionized water before it was dried in an oven at 50 °C for 24 hours.

2.4 Preparation of polymer/taranakite composites

All polymers except PVA were prepared by melt blending methods in a Brabender mixer[95]. The loading for all the polymer/taranakite composites was maintained at 3, 5 and 10 wt% of

taranakite or AL-SDS. The requisite amounts of polystyrene (PS), polypropylene (PP), and taranakite were premixed in a beaker and stirred, then transferred to a Brabender Plasticorder operated with a screw speed of 60 rpm and residence time of 20 min. The temperature for melt blending was 200°C for PS and 185 °C for PP.[96] The reference samples of pure PS and PP were obtained using the same treatment procedure, without the additives.

The PVA/taranakite composite was prepared using a solution method.[97] The 5 g of PVA was dissolved in 200 mL deionized water held at 80 °C with vigorous stirring. Different masses of taranakite were added to obtain loadings of 3%, 5% and 10 wt%. The mixture was kept stirring for a week at a temperature 80°C, then the mixture solution was dried at room temperature. The PVA/AL-SDS composite was prepared using same method with PVA/taranakite, but it was found that AL-SDS is not compatible with the PVA polymer because the AL-SDS precipitated after stirring, therefore the PVA/AL-SDS system was not included for further experiments.

Chapter 3 Results and Discussion

3.1 Characterization of the layered aluminum phosphates

3.1.1 X-ray diffraction of taranakite and AL-SDS

The X-ray diffraction patterns of layered aluminum phosphate prepared by using different methods are shown in Figure 3.1(I). Curves (a) and (b) are for samples synthesized via the co-precipitation method with the Al:P molar ratio of 1:2 and 2:3 respectively, and curves (c) and (d) were obtained with samples synthesized via the hydrothermal method with the Al:P molar ratio

of 1:2 and 2:3 respectively. The ALP samples prepared using co-precipitation method shows a good layered crystalline structure. The ALP synthesized using hydrothermal method shows crystalline structure, but not a good layered structure. The different molar ratios of Al:P also resulted in different structures. The co-precipitation ALP was used for the rest of the fire retardancy studies because it has better layered crystalline structure, and also it contains no organic composition.

Figure 3.1 (II) shows the XRD of (a) co-precipitation ALP and (b) taranakite. The pattern shows many sharp reflection peaks which are indicative of a crystalline material. Peak positions are all consistent with the XRD of taranakite mineral (PDF 29-981) in literature.[98] Table 3.1shows the 2θ, intensities of peaks and d-spacing of literature assignment for taranakite and the observed values for our sample. Therefore, the co-precipitation ALP sample is assigned to be taranakite.

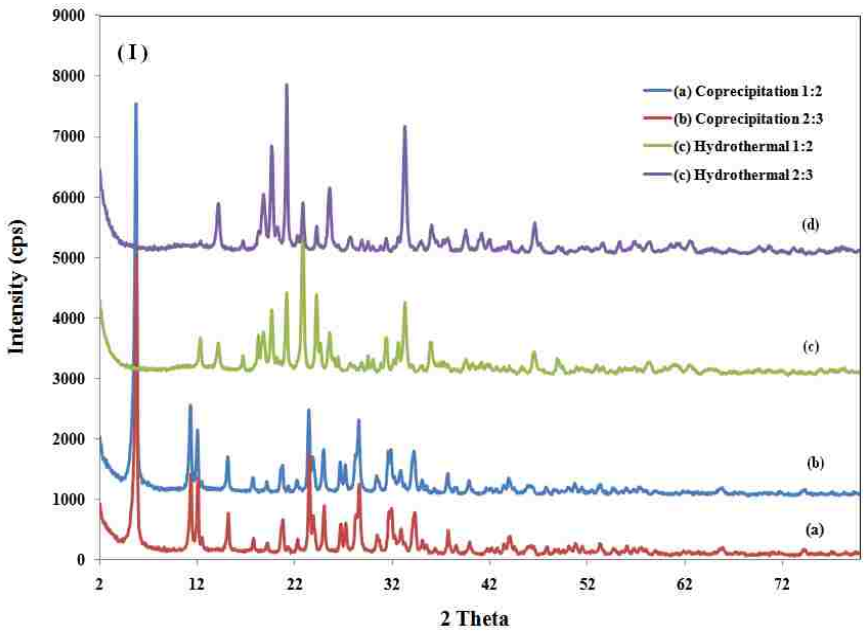

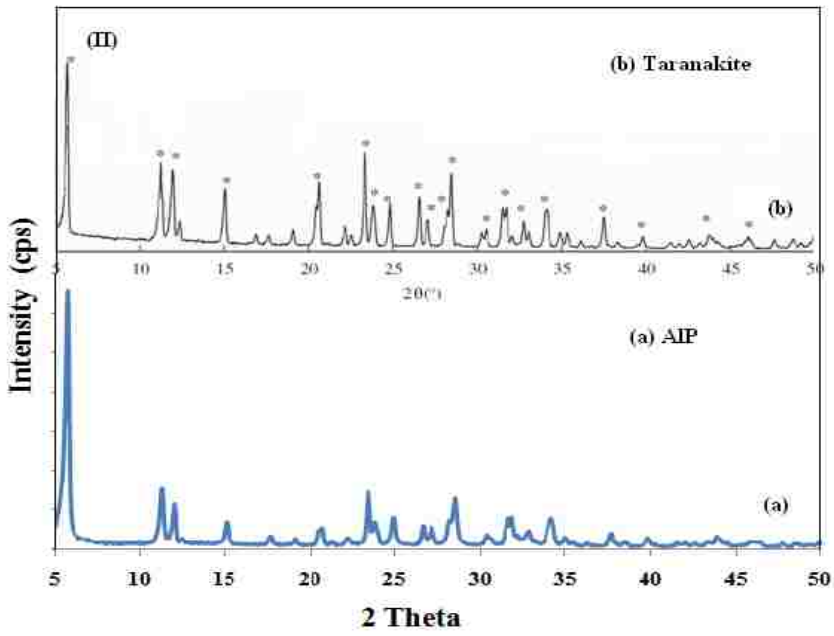

Figure 3.1 X-ray diffraction patterns of layered aluminum phosphate, (I) XRD of ALP at different conditions, which (a) and (b) are co-precipitation method with Al:P molar ratio at 1:2 and 2:3, (c) and (d) are hydrothermal method with Al:P molar ratio at 1:2 and 2:3. (II) XRD of co-precipitation ALP compared with taranakite.

Table 3.1 The 2θ, intensity and d-spacing of Taranakite and ALP

Taranakite (PDF 29-981)			**ALP**		
2Theta (°)	**Intensity (%)**	**d-spacing(Å)**	**2Theta(°)**	**Intensity (%)**	**d-spacing (Å)**
5.58	100	15.84	5.65	100	15.65
11.17	11.9	7.92	11.25	11.95	7.87
11.89	16.72	7.44	12.00	16.77	7.38
12.32	3.41	7.18	12.45	3.46	7.11
15	9.48	5.91	15.05	9.53	5.89
17.58	2.33	5.04	17.60	2.38	5.04
19.02	1.88	4.67	19.06	1.93	4.66
20.41	3.44	4.35	20.45	3.49	4.34
20.6	7.63	4.31	20.64	7.68	4.30
21.17	1.66	4.20	21.21	1.71	4.19
22.11	2.68	4.02	22.15	2.73	4.01
23.32	24.92	3.81	23.36	24.97	3.81
23.74	5.51	3.75	23.78	5.56	3.74

23.91	2.45	3.72	23.94	2.46	3.72
24.82	12.51	3.59	24.86	12.52	3.58
26.54	5.69	3.36	26.58	5.73	3.35
27.06	7.85	3.29	27.10	7.9	3.29
28.04	4.54	3.18	28.08	4.54	3.18
28.17	2.58	3.17	28.21	2.62	3.16
28.45	19.39	3.14	28.49	19.44	3.13
30.27	4.46	2.95	30.29	4.51	2.95
30.52	1.87	2.93	30.56	1.91	2.93
31.42	1.03	2.85	31.46	1.06	2.84
31.5	8.3	2.84	31.54	8.34	2.84
31.76	11.5	2.82	31.80	11.52	2.81
32.11	3.52	2.79	32.15	3.57	2.78
32.72	5.9	2.74	32.76	5.95	2.73
32.82	1.14	2.73	32.86	1.19	2.73
33.11	1.69	2.71	33.15	1.74	2.70
33.95	3.73	2.64	33.99	3.78	2.64
34.13	2.89	2.63	34.17	2.94	2.62
34.17	6.55	2.62	34.21	6.61	2.62
34.93	3.23	2.57	34.97	3.28	2.57
35.36	1.91	2.54	35.40	1.96	2.54
36.2	1.35	2.48	36.24	1.38	2.48
37.56	4.81	2.39	37.60	4.86	2.39
37.56	1.38	2.39	37.60	1.43	2.39
38.38	2.11	2.35	38.42	2.16	2.34
39.77	1.95	2.27	39.81	1.97	2.26
42.02	1.73	2.15	42.06	1.78	2.15
43.3	2.41	2.09	43.31	2.48	2.09
43.82	5.19	2.07	43.86	5.24	2.06
44.05	1.84	2.06	44.09	1.89	2.05
44.37	1.58	2.04	44.41	1.68	2.04
45.82	1.32	1.98	45.86	1.37	1.98
46.11	1.41	1.97	46.15	1.46	1.97
46.38	1.67	1.96	46.42	1.72	1.96
47.69	2.44	1.91	47.73	2.46	1.91
48.83	1.08	1.87	48.87	1.13	1.86
49.31	1.13	1.85	49.35	1.18	1.85
49.98	1.81	1.82	50.02	1.87	1.82
50.65	2.04	1.80	50.69	2.09	1.80
50.78	1.15	1.80	50.82	1.2	1.80
51.33	2.41	1.78	51.37	2.44	1.78

52.39	1.39	1.75	52.44	1.44	1.75
53.22	2.64	1.72	53.26	2.68	1.72
54.58	1.05	1.68	54.62	1.1	1.68
55.91	2.69	1.64	55.92	2.74	1.64
57.21	1.76	1.61	57.25	1.77	1.61
57.81	1.04	1.60	57.85	1.09	1.59
61.75	1.13	1.50	61.79	1.15	1.50
65.48	1.04	1.43	65.49	1.09	1.43
74.02	1.13	1.28	74.06	1.17	1.28
74.24	1.07	1.28	74.27	1.12	1.28

Taranakite is one type of alkyl aluminum phosphate mineral reported by Hector and Skey ,[99] which was found in caves. The unit cell of taranakite contains six layers with the composition $K_3Al_5(PO_4)_2(HPO_4)_6 \cdot 18H_2O$.[100] Taranakite crystallizes in the hexagonal crystal system. The unit cell dimensions are a = 870.25 pm and c = 9505 pm, enclosing a volume of 6.234 nm^3 and the c-axis of taranakite is the longest of all known minerals.[101] Figure 3. 2 is the schematic structure of taranakite, which six layers are stacked with the interlayer water molecules.

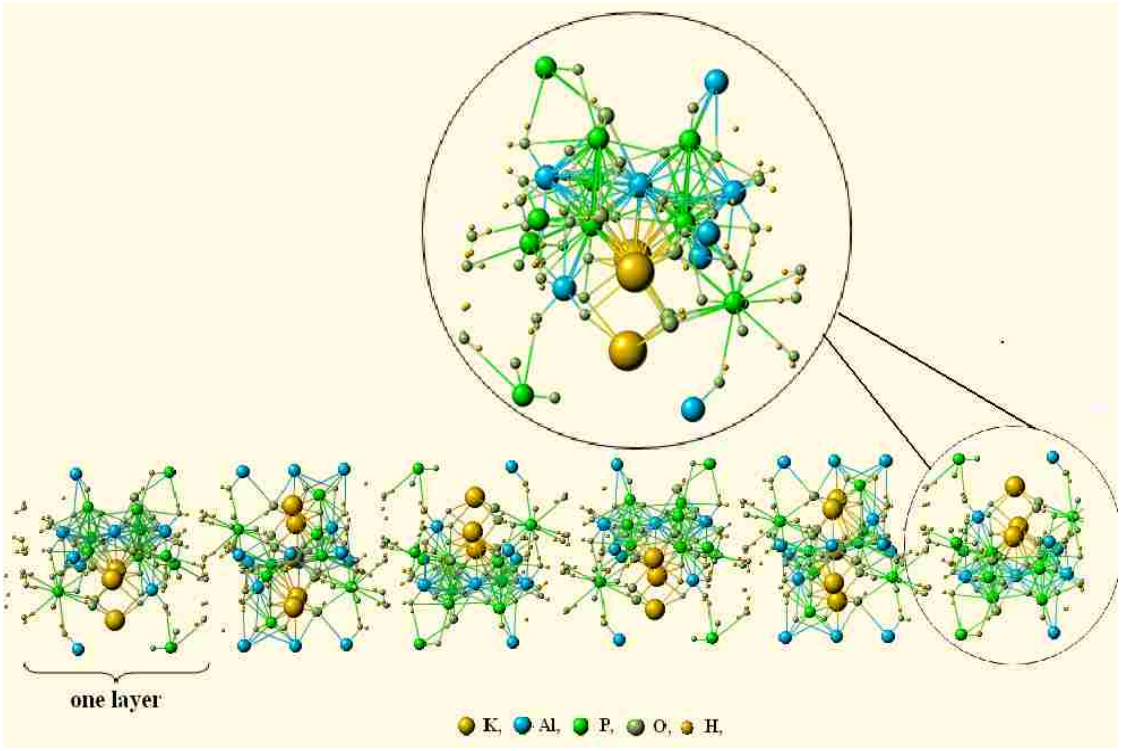

Figure 3.2 Schematic structure of taranakite crystal.[102]

Figure 3.3 shows an overlay of the XRD patterns for the pristine taranakite (a) and AL-SDS (b). The AL-SDS pattern shows three sharp reflection peaks which also indicate good layer structure in the AL-SDS, and the absence of taranakite peaks in AL-SDS pattern indicates the completeness of the ion-exchange process. All of the peaks, including the first diffraction peak that is associated with the interlayer space, moved to lower 2θ than ALP pattern, which means the expansion of interlayer distance. This is consistent with the intercalation dodecyl sulfate ions with an increase in d-spacing of the pure taranakite from 15.9 Å to 30.9 Å. The d-spacing upon intercalation of the dodecyl sulfate ion, is 17.1 Å, which is calculated by subtracting the solid layer thickness of 13.78 Å.[101] The increase is consistent with the potential replacement smaller PO_4^{3-} with a larger dodecyl sulfate anion (16.4 Å). The chain length of SDS was calculated using Gaussian 98 program and carried out at DFT (B3LYP) level of theory with 6-311G* basis set.

The chain length was calculated as the inter-atomic distance between the sulfate oxygen and the hydrogen atom of the furthest methyl group. Figure 3.4 shows the intercalation process of SDS anion in ALP, and the proposed arrangement of dodecyl sulfate anions into the layer is an intercalated structure (interdigited or tilted orientation).

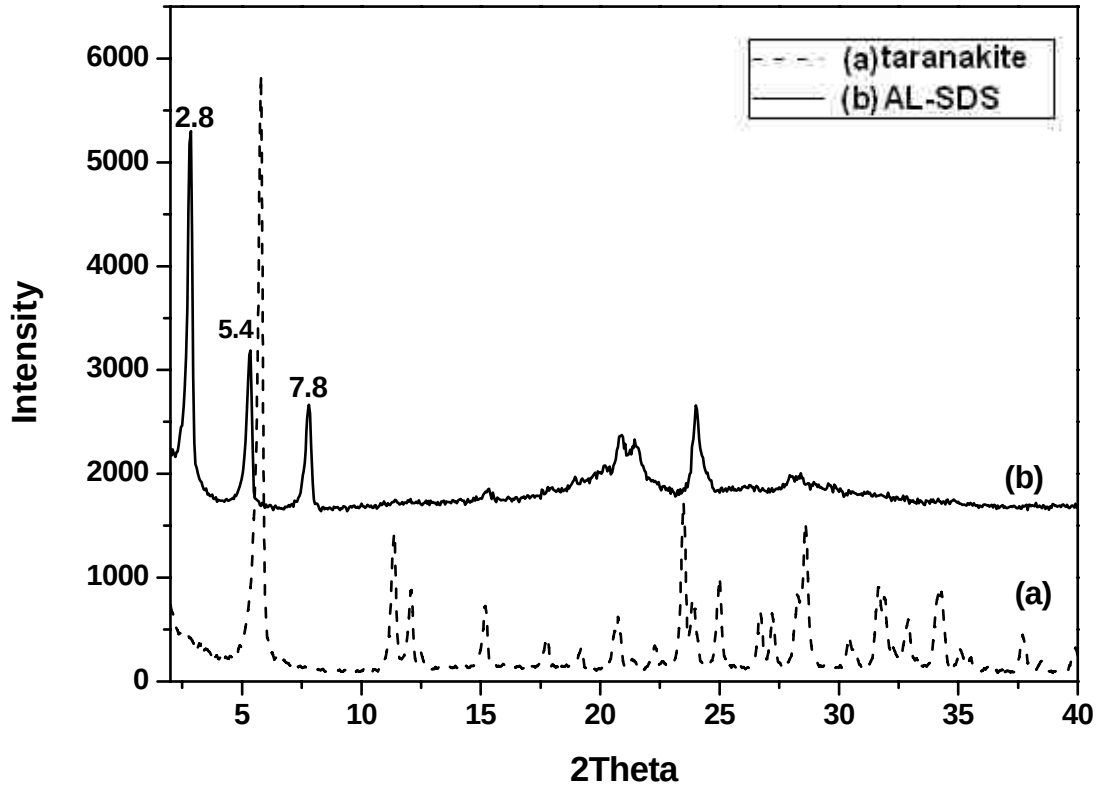

Figure 3.3 XRD pattern of AL-SDS (b) compared with pure taranakite (a)

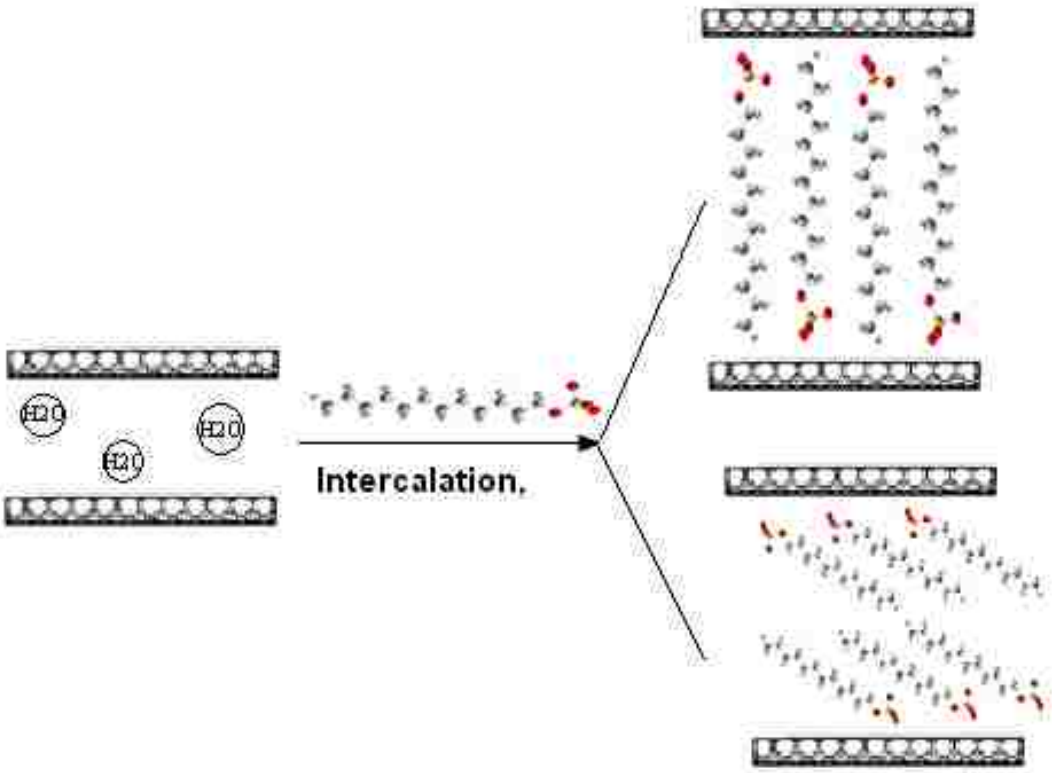

Figure 3.4 Modification process of taranakite by SDS

In the XRD, the first three 2θ values 5.65°, 11.25° and 12.0° are for (006), (00(12)) and (012) peaks of taranakite respectively. The d-spacing of taranakite was calculated by using the Bragg equation with the d_{006} peak to be 15.7 Å. Crystallite sizes in the c-axis dimension were estimated using the Scherrer equation:

$$\tau = \frac{\kappa\lambda}{\beta cos\theta} \qquad (1)$$

where τ is the crystallite size and κ is a constant (shape factor = 0.9 for powders), β is the full width at the half maximum (Full-Width Half-Maximum, FWHM) of the diffraction peak after correcting for instrumental broadening. The instrumental broadening was corrected by the silicon

111 peak at 28.4° where the FWHM of 111 peak of silicon was deducted from the FWHM of the sample's first peak. λ is the X-ray wavelength which is 1.54 Å for Cu-$\kappa_{\alpha 1}$. The 00ℓ (ℓ= 1, 2, 3…) peaks were used to estimate the average crystallite size, which is 29 nm for taranakite and 25 nm for AL-SDS. The layers stacked of taranakite and AL-SDS for one crystal could be calculated by the average c-axis crystallite size and d-spacing obtained from XRD, which are 12 layers stacked for ALP crystal and 8 layers for AL-SDS crystal.

3.1.2 Infrared spectrum of taranakite and AL-SDS

The infrared spectrum of taranakite is shown in Figure 3.5. The spectrum agrees with that reported by Sakae *et al*.[102] The phosphate absorption bands were observed from 876 to 1200 cm^{-1}, bands from 1100 to 1200 cm^{-1} were assigned as the stretching bands of P = O bond. The absorption bands of 1643 and 3063 cm^{-1} were from H_2O, while broad band at about 3372 cm^{-1} can be assigned to the stretching of water hydroxyl groups, suggesting that taranakite has adsorbed water molecules. FT-IR spectrum also confirmed the absence of other anions, such as nitrate and carbonate that normally appear at 1385 cm^{-1} and 1365 cm^{-1}, respectively.

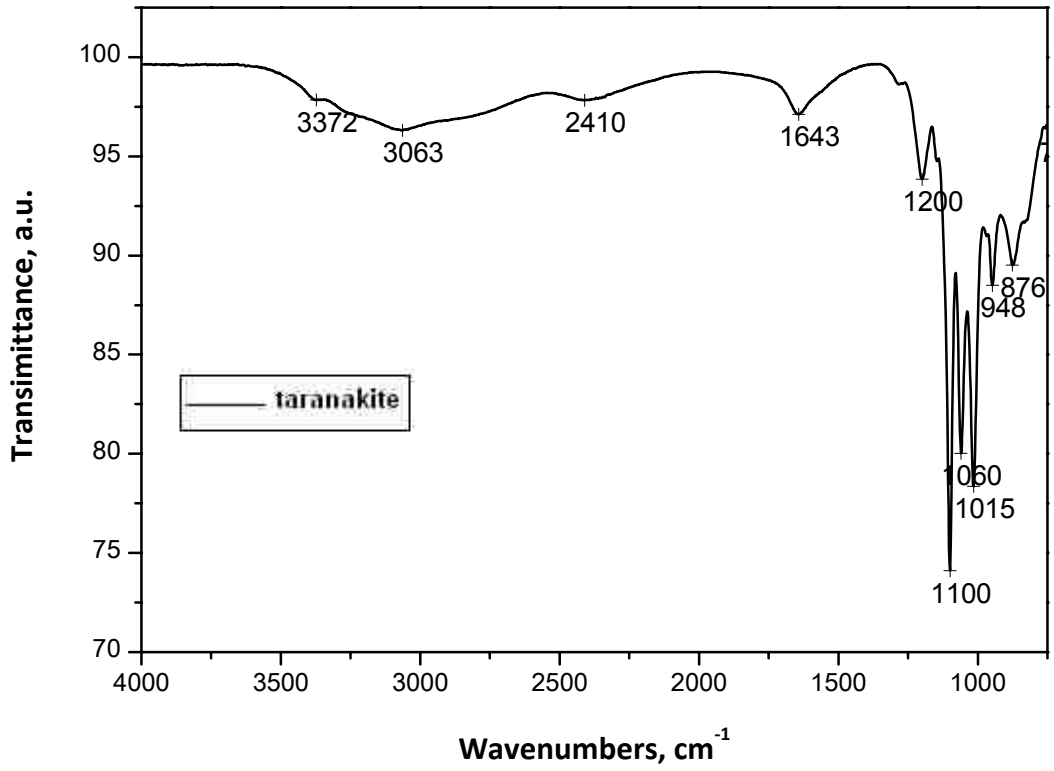

Figure 3.5 FTIR spectrum of taranakite

The FTIR spectrum of AL-SDS is shown in Figure 3.6, along with the taranakite and pure SDS spectra. After ion exchange, the phosphate absorption bands (876 to 1200 cm^{-1}) disappeared and S = O stretching bands appeared at 1210 cm^{-1} and 1047 cm^{-1}. The absorption band at 803 cm^{-1} is assigned as the S-O stretching band. The absorption bands of 2913 cm^{-1} and 2856 cm^{-1} are assigned as the C-H stretching bands of alkyl chain. The FTIR spectroscopy thus confirms the presence of dodecyl sulfate in AL-SDS.

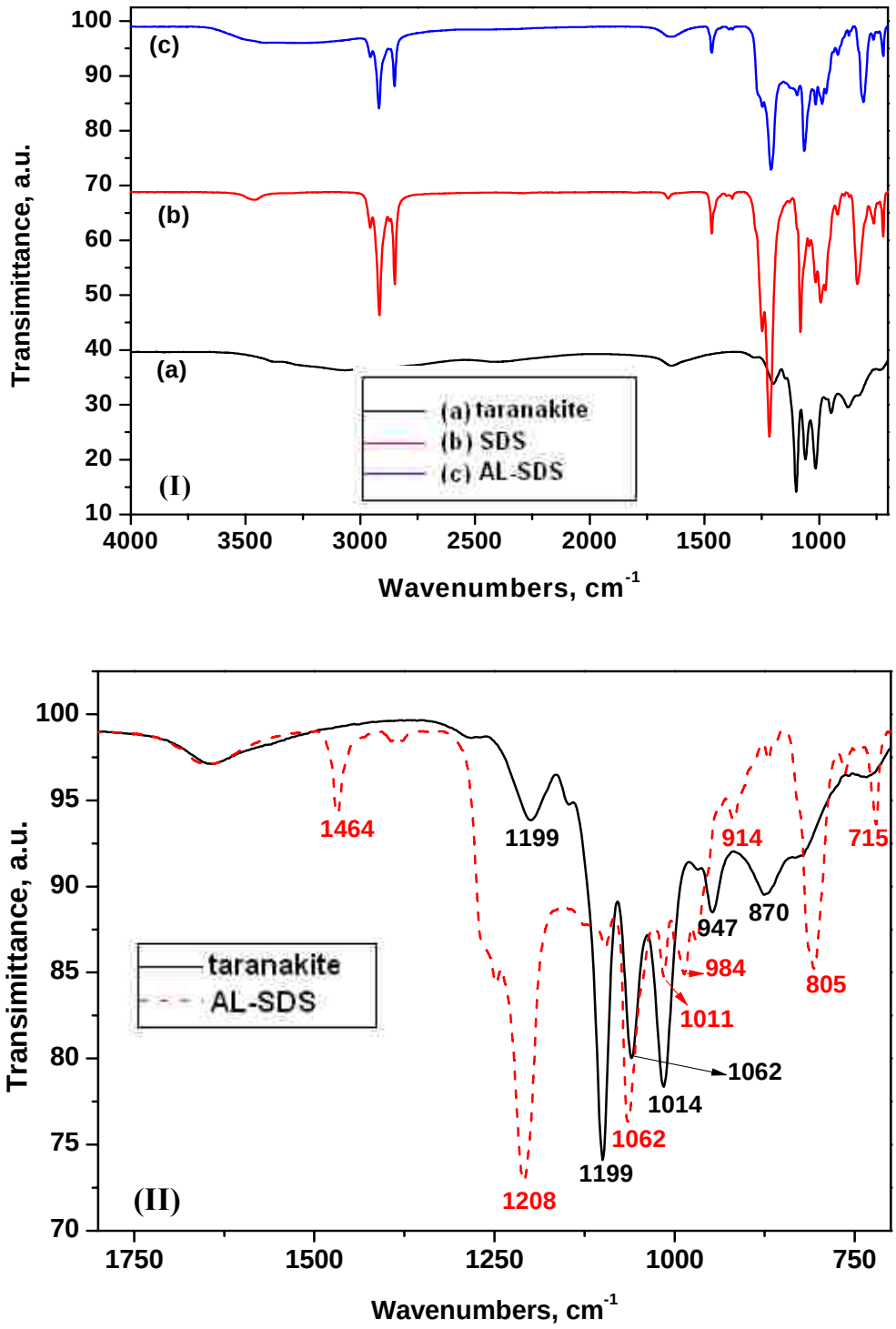

Figure 3.6 FTIR spectra of (I) AL-SDS (c) compared with taranakite (a) and SDS (b). (II) ALP overlaid with AL-SDS

3.2 Characterization of polymer/taranakite composites

The nature of polymer/taranakite composites was evaluated by monitoring the XRD data. The formation of an intercalated composite results in an extended basal spacing of the XRD pattern, while the formation of an exfoliated composite leads to the complete loss of registry between the layers and therefore no peak is observed. It is noted that the absence of a peak is not proof of exfoliation because the disappearance of peaks from the XRD trace could be due to various types of disorder.[103] The presence of an XRD peak at a lower 2θ indicates the formation of an intercalated structure, while the presence of a small, diffuse peak may suggest a mixed intercalated-disordered structure.

Figure 3.7 shows X-ray diffraction patterns of the PS, PP, PVA composites. The peaks for the composites at the lower 2θ disappeared for the PS and PP composites, which suggested that the taranakite and AL-SDS are disordered in some way. Figure 3.7(c) is the XRD of PVA/taranakite composite, and it shows the small, broad peaks which indicate an intercalation structure. When increasing the amount of taranakite to 5 wt%, there is a broad peak at 4.9° with a d-spacing of 18.01 Å, increased from 15.6 Å of pristine taranakite. The increase of d-spacing is consistent with intercalation of PVA molecules.

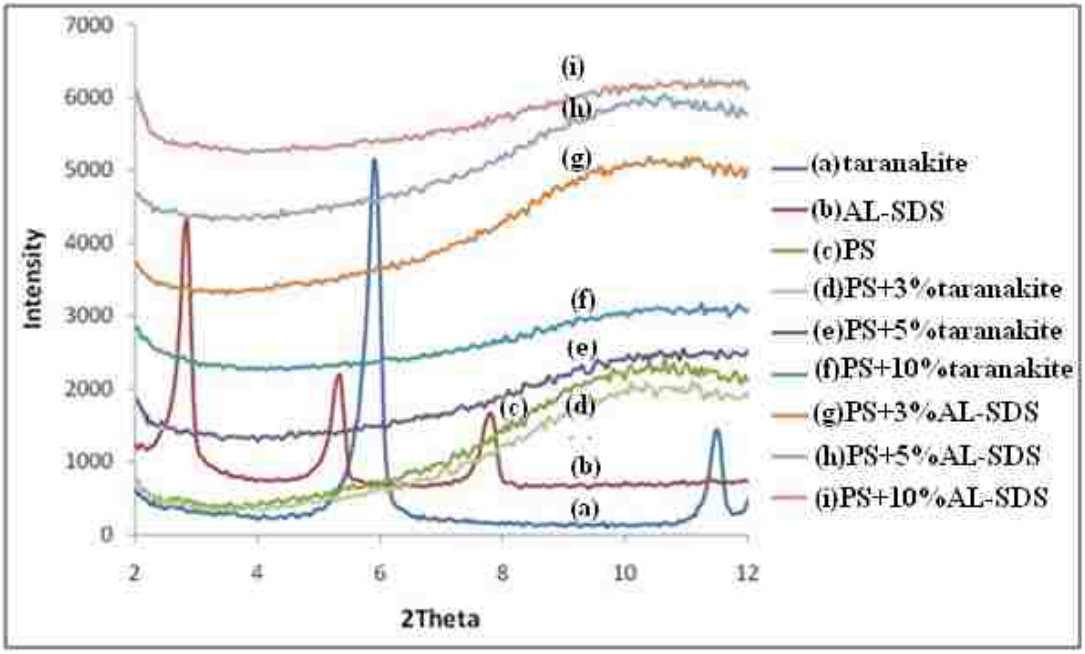
Intensity
2Theta
(a)taranakite
(b)AL-SDS
(c)PS
(d)PS+3%taranakite
(e)PS+5%taranakite
(f)PS+10%taranakite
(g)PS+3%AL-SDS
(h)PS+5%AL-SDS
(i)PS+10%AL-SDS

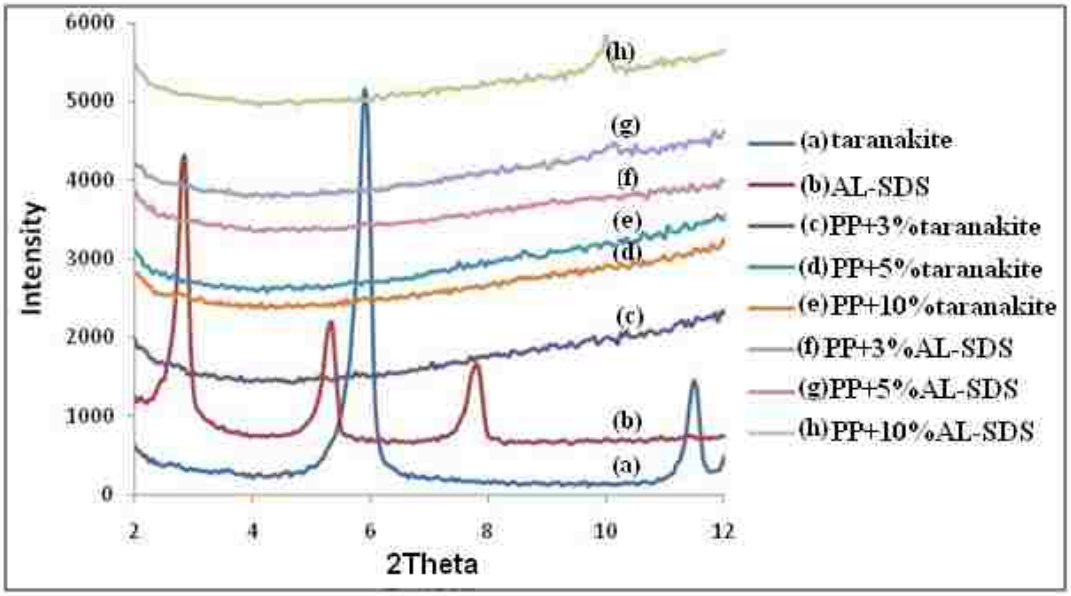
Intensity
2Theta
(a)taranakite
(b)AL-SDS
(c)PP+3%taranakite
(d)PP+5%taranakite
(e)PP+10%taranakite
(f)PP+3%AL-SDS
(g)PP+5%AL-SDS
(h)PP+10%AL-SDS

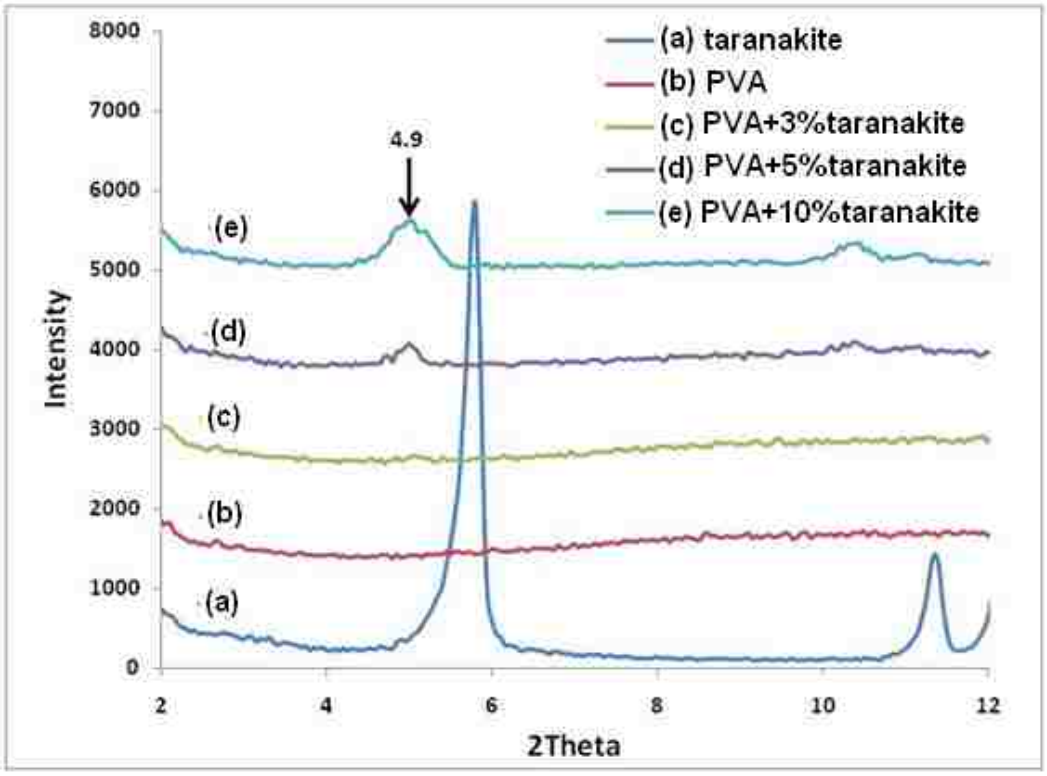

Figure 3.7 XRD spectra of PS (a), PP (b) and PVA (c) composites

3.3 Thermal stability of polymers/taranakite composites

The thermal decomposition of layered inorganic/organic hydrids is generally divided into three stages[104]: (I) dehydration of physiosorbed and intercalated water; (II) dehydroxylation and (III) oxidative degradation of the organic anions. Figure 3.8 below shows the thermogravimetric analysis curves for our sample of taranakite, which is same as the literature.[102] The DTA curve reveals three stages during the heating of taranakite. The first peak in the temperature region 80 °C to 100°C is assigned to the loss of intercalated water, while the second peak at 150 °C suggests the modification is due to a sluggish phase transformation. Then the residue tends to be constant after 200°C which is about 67.2% of the original weight. XRD was used to study the

residue at different temperatures. Figure 3.9 shows the XRD of taranakite after heating at different temperatures. The XRD data indicates that when the heating temperature is lower than 200°C, the taranakite shows the same structure with the original one. However, when the temperature is at 200°C, the taranakite loses its crystalline structure, which indicates that the decomposition happened at this temperature. The TG curve shows that loss weight is from the loss of intercalated water. This indicates that there are large amount of water at the interlayer of taranakite.

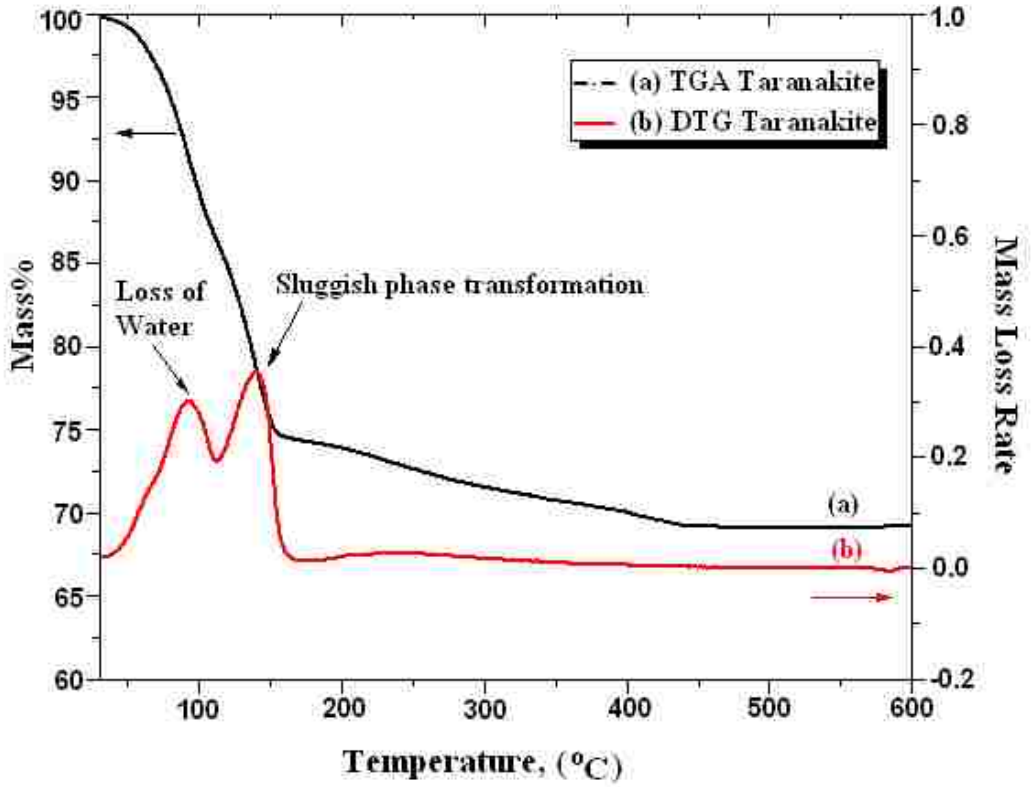

Figure 3.8 TGA and DTA curves of ALP

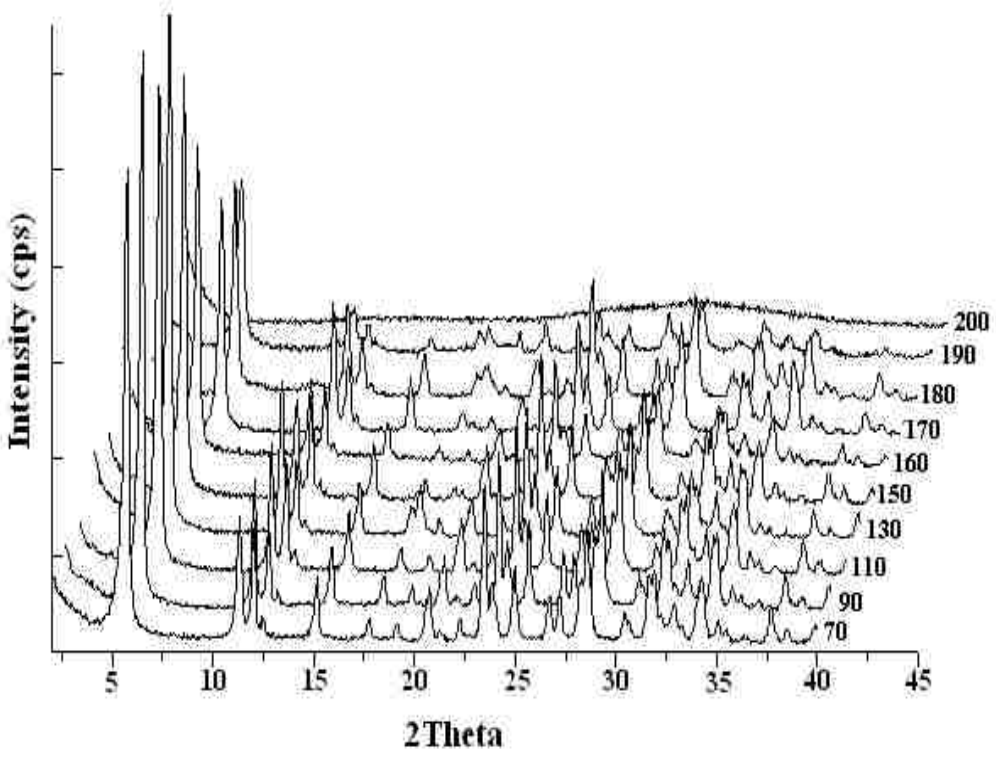

Figure 3.9 XRD of taranakite heated at different temperatures.

Figure 3.10 shows the thermogravimertic analysis traces of pure PS and its nanocomposites. The degradation of PS follows a single step and composites containing the taranakite or AL-SDS exhibit enhanced thermal stability. This is similar to behavior typically seen with montmorillonite (MMT) systems, where the addition of MMT brings about an increase in both $T_{0.1}$ and $T_{0.5}$, [105-107] but unlike some layered double hydroxides (LDH) which the $T_{0.1}$ and $T_{0.5}$ decrease with added LDH.[96] The onset degradation temperature (temperature at 10% mass loss, $T_{0.1}$) is increased by 5-15 °C for all loading composites. The mid-point temperature ($T_{0.5}$) is also increased compared to the pure polymer by 4-16 °C for the composites. Based on the fraction of non-volatiles taranakite and AL-SDS, one expects to obtain between 2 - 7 wt% residues in these composites and the experimental amount is in this range (2.1- 6.7 wt%), which indicates that all residues are due only to the presence of the additive. Table 3.2 is the summary of the $T_{0.1}$ and $T_{0.5}$

of PS composites with different taranakite and AL-SDS loading. The data indicates that there is no significant difference between the taranakite and AL-SDS. The expected char% and experimental char% are compared in the table. The expected char% is the sum of taranakite char% calculated from TGA and pure PS char%. And the experimental char% is the collected data from the TG instrument. These two data are similar as showed in the table, which indicates the complete degradation of PS during the heating.

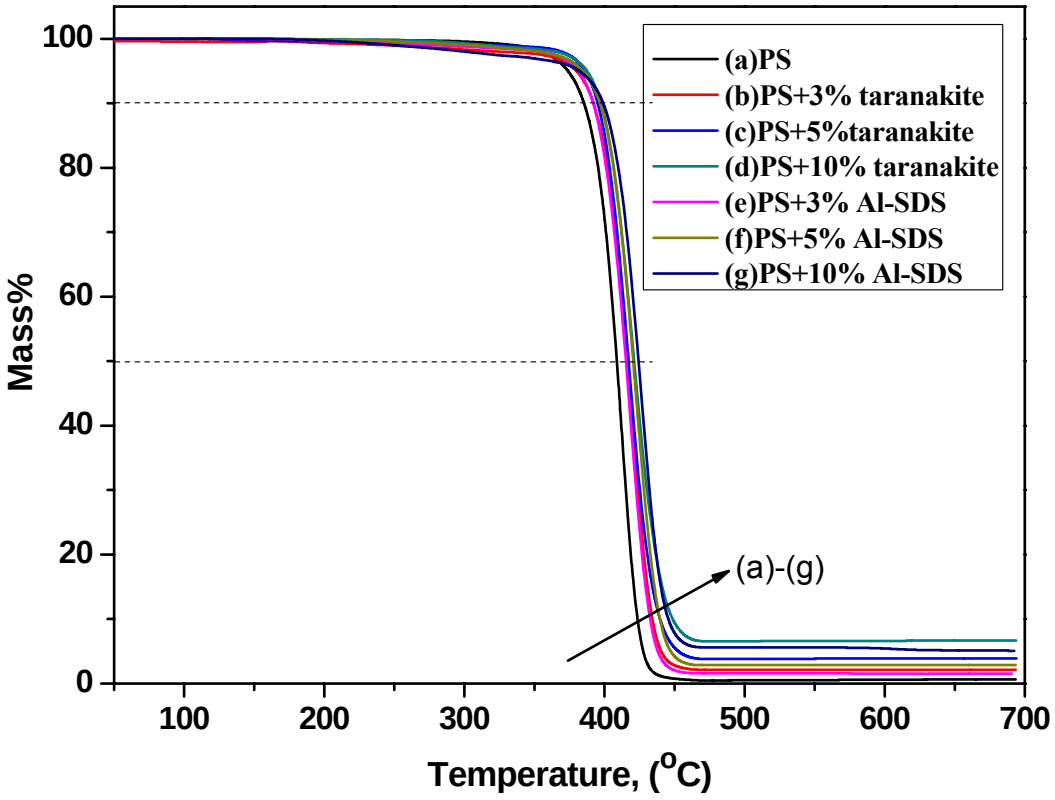

Figure 3.10 TGA curves of PS composites

Table 3.2 TGA summary results for PS and its composites

Formulation	$T_{0.1}$	$T_{0.5}$	Experimental Char (%)	Expected Char (%)
Pure PS	385 ± 1	408 ± 1	0.6 ± 0.2	NA
PS+3% taranakite	390 ± 2	412 ± 3	2.1± 0.3	2.5
PS+5% taranakite	395 ± 3	416 ± 3	3.9 ± 0.3	4.0
PS+10% taranakite	397 ± 2	421 ± 2	6.7 ± 0.1	7.0
PS+3%AL-SDS	392 ± 3	415 ± 1	1.5 ± 0.4	1.8
PS+5%AL-SDS	396 ± 2	420 ± 2	2.8 ± 0.2	2.6
PS+10%AL-SDS	399 ± 1	424 ± 3	5.1 ± 0.1	4.6

Figure 3.11 shows the TGA curves of PP and its composites. The degradation of PP also follows a single step, and the loading of taranakite or AL-SDS increases the onset temperature and mid-point temperature. Table 3.3 is the summary of TGA results. The data show that the onset temperature of polymer composites increase by the increasing loading of taranakite, and at the loading of 10 wt%, the $T_{0.1}$ increased by 12°C which is a significant improvement for the heat stability of PP, while usually there is a decrease with LDH as additive.[117] The onset temperature temperature of PP/AL-SDS remains constant or exhibits a slight decrease compared to pure PP, while the PP/taranakite exhibits an increase in $T_{0.1}$. The reason for this may possibly be the lower heat stability of SDS. The comparison of expected char% with experimental char% indicates the complete degradation of PP for all compositions.

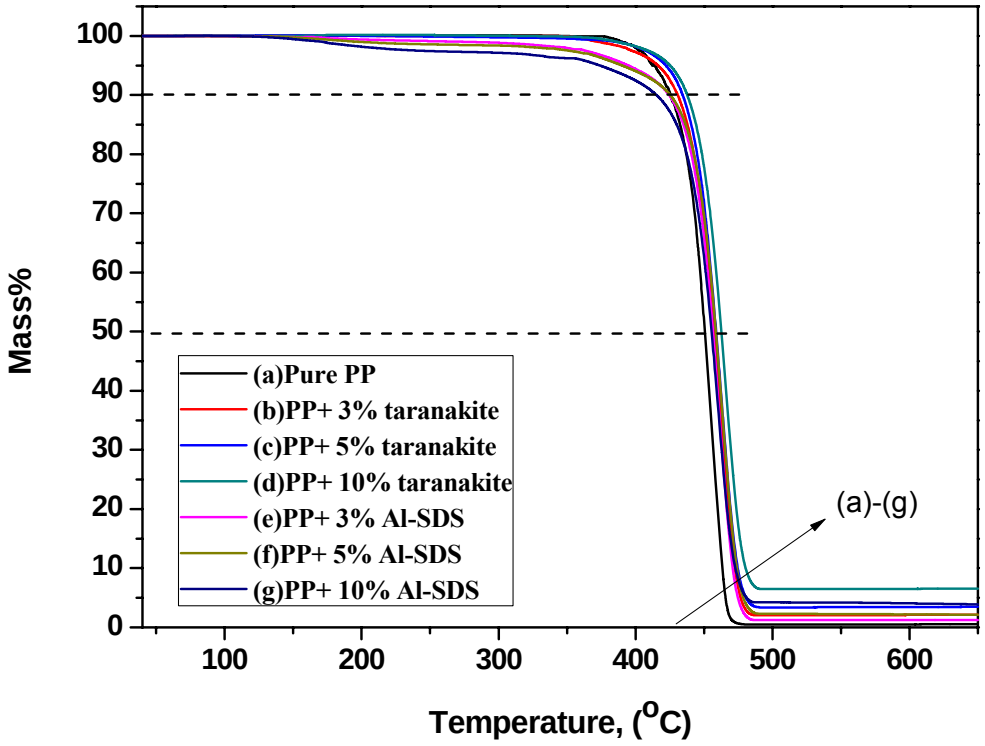

Figure 3.11 TGA curves of PP and its composites

Table 3.3 TGA summary results for PP and composites

Formulation	$T_{0.1}$	$T_{0.5}$	Experimental Char (%)	Expected Char (%)
Pure PP	425 ± 1	450 ± 1	0.2 ± 0.1	NA
PP+3% taranakite	430 ±2	457 ± 2	2.2 ± 0.3	2.2
PP+5% taranakite	434 ± 2	459 ± 1	3.4 ± 0.2	3.8
PP+10% taranakite	437 ± 2	463 ± 2	6.5 ± 0.0	6.7
PP+3%AL-SDS	424 ± 3	456 ± 2	1.2 ± 0.2	1.4
PP+5%AL-SDS	425 ± 2	459 ± 3	2.3 ± 0.1	2.2
PP+10%AL-SDS	415 ± 3	456 ± 3	4.5 ± 0.4	4.2

Figure 3.12 shows the TGA curves of PVA and its composites. Unlike PS and PP, PVA is a polar copolymer. Polar polymers typically are expected to exhibit a better compatibility

with polar layered materials than non-polar polymers such as PS and PP. The degradation of PVA is reported to be a two step degradation mechanism.[108] The first step, at a temperature around 300°C, is the elimination of water and residue acetate groups, since a large number of acetate groups remain in the PVA chains due to the incomplete hydrolysis. This process is shown in Figure 3.13 (Scheme 1).[108] The second step, at the temperature of approximated 430 °C, is dominated by chain-scission reactions, side-reactions and cyclization reactions. An early weight loss process in the temperature range 100–140 °C is attributed to the loss of absorbed water, and is not counted as an additional step. The two-step degradation is shown by DTA curves in the Figure 3.12.

The TGA curves show that the PVA/taranakite composites exhibit a significantly improved thermal stability Unlike the other layered material additives (such as α-zirconium phosphate) that lower the degradation temperature of PVA at the first step,[109] degradation temperatures of PVA/taranakite composite are markedly higher, especially when the content is 10 wt% (increased by 31°C). The temperature for the second step of PVA degradation increased even more with the taranakite additives; it increased by 65°C with a 10 wt % loading. All composites exhibit thus enhanced thermal stability. The table 3.4 contains a summary of the parameters collected from TGA. The experimental char% data are almost same as predicted, indicating complete degradation of PVA.

Similar to the pure PVA, the thermal degradation of the PVA/taranakite composite can be regarded as two-step degradation. The mechanism of improvement of thermal stability of PVA by adding taranakite could be due to the formation of hydrogen bonding by OH group in PVA and the phosphate ions between the taranakite layers. This may impede the first step of degradation, as shown in Figure 3.13 (Scheme 2).

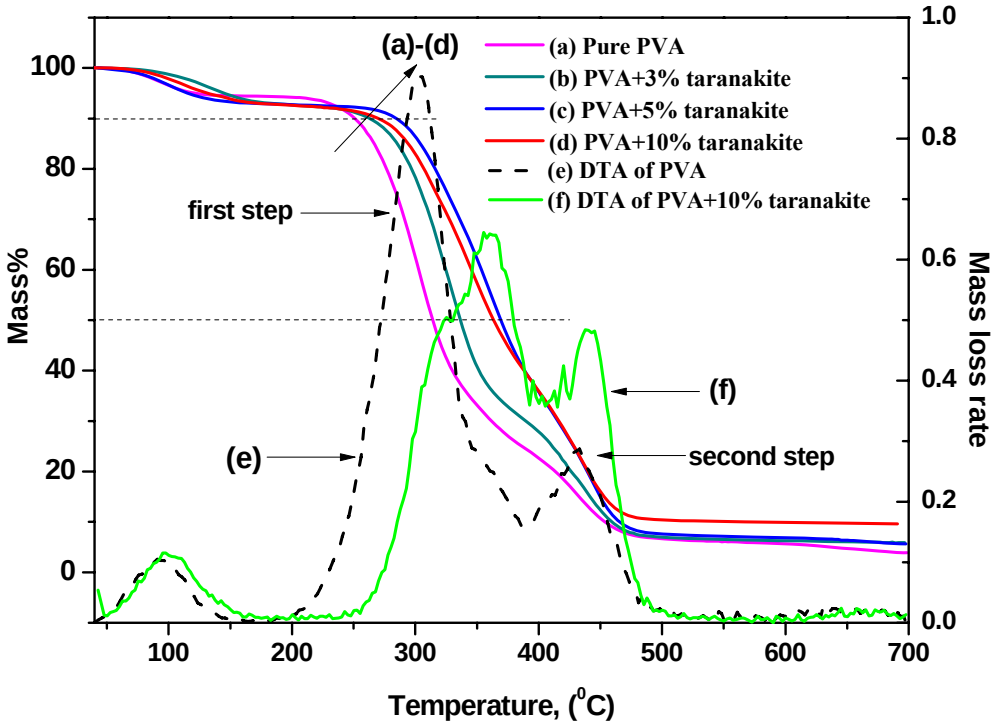

Figure 3.12 TGA and DTA curves of PVA and its composites

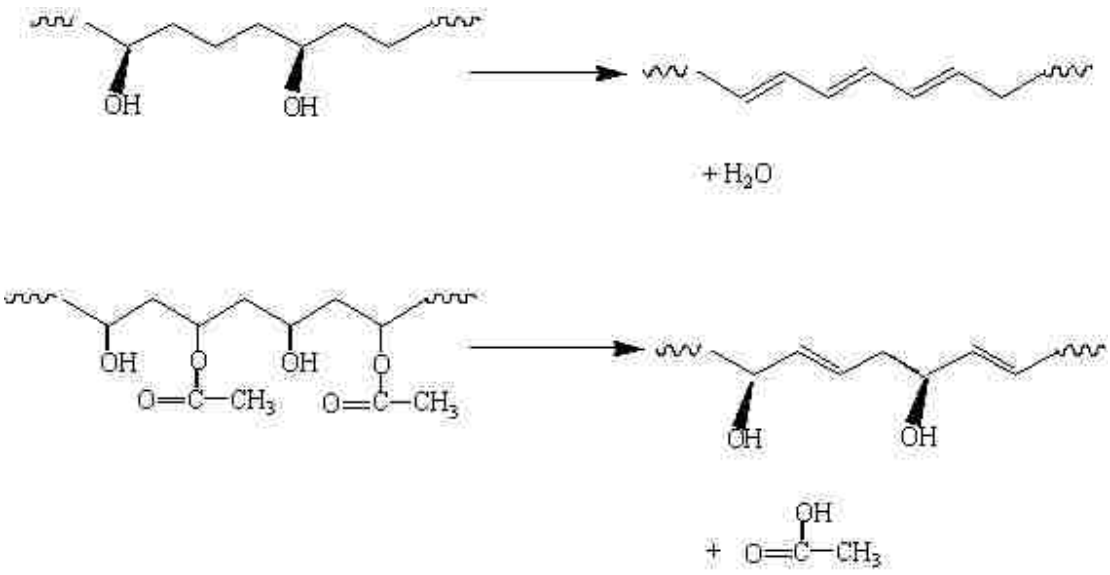

Scheme 1 Dehydration and eliminations of residue acetate groups

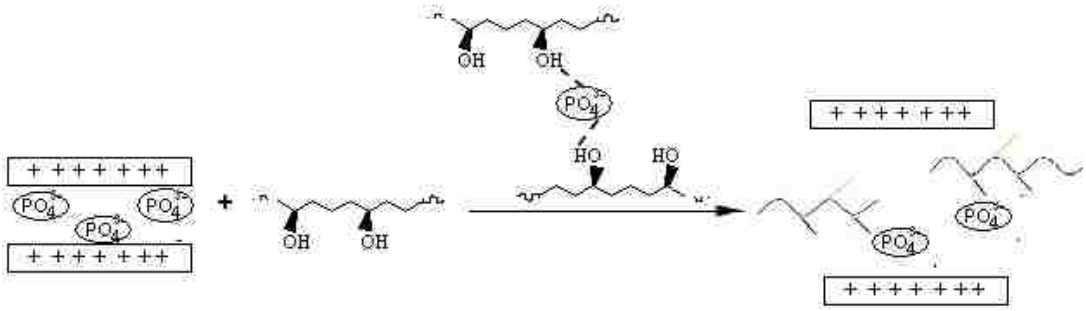

Scheme 2 Hydrogen bond formation process in the first step

Figure 3.13 Two steps of the decomposition of PVA

Table 3.4 TGA results summary for PVA nanocomposites

Formulation	$T_{0.1}$	$T_{0.5}$	Experimental Char (%)	Expected Char (%)
PVA	257 ± 3	313 ± 3	4.0 ± 0.2	NA
PVA+3%taranakite	264 ± 2	337 ± 1	6.3 ± 0.3	6.0
PVA+5%taranakite	285 ± 2	367 ± 2	6.9 ± 0.1	7.3
PVA+10%taranakite	288 ± 3	378 ± 3	9.7 ± 0.2	10.0

3.4 Fire retardancy of the nanocomposites

Cone calorimetry is one of the most efficient methods to evaluate the flammability performance of polymeric materials.[110] The peak heat release rate (PHRR) reduction is usually considered to be the most important.[111]

Table 3.2-3.3 contain summaries of cone data results for the fire properties of PS, PP with taranakite and AL-SDS, measured at a heat flux 35 kW/m^2. As shown in the Table 3.2 and

Figure 3.10, the presence of taranakite reduces the PHRR significantly in PS, while the presence of AL-SDS has less effect on the PHRR.

Based on work with MMT, a small PHRR reduction or no reduction is usually associated with microcomposite formation while a larger PHRR reduction may associate with the formation of nanocomposites.[112] In general, the polar layered materials (such as layered double hydroxides or clays) without organic modification are less compatible with the non-polar polymers such as PS and PP, which will results microcomposite formation. In this case, the fire properties of these types of polymer do not exhibit significant improvement. However, in contrast to other layered materials, taranakite with PS exhibits significant improvement on PHRR reduction that increases with the loading of taranakite. The smoke, as measured by the ASEA, increased for all the composites with taranakite and the time to ignition (t_{ig}) was reduced; the lowering of the t_{ig} may be attributed to a decrease in the specific heat capacity.[113] No significant change in total heat release (THR) was observed for PS and PP, this is expected based upon the previous work with MMT.[114] The reason the composites with AL-SDS as an additive show less improvement on PHRR of polymers might be the low thermal stability of SDS.

The effect of taranakite on polymer flammability can be considered as due to the following reason:

At the temperature higher than 200 °C, the phosphate ions produced by decomposition of taranakite could react with the polymer to form ester by the mechanism similar to that reported by Kishore *et al* in 1981. The flame retardant effect of phosphorus compounds involves the phosphate ions acting mainly in the condensed phase via a char formation mechanism. The phosphate groups link to the polymer chain by ester groups which are readily eliminated forming conjugated double bonds, and finally give the char.[115] Figure 3.16 shows the process of the

degradation of PS with the phosphate additive. The mechanism can be classified into five important stages, (i) hydroperoxide formation; (ii) decomposition of the hydroperoxide; (iii) ester formation with phosphoric acid; (iv) dehydration of the ester, forming double bonds; and (v) char formation of the unsaturated substrate.[115] For PS/taranakite composite, the taranakite already decomposes during mixing with PS in the Brabender mixer at 200 °C, so the fire retardancy effect on PS only at the third step which is the formation of ester.

Table 3.5 Cone calorimetric data for PS, PS/ ALP, and PS/AL-SDS

Formula	PHRR (kW/m^2)	PHRR Reduc. (%)	THR (mJ/m^2)	AMLR ($g/s\ m^2$)	ASEA (m^2/kg)	t_{ig} (s)
Pure PS	1557 ± 44	NA	98 ± 7	34 ± 10	784 ± 55	38 ± 2
PS+3%taranakite	1412 ± 65	9	93 ± 9	25 ± 2	913 ± 59	28 ± 2
PS+5%taranakite	1342 ± 47	14	111 ± 5	25 ± 2	907 ± 27	26 ± 1
PS+10%taranakite	1168 ± 51	25	102 ± 5	27 ± 1	1006 ± 17	19 ± 1
PS+3%AL-SDS	1528 ± 47	2	105 ± 3	33 ± 1	880 ± 23	30 ± 2
PS+5%AL-SDS	1489 ± 45	4	105 ± 4	30 ± 2	962 ± 28	27 ± 2
PS+10%AL-SDS	1475 ± 60	5	102 ± 11	28 ± 4	1013 ± 64	18 ± 2

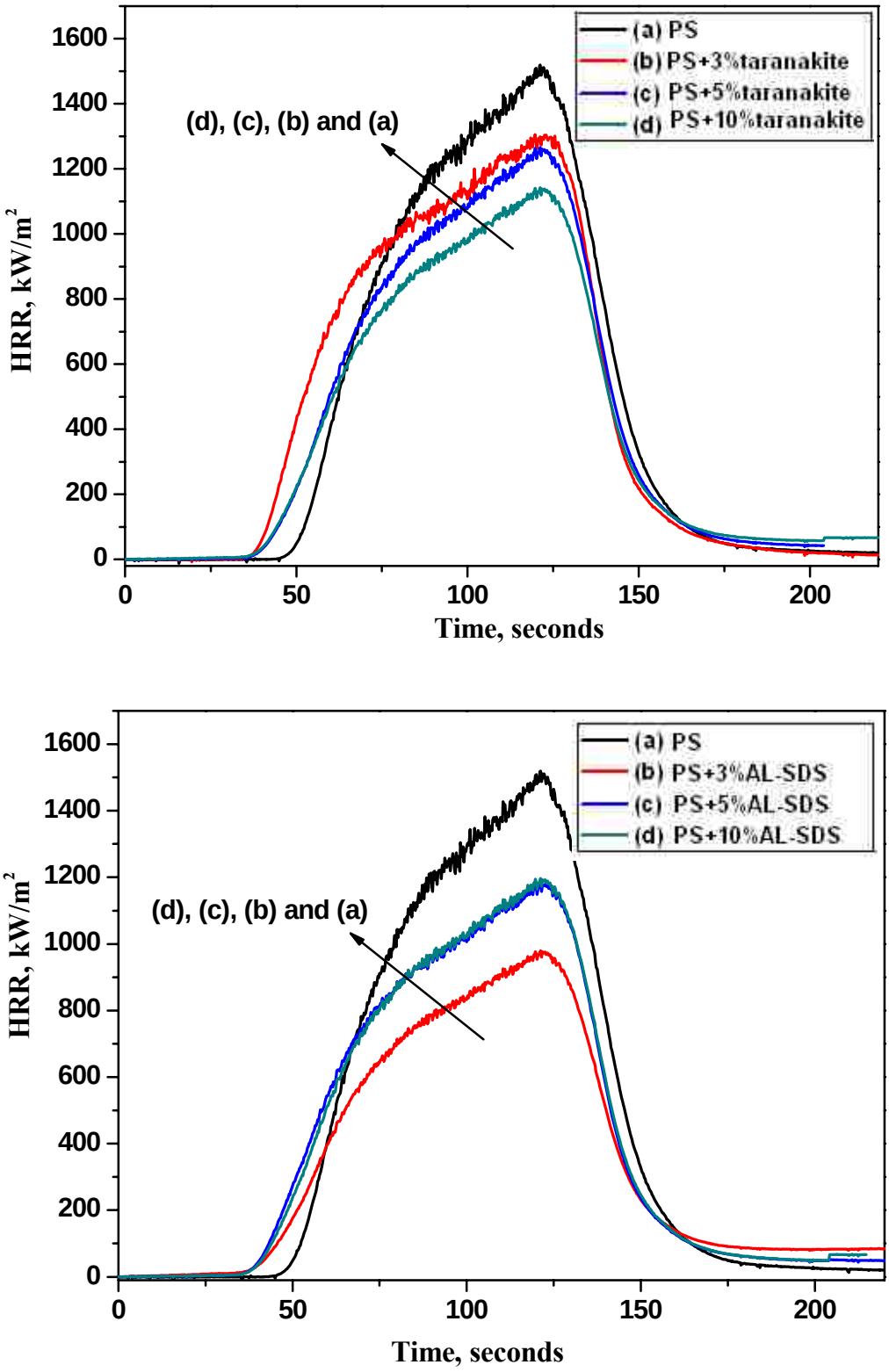

Figure 3.14 HRR curves for PS/taranakite and PS/A-SDS

Table 3.6 Cone calorimetric data for PP, PP/taranakite and PP/AL-SDS

	PHRR (kW/m^2)	Reduction (%)	THR (mJ/m^2)	AMLR (g/s m^2)	ASEA (m^2/kg)	t_{ig} (s)
Pure PP	1726 ± 29	NA	99 ± 7	34 ± 1	361 ± 5	30 ± 6
PP+3%taranakite	1564 ± 46	9	93 ± 8	25 ± 2	425 ± 8	29 ± 2
PP+5%taranakite	1462 ± 58	15	107 ± 10	25 ± 3	439 ± 11	26 ± 4
PP+10%taranakite	1395 ± 46	19	104 ± 8	27 ± 4	402 ± 6	23 ± 1
PP+3%AL-SDS	1644 ±50	5	95 ± 15	33 ± 4	357 ± 29	33 ± 3
PP+5%AL-SDS	1542 ±20	10	94 ± 20	30 ± 8	414 ± 8	32 ± 1
PP+10%AL -SDS	1486 ± 20	14	102 ± 11	28 ± 3	411 ± 5	27 ± 2

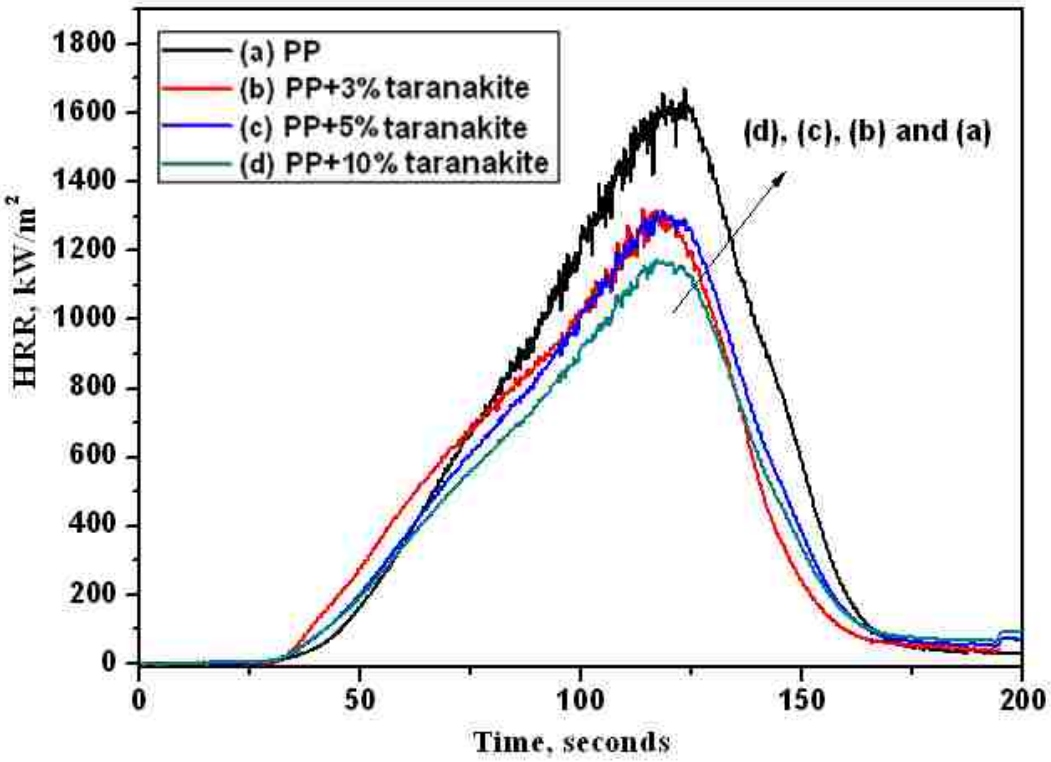

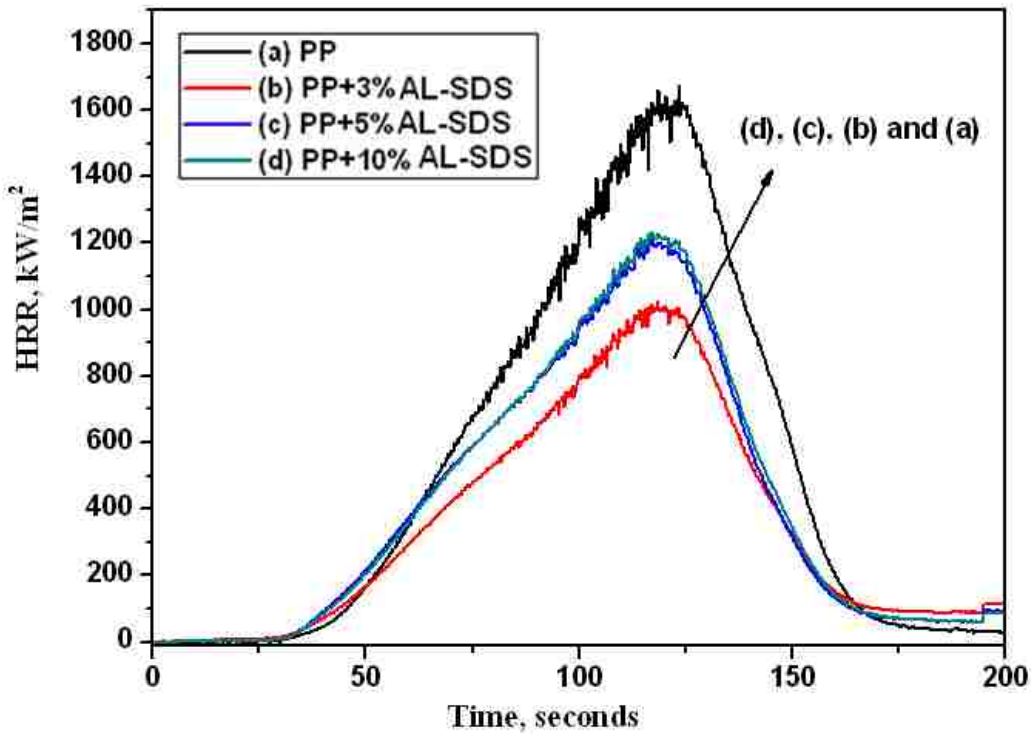

Figure 3.15 HRR curves for PP/taranakite (i) and PP/AL-SDS (ii)

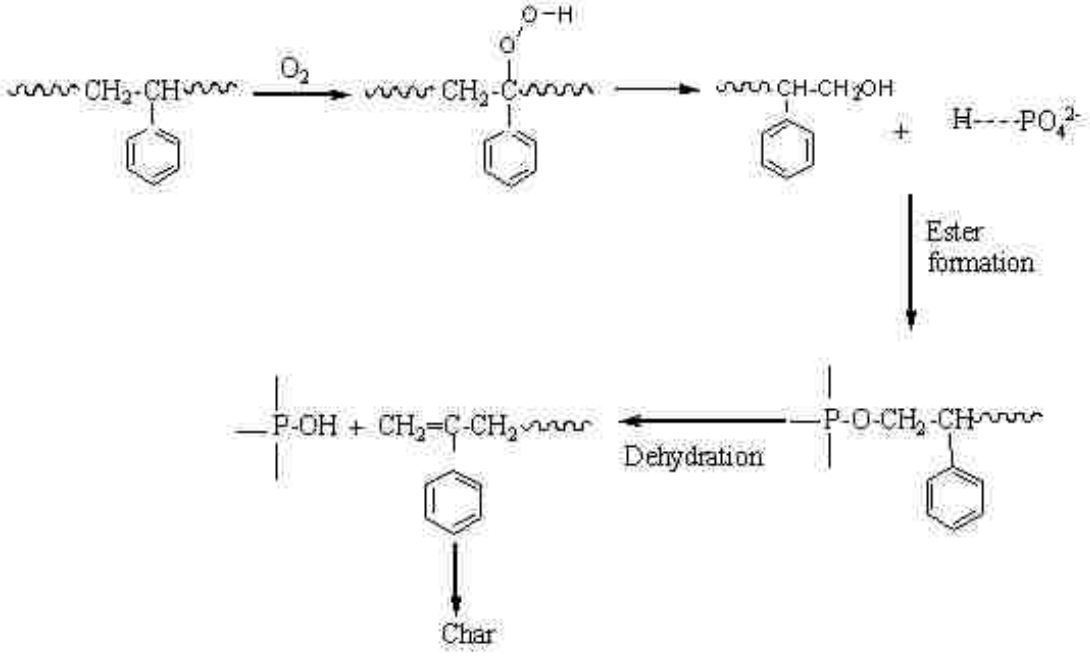

Figure 3.16 The schematic fire retardancy effect of phosphate on the degradation of Polystyrene

For the PVA system, it was difficult to prepare the standard plaques for the cone tests. The micro-combustion calorimeter (MCC) was employed to assess the flammability performance of its nanocomposites, since only a small amount (less than 5 mg) of the sample is needed. By measuring the heat of combustion of pyrolysis products, the primary parameters, peak heat release rate (PHRR), heat release capacity (HRC), total heat released (THR) and temperature at PHRR (T_p), can be acquired. In particular, HRC and PHRR are used to screen the flammability of the samples.

The results of MCC experiment listed in Table 3.7 clearly show that the THR, HRC and PHRR (the first peak of heat release rate) decrease significantly as the taranakite additive increases. The change of the char yields in the MCC exhibits the same tendency as in the TGA, indicating complete loss of PVA.

Table 3.7 Cone calorimetric data for PVA and PVA/ taranakite

	Peak HRR (W/g)	PHRR Reduction (%)	Temp. of PHRR (°C)	HR Capacity (J/g-k)	Total HR (kJ/g)	Char (%)
PVA	194 ± 3	0	347 ± 1	194 ± 4	18 ± 0.2	4.0 ± 0.1
PVA+3%taranakite	166 ± 3	14	347 ± 8	186 ± 3	17 ± 0.2	4.6 ± 0.7
PVA+5%taranakite	146 ± 8	25	399 ± 3	146 ± 5	17 ± 0.5	5.3 ± 0.6
PVA+10%taranakite	138 ± 5	30	393 ± 2	138 ± 4	16 ± 0.1	7.6 ± 0.5

Figure 3.17 shows the influence of taranakite on the heat release rate (HRR) in the MCC comparison with the mass loss rate (MLR) in differential thermal analysis (DTA) (DTA is the first derivative of TGA data). The HRR curve of pure PVA shows features similar to the DTA, but the HRR peaks shift to higher temperature due to the higher heating rate (60 °C /min for

MCC vs 10 °C /min for DTA). Figure 3.17 further compares the changes of the maximum mass loss rate (MMLR) of the PVA/taranakite nanocomposites in the first stage and the first peak of HRR-MCC. These two curves show similar trends in that the MMLR and HRR decrease with increasing taranakite content, and two factors decrease sharply with the loading from 0-5%, while the loading from 5%-10%, the effects of taranakite on PVA tends to be less. The decreased MMLR at a lower loading of taranakite may be attributed to the taranakite nanoplatelets slowing the volatilization of degradation products. With an increased loading, there is a competition between the segregation effect of taranakite nanoplatelets and the catalytic degradation of PVA.[109] The stacked taranakite nano-layers cannot efficiently work as a mass transport barrier to suppress the volatilization and lead to a weak effect on MMLR.

Table 3.8 is the summary of PHRR, T_p and MMLR, T_m with different taranakite amounts for two steps of degradation of PVA. At the first step (Step I) of degradation, the presence of taranakite composites lowers the PHRR and MMLR both, and increases the T_p and T_m significantly. Then at the second step, the PHRR and MMLR increase with the increasing loading of taranakite, opposite of what is observed for the first step. The significant PHRR reduction on the first step degradation of PVA nanocomposites (shows in Table 3.8) is consistent with the formation of hydrogen bonding between phosphate ions and O-H group in PVA as the main reason for its thermal stability.

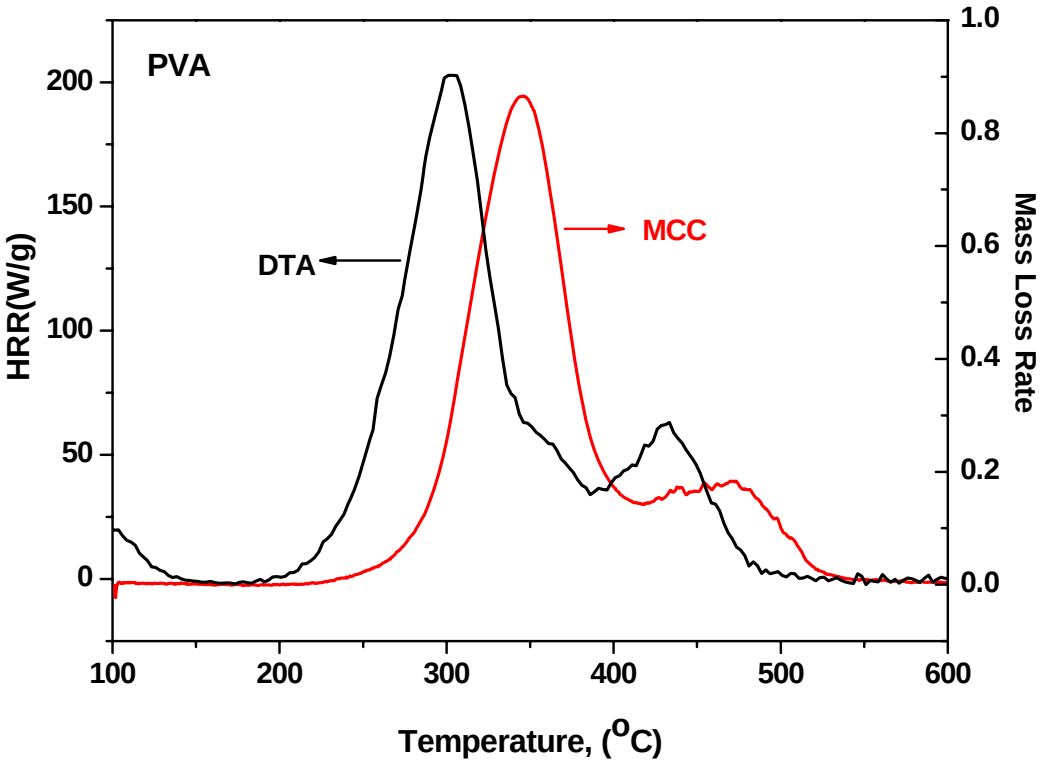
PVA
DTA
MCC
HRR(W/g)
Mass Loss Rate
Temperature, (°C)
0
50
100
150
200
0.0
0.2
0.4
0.6
0.8
1.0
100
200
300
400
500
600

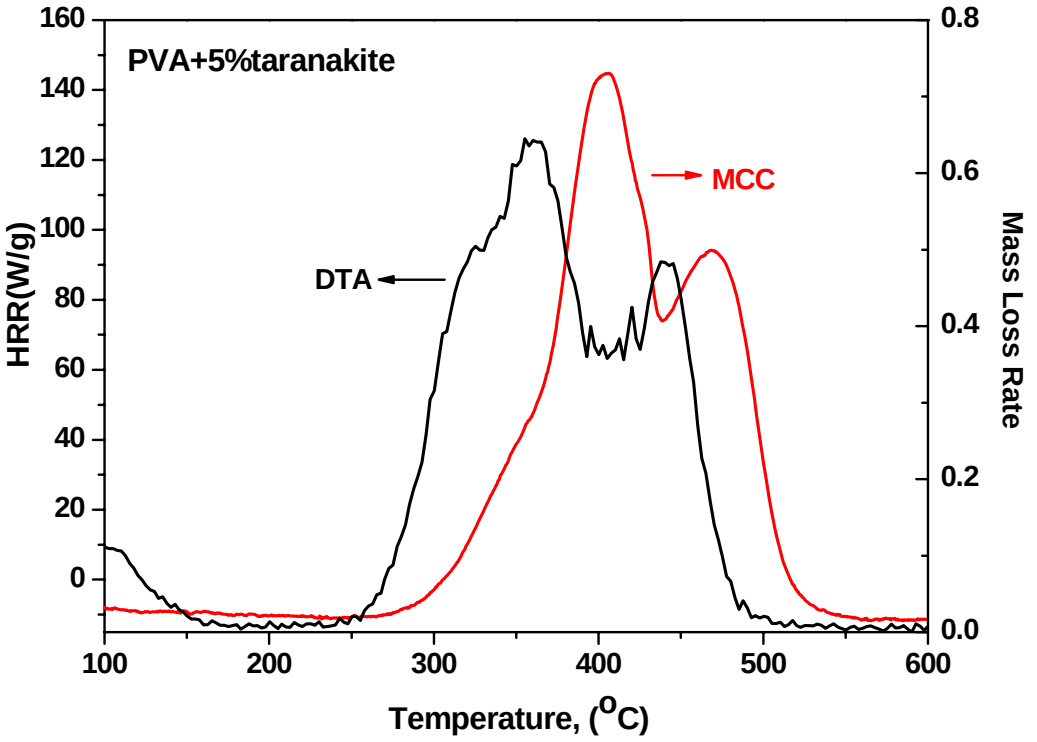
PVA+5%taranakite
DTA
MCC
HRR(W/g)
Mass Loss Rate
Temperature, (°C)
0
20
40
60
80
100
120
140
160
0.0
0.2
0.4
0.6
0.8
100
200
300
400
500
600

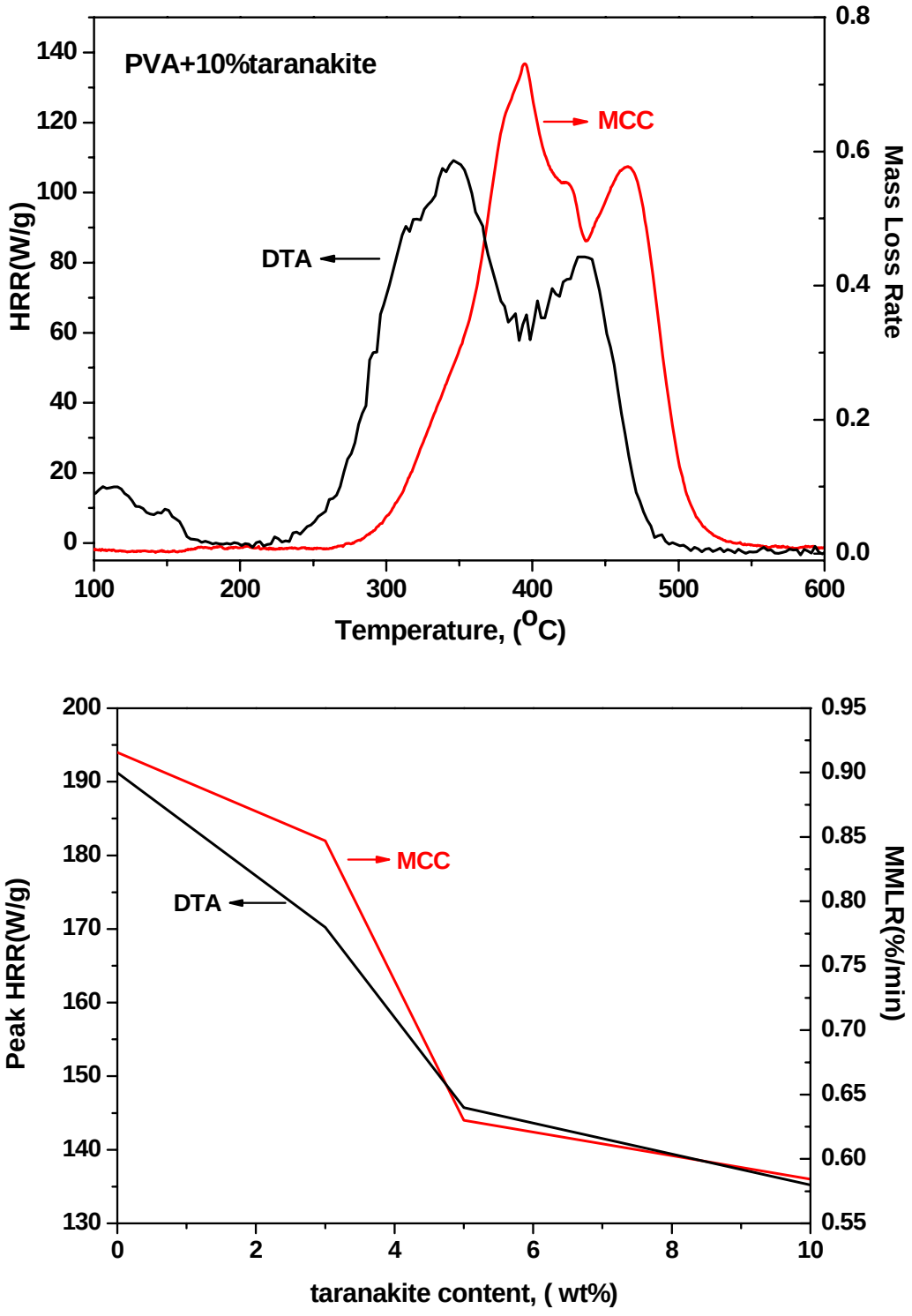

Figure 3.17 MCC and DTA curves for PVA and PVA/taranakite nanocomposites, and the changes of MMLR and the first peak HRR-MCC with increasing taranakite content

Table 3.8 The summary of PHRR, MMLR, T_P, and T_m of PVA and its composites at two steps

Degradation process	Contents (wt%)	MCC			DTA	
		PHRR (W/g)	PHRR Reduction (%)	T_P (°C)	MMLR (%/min)	T_P (°C)
Step I	Pure PVA	203	NA	303	0.90	304
	3%	182	10.3%	352	0.78	350
	5%	144	29.0%	404	0.64	359
	10%	136	33.0%	397	0.58	347
Step II	Pure PVA	39	NA	468	0.28	432
	3%	54	-38.5%	477	0.39	439
	5%	94	-141%	470	0.48	442
	10%	107	-174%	467	0.44	434

3.5 Char information after cone calorimetry

Figure 3.18 shows the photographs of the residue that remains after cone calorimetry experiments. For pure PS and PP, there is almost no residue after burning, while with the samples that include taranakite or AL-SDS as additives, there is more residue covering a larger area of the sample pan. The distribution of residue in the pictures suggests that the PP/AL-SDS system has a better dispersion than taranakite system which shows some cluster in the residue. This may be because PS and PP are non polar polymers which are not expected to disperse the polar taranakite additive as would be the case for an SDS-modified additive.[116]

100% PS

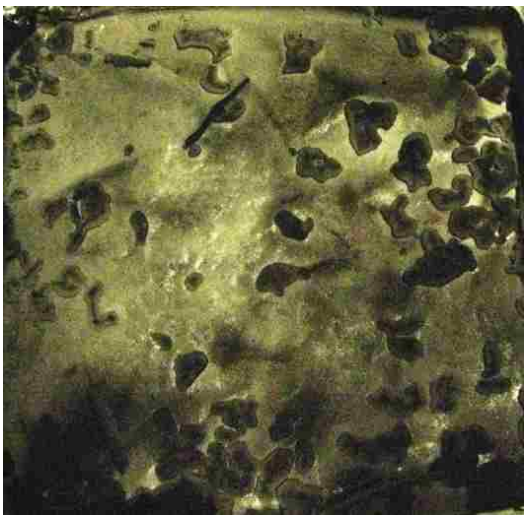

90%PS +10% taranakite

90%PS +10% AL-SDS

100% PP

90%PP+10% taranakite

90%PP+10%AL-SDS

Figure 3.18 The photographs of residues of polymer/taranakite or polymer/AL-SDS composites

Figure 3.19 contains the FTIR spectra of the residues of PP with taranakite and AL-SDS composites. The spectra band of PP/taranakite composites at 1117 cm^{-1} is P=O stretching frequency, while the band at 932 cm^{-1} is Al-O stretching frequency and the band at 770 cm^{-1} is Al-O-P stretching mode. At the 10% taranakite loading, the spectrum shows bands at

approximately 2950 cm^{-1}, assigned as C-H stretching modes, and bands at 1464 cm^{-1} and 1383 cm^{-1}, which are C-H bending modes. The bands observed in the PP/AL-SDS composite residues at 1078 cm^{-1} is S=O stretching mode, while the band at 700 cm^{-1} is S-O stretching frequency. At the 5% and 10% AL-SDS loadings, the IR spectra of residues also show the C-H stretching bands and C-H bending bands.

Figure 3.20 are the FTIR spectra of the residues of the composites of PS, with taranakite and AL-SDS. At the 3% and 5% taranakite loadings, the spectra only show the P=O, Al-O stretching modes which are same with PP composites, while at the 10% loading, the spectrum also shows the C-H stretching and bending frequencies. The spectra of PS/AL-SDS composites with different AL-SDS loading show the same bands which are S=O and S-O stretching modes.

The FTIR spectra of PP, PS composites all show the C-H strectching and bending modes at the 10% loading of taranakite, which indicates the incomplete combustion of the polymers. However, at the 3% and 5% taranakite loadings, the residues are only from the taranakite.

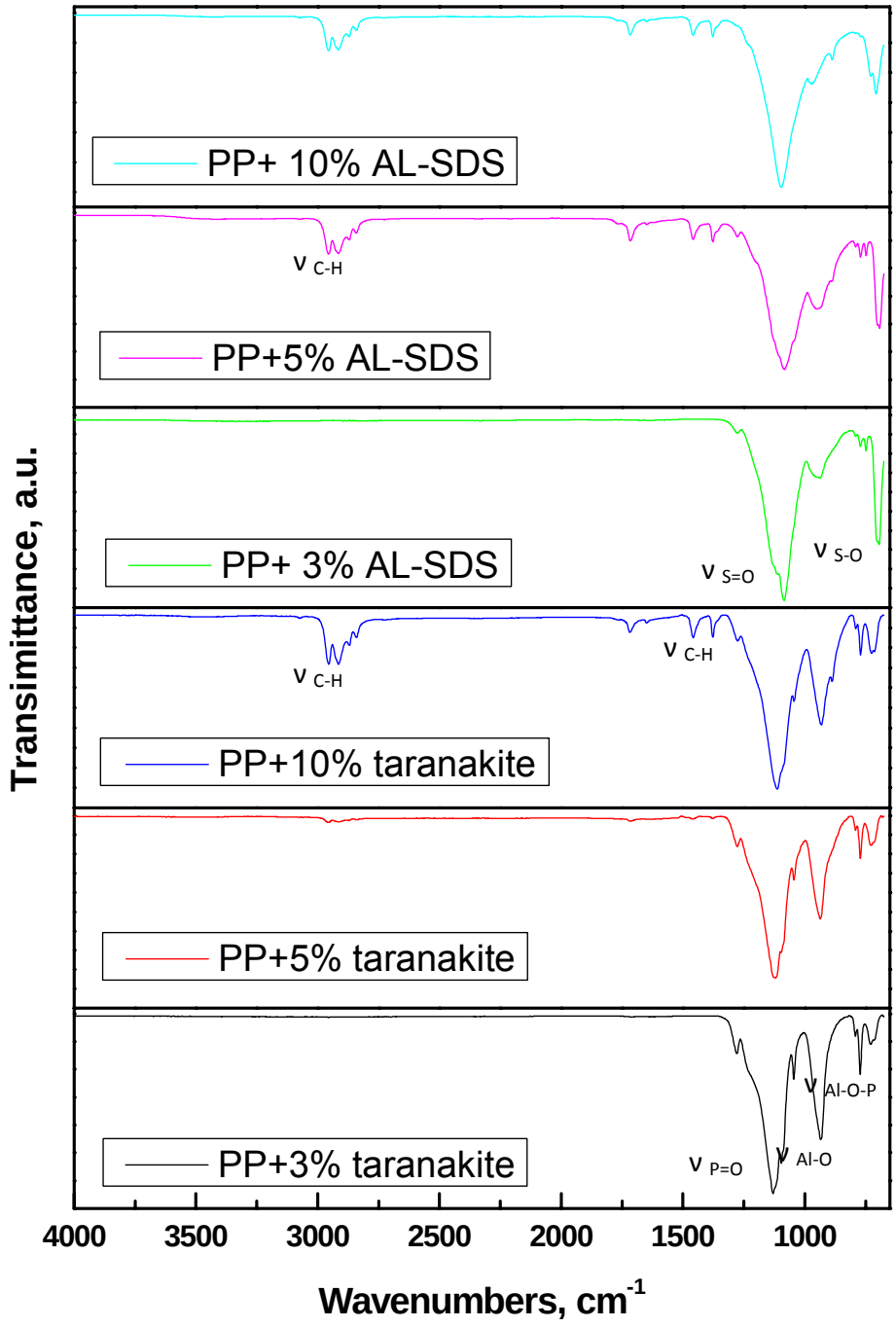

Figure 3.19 FTIR spectra of PP/taranakite, PP/AL-SDS residues

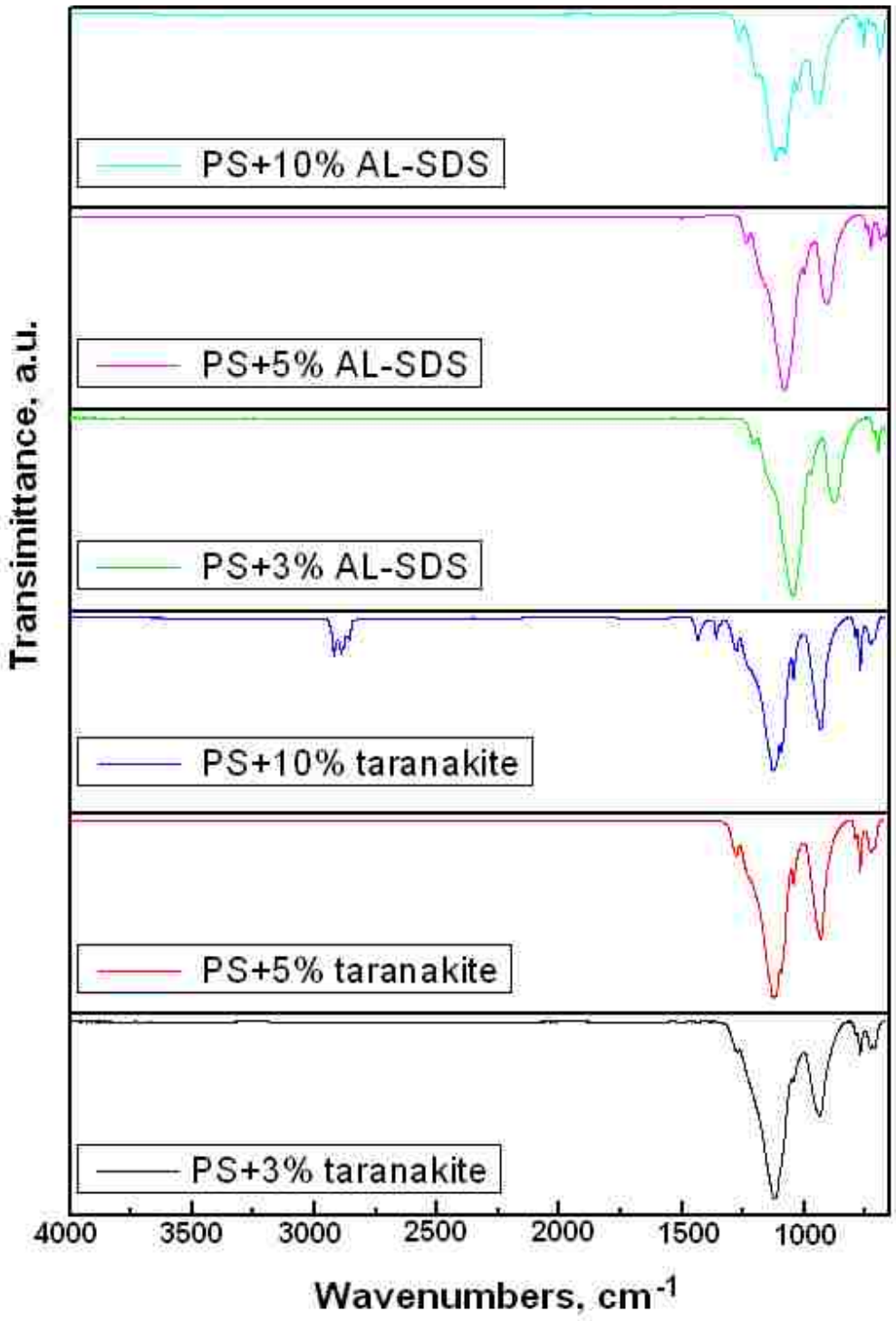

Figure 3.20 FTIR spectra of PS/taranakite, PS/AL-SDS residues

3.6 Comparison of the effect of taranakite and Ammonium polyphosphate (APP) on polystyrene flammability

The fire properties of taranakite and commercial ammonium polyphosphate (APP) on polystyrene were studied to compare the fire retardancy of these two different phosphate compounds. APP is classic fire retardant which shows great effect on PS as discussed in the introduction. The fire retardant action is well understood. It acts mainly in the condensed phase via a char formation mechanism. The phosphoric acid decomposed from APP at high temperature links to the cellulose chain by ester groups which are readily eliminated forming conjugated double bonds, and finally give the char.[117]

The PS/APP or ALP composites were prepared using melt blending method same as the previous part. Table 3.9 lists the formulations of taranakite, APP and PS.

Table 3.9 Formulation of PS, ammonium phosphate and taranakite

Formula	Polystyrene (%)	ALP (%)	APP (%)
Pure PS	100	0	0
PS+5%APP	95	0	5
PS+10%APP	95	2.5	2.5
PS+2.5%APP+2.5%taranakite	95	5	0
PS+5%APP+5 taranakite	90	0	10
PS+5%taranakite	90	5	5
PS+10%taranakite	90	10	0

3.6.1 X-ray diffraction studies

Figure 3.21 shows the XRD of PS composites with taranakite and APP. The patterns of PS melt blended with APP show the sharp peaks for 5% loading of APP which are typical peaks for APP. All of the sharp peaks disappeared in samples containing both additives, suggesting disordered structures.

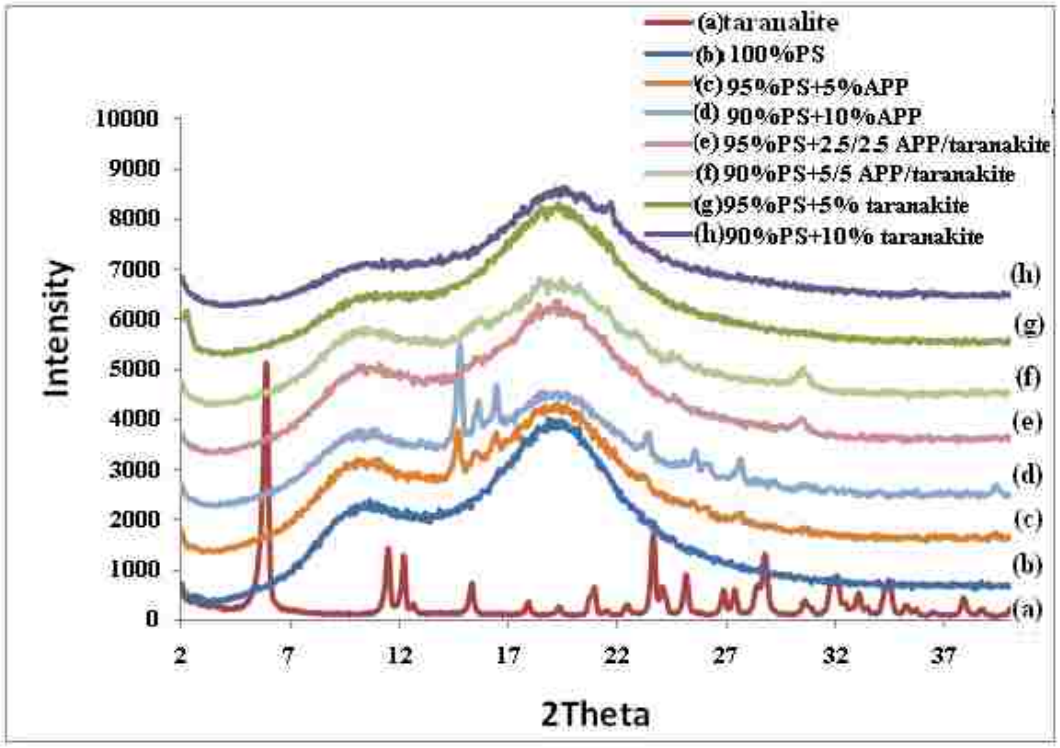

Figure 3.21 XRD patterns of PS melt blending with APP and taranakite

3.6.2 Evaluation of thermal stability

Figure 3.22 illustrates the TGA curves of pure PS and the taranakite composites. Table 3.10 contains a summary of the onset temperature of degradation ($T_{0.1}$), mid-point temperature of degradation ($T_{0.5}$) and the fraction of the non-volatile residue remaining at 700˚C. The onset

temperatures of the degradation when adding APP or the APP and taranakite mixture are similar to pure PS, but exhibit a greater improvement when using taranakite alone as additive. The mid-point temperature of degradation increases with the the addition of adding the APP or taranakite and APP mixtures to the polymer. Based on the fraction of non-volatile in taranakite, the expected char there should be between 4% and 8% residue in the composites and the experimental amount is also in this range, so it appears that all residues are due to the additive.

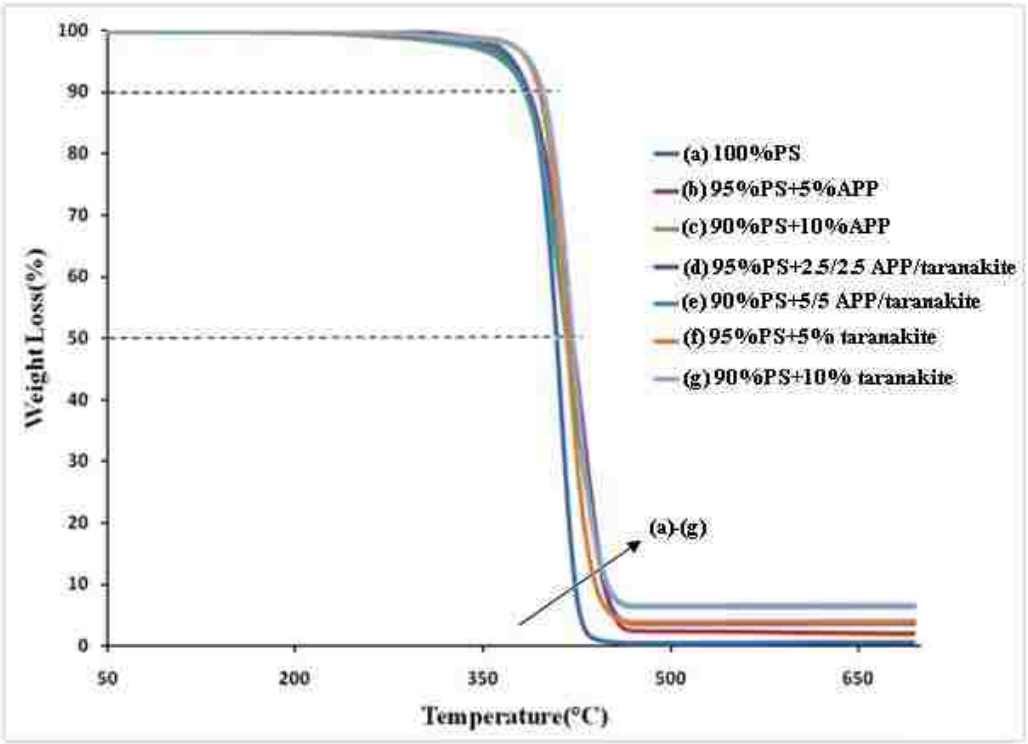

Figure 3.22 TGA curves of PS/ taranakite /APP composites

Table 3.10 TGA summary results for PS and composites

Formulation	$T_{0.1}$ (°C)	$T_{0.5}$ (°C)	Char (%)
Pure PS	385 ± 1	408 ± 1	0.6
PS+5%APP	384 ± 2	421 ± 3	2.1
PS+10%APP	385 ± 2	416 ± 3	6.4
PS+2.5%APP+2.5%taranakite	386 ± 3	420 ± 2	3.7
PS+5%APP+5%taranakite	382 ± 2	417 ± 3	6.4
PS+5%taranakite	395 ± 3	416 ± 3	3.9
PS+10%taranakite	397 ± 2	421 ± 2	6.7

3.6.3 Evaluation of fire properties – cone calorimetry

The cone calorimetric data for the PS composites, obtained at a heat flux of 35 kW/m^2, are shown in Table 3.11. The table shows that time to ignition was reduced when the APP and taranakite were added. The lowering of the t_{ig} is because the decreased specific heat capacity, or decreased ignition temperature, or changed decomposition products of the polymer composites.[118] The presence of APP /taranakite and taranakite reduced the PHRR significantly at 5% and 10% loading.

Table 3.11 Cone calorimetric data for PS, taranakite and APP

Formulation	PHRR (kW/m^2)	PHRR Red. (%)	THR (mJ/m^2)	AMLR (g/s m^2)	ASEA (m^2/kg)	t_{ig} (s)
Pure PS	1532 ± 58	NA	92 ± 1	37 ± 1	1389 ± 60	38 ± 1
PS+5%APP	1509 ± 27	2	100 ± 0	32 ± 1	1354 ± 10	28 ± 2
PS+10%APP	1333 ± 12	13	96 ± 3	30 ± 1	1353 ± 45	21 ± 3
PS+2.5%APP+2.5%taranakite	1355 ± 25	12	97 ± 3	30 ± 1	1332 ± 65	21 ± 1
PS+5%APP+5%taranakite	1164 ± 39	24	94 ± 5	29 ± 1	1364 ± 39	20 ± 2
PS+5%taranakite	1314 ± 62	14	98 ± 2	31 ± 1	1473 ± 60	24 ± 2
PS+10%taranakite	1162 ± 7	24	92 ± 3	30 ± 0	1298 ± 16	20 ± 2

The HRR curves as a function of time for pure PS and APP/taranakite are shown in the figure 3.23. The HRR curves of the taranakite composite are spread over a wide range, indicating that the composites burn for a longer time. The addition of APP and taranakite brings a significant reduction in PHHR. The PHRR decreases with an increasing loading of APP and taranakite. This should be compared to PS-APP composites in which the reduction in the PHRR is in the range of 2-13%, the taranakite is more effective in reducing the PHRR than APP.

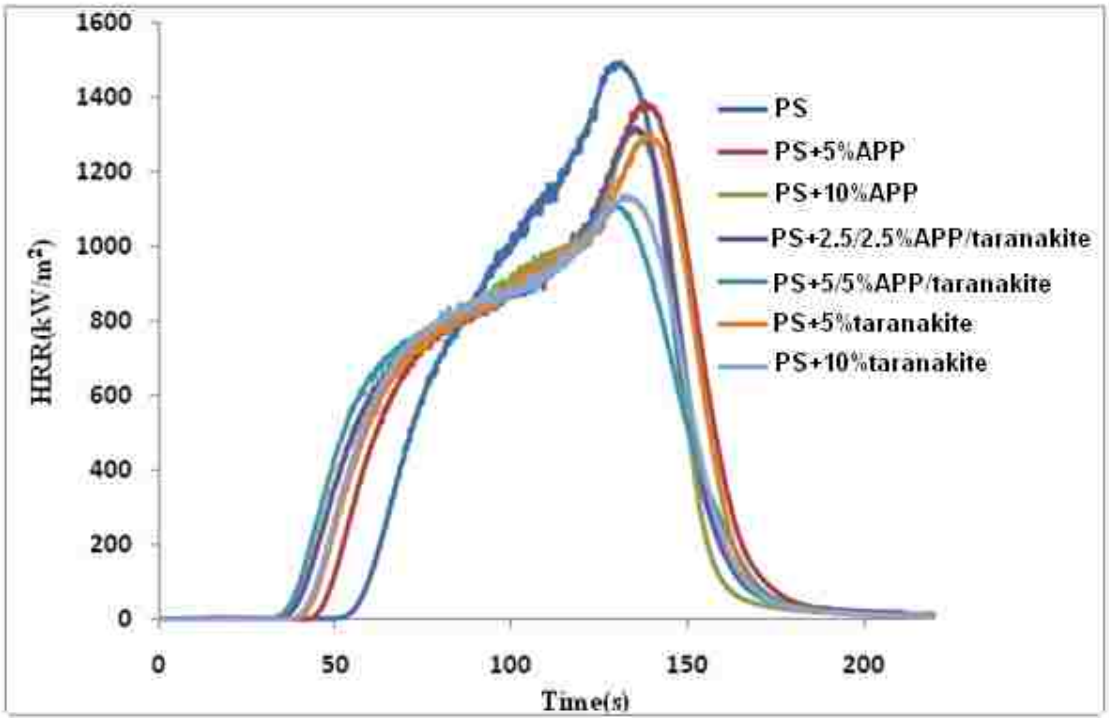

Figure 3.23 Heat release rate (HRR) curves for PS and APP/ taranakite

The better fire retardancy performance of taranakite compared with APP could be due to decomposition of taranakite which will release the phosphate ions. The char formation by phosphate ions and polymers will lead to the fire retardancy of polymers which is the same mechanism as APP on polymers.

3.7 Comparison the fire retardancy of taranakite with other layered materials.

Montmorillonite (MMT) is the most common of the mineral clays tested as potential fire retardants. Because of the weak electrostatic interaction between MMT layers, polymer molecules can easily intercalate into the d-spacing, resulting in exfoliation. When used as the additive for polymers, MMT is typically modified by organic molecules. This process increases d-spacing for the intercalation of polymers and can also improve compatibility with non-polar polymers. The reported reduction of PHRR using modified MMT as additive for specific polymers (such as PMMA) can be as high as 55%.[119] However, MMT nano-particles were found to be inefficient in polypropylene because of the lack of a heat insulating char layer and because of the decomposition of the modified surfactant layer on nanoparticle surface.[120]

Layered double hydroxide (LDH) and hydroxy double salts (HDS) are another class of layered materials that have been tested for use as fire retardant because of the layered structure and tunable metal composition. However, these materials show strong interactions between the nano-layers, making it difficult to exfoliate them when mixing with polymers. LDHs compounds are also usually modified by long-chain organic molecules to increase the interlayer space and the compatibilities with polymers. The reported reduction of PHRR by using modified LDHs as additive for polar polymers (PMMA) have been as high as 34%, but usually only modified with long chain organic molecules will result a good reduction for non-polar polymers[121]. Nyambo *et al.* reported that the Mg-Al-LDH modified with 10-undecenoin acid shows the 7% reduction on PHRR for PP and 20% reduction for PS with the 10% loading.[121] Wang *et al.* also reported that the Mg-Al-LDH modified with bis(2-ethylhexyl) phosphate (HDEHP) and sodium dodecyl benzenesulfonate (SDBS) exhibits 32% and 49% reduction, respectively, on PHRR for PS at 10% loading. The larger reduction in PHRR with modification by HDEHP and SDBS is because the

longer chain of these organic molecules compared with 10-undecenoic acid, which will lead to larger increase in d-spacing of LDH.[9] The modification by these long chain organic molecule lead to other environmental concerns, however. For example, the cone results show the high ASEA increase with these modified LDH (50% increase for PS with 10% loading of 10-undecenoin acid modified Mg-Al-LDH), which indicates more smoke will be produced during the burning.[121]

The mechanism of fire retardancy on polymers by these layered materials is the char formation mechanism, which is a charring barrier mechanism of carbonaceous char formation as an insulator to the heat and a mass transport barrier during the combustion of the nanocomposites.[122]

Taranakite without any modification shows better compatibility with polar and non-polar polymers than MMT and layered double hydroxides. Besides the char formation, fire retardancy of this compound is also because of the large amount of interlayer water and the phosphate ions produced at the decomposition. The reduction in PHRR by taranakite on polymers was found to be 25% for non-polar polymers and 30% for polar polymer at 10% loadings. In addition, the onset temperature for thermal degradation of polymer/taranakite nanocomposites is higher than for virgin polymers, an effect that is different from that observed with some nanocomposites containing LDH or MMT. However, the time to ignition in cone calorimetry decreases with addition of taranakite.

Chapter 4 Conclusions and potential future directions

Taranakite was synthesized and modified by sodium dodecyl sulfate. The TGA data shows that the taranakite is stable when the temperature is lower than 200 °C, while decomposition occurs at temperatures higher than 200 °C.

The materials were used as additives to non-polar and polar polymers to study the fire retardancy. For non-polar polymers, PS and PP, the taranakite or AL-SDS composites were prepared using melt blending methods. Based on the XRD patterns, one can expect the formation of nanocomposites by these non-polar polymers and taranakite/AL-SDS. Further experiments are needed the confirm this. The thermal stabilities of PS or PP/taranakite composites were significantly improved. The reduction in peak heat released rate (PHRR), which is the most important parameter in the flame retardancy of testing polymers, increased with increasing loading of taranakite. The possible reason for polar taranakite improving the fire retardancy of non-polar polymers could be the formation of ester by hydroperoxide and phosphate ions during the degradation of polymer improve the thermal stability of polymer.

The fire retardancy of a polar polymer with taranakite was also studied. PVA/taranakite composites were prepared using solution method at 80 °C. The XRD provides the evidence of the formation of intercalated nanocomposites. The thermal stability of these nanocomposites was significantly improved, as shown in the TGA results. The fire properties which were acquired from the micro-cone calorimetriy (MCC), were improved for PVA/taranakite nanocomposites. This was indicated by the 30% reduction of PHRR obtained from 10 wt% loading of taranakite, and also the corresponding decreased mass loass rate for the nanocomposites when compared with the pristine PVA. The HRR curves and the summary of the PHRR and MMLR (Table 3.5.4)

indicate the presence of taranakite could be the inhibitor at the first step of degradation of PVA. This can be expected the formation of hydrogen bonding between PO_4^{3-} ions in the taranakite layers and –OH groups of PVA.

Taranakite is a promising compound for fire retardant formulations for both polar and non-polar polymers. The mechanism of the fire retardancy by taranakite is different from that of other layered materials, which is of interest for further investgation. Further studies are required on polymer/taranakite nanocomposites to identify the process that occur in these systems, and different organic- modified taranakites would be of interest for further fire retardancy studies.

Part B. Computational methods combined with experiments to study the modification of α-zirconium phosphate and adsorption of organic pollutant

Chapter 5 Introduction

5.1 Preparation of α-Zirconium phosphate

The metal salts of phosphoric acid have been studied for over a century.[123] These materials can be used in many applications, such as: molecular sieves, catalysts, ion and proton conductors, and matrices for chemical modification. Since the initial report of the ion exchange properties of zirconium phosphate gels in the 1960s, these compounds have been the subject of continuous interest because of their ion exchange ability.[124-129]

α -Zirconium Phosphate, α -$Zr(HPO_4)_2 \cdot H_2O$ (abbreviated as α-ZrP) is an example of a metal salt of phosphoric acid. It has great crystalline morphology,[130] high stability in aqueous and organic solvents,[131] and good thermal stability.[131] α-ZrP is composed of two dimensional layered macromolecular units that are weakly interacting with each other[132]. It has a clay-like structure with an interlayer distance of 7.6 Å, and each layer consists of a plane of zirconium atoms bridged by three oxygen atoms of the tetrahedral phosphate group- anions,[125] Figure 5.1 shows the schematic structure of α-ZrP. These phosphate groups serve as active Brönsted acidic species,[133;134] and then interact easily with molecules containing basic group such as alkyl amines or aniline. The theoretical cation exchange capacity (CEC) of α -zirconium phosphate is 6.67 mmol/g.[135;136]

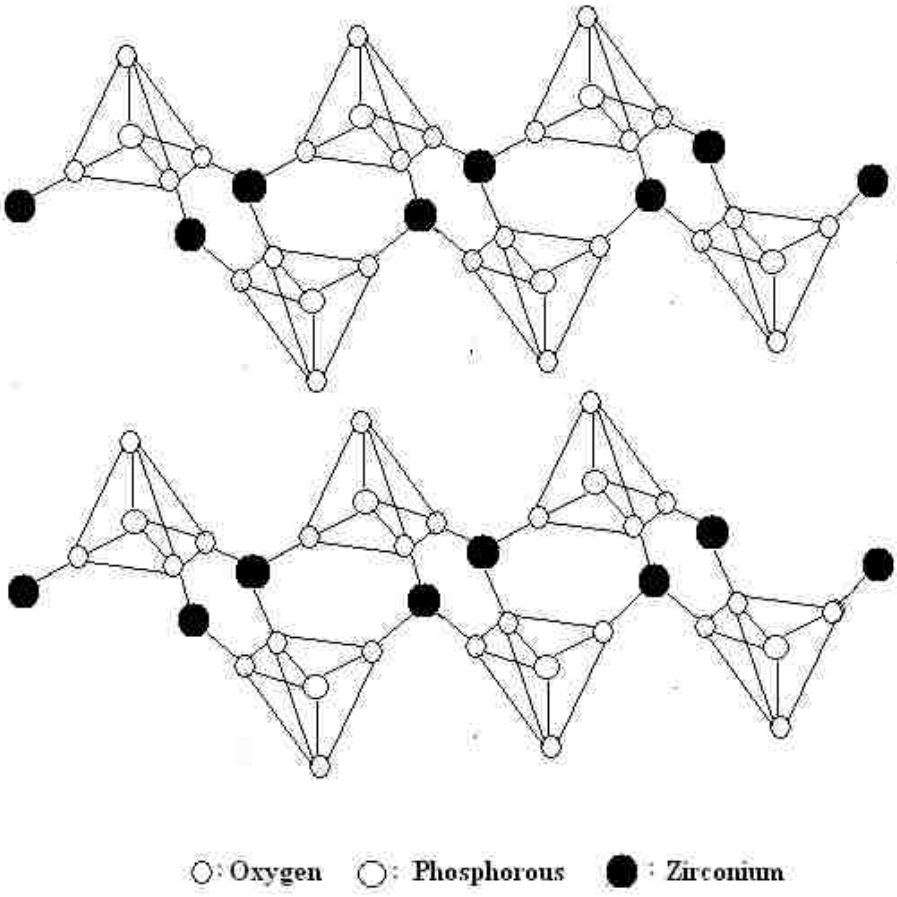

Figure 5.1 Schematic structures of the arrangement of three adjacent macro anions in α-ZrP. The distance between two planes passing through the baricenters of $O^{(-)}$ belonging to the two sides of the macro anion is 6.3Å (ref. 130).

The first reported crystalline α-ZrP was obtained by reflux in H_3PO_4 of a zirconium phosphate gel.[127] It can also be synthesized by hydrothermal methods or by direct precipitation with prior formation of zirconium (IV) fluoro complexes.[137]

5.2 Intercalation of alkylamines in α-zirconium phosphate

Intercalation chemistry is of interest because of the alteration of the host's properties brought about by the intercalation process.[138] For example, incorporation of amines into the

interlayer space of clays not only increases the separation of the clay layers but can be used to mediate the hydrophilic–hydrophobic character of the composite. The intercalated compounds can be used to absorb organic species.[139] More recently, amine intercalates have been prepared to make the clay more compatible with any number of organic materials or polymers to which they are admixed, and such intercalates can also be used as precursors to pillaring reactions.[140;141]

α-zirconium phosphate is an important compound for intercalation chemistry due to its two-dimensional (2D) layered packing structure. The presence of P–OH groups on the surface of the layers helps the alkylamine molecules access the interlayer region by the acid-base reaction.[136] This compound is able to act as a host for cationic or molecular polar guest species.[142;143] The intercalation of aliphatic monoamines and diamines has been investigated by several researchers.[144-147] MacLachlan *et al*. reported the relationship between the amount of alkylamine and its arrangement in the interlayer region of α-ZrP, and clarified that an alkylamine with a short alkyl-chain, such as butlyamine, has various conformations in the interlayer region, depending on the amount of alkylamine.[148;149] The intercalation compound has an interdigited structure at lower loading of alkylamine and then transforms to a bilayer structure, with an increase of the interlayer distance at higher amine loading. α-ZrP is capable of incorporating a maximum of 2 mol of n-alkylamines with formation of a bilayer in the interlayer space.[135;136] The alkylamine intercalated α-ZrP with a bilayer structure has a large hydrophobic region in the interlayer space.

Experimental characterization of the amine interlayer orientation has been explored via XRD, FTIR, and computational methods.[150-153] Benes *et al*. reported that the cross sectional area is an important factor that would have effects on the arrangement.[154] Stoichiometric intercalation can occur when the cross section area of amine does not exceed the free area of the α-ZrP which

24 $Å^2$. If the cross section area of amine is higher than free area of α-ZrP, the interdigited arrangements of amine will be formed.

5.3 Adsorption of organic pollutant by organo-modified layered α-zirconium phosphate

Elimination of harmful environmental pollutants such as pesticides and environmental hormones has become increasingly important and many chemists have devoted their research to green chemistry. Hayashi *et al*. reported polyamine-intercalated α-ZrP adsorbed gaseous carboxylic acid and formaldehyde by the interaction of those gases with polyamine in the interlayer region.[153, 154] Formaldehyde is a compound that causes the sick-house syndrome.[155]

Very small amounts of chlorophenols are contained in city water and their acceptable limits are strictly determined.[156] The main pollution sources containing chlorophenols are the waste water from pesticide, paint, pharmaceutics, wood, paper and pulp industries as well as water disinfecting process.[156] Chlorophenols are weak acids which permeate human skin and are readily absorbed by the gastro-intestinal tract. Due to its high toxicity, carcinogenic properties, structural stabilization and persistence in the environment, the removal of chlorophenol from the environment is crucial.[157]

Various treatment methods have been applied to remove chlorophenol molecules from aqueous solutions, such as biological treatment using anaerobic granular sludge,[156] catalytic wet oxidation,[158] photochemical treatment,[159] adsorption technology using activated clay,[160] and activated carbons prepared from various precursors.[161;162] Adsorption on activated carbon is one of the most effective and widely used techniques in treating low concentration of phenol waste water. However, the usage of activated carbon has been limited by its high cost due to the use of non-renewable and relatively expensive starting materials such as coal, which is a major

economic consideration.[163] This has prompted growing research interest in the production of low-cost adsorbents such as activated carbons for application in wastewater treatment. Therefore, the interest in the development of absorbents with low cost and high efficient such as nano-crystalline metal oxides,[164] layered nano-dimensional materials[165-167] and organic-modified clay,[168;169] has also significantly increased in recent years. Clays treated with organic compounds with long alkyl chains, or clays pillared by surfactants could adsorb phenols and chlorinated phenols. Their adsorption mechanism is mainly hydrophobic interaction of long alkyl chain or surfactant with phenols.[170;171] Hayashi *et al* first reported that butylamine-intercalated α-ZrP could adsorb harmful pollutants such as phenol, chlorophenol, and 2, 4- dichlorophenol. Phenols were co-intercalated into the interlayer region and the adsorption reactions of phenols reached equilibrium within 15 min. This makes the alkylamine-intercalated α-ZrP a potential candidate to be an adsorbent for harmful phenols[172]. Recent work in our laboratory has reported the effects alkylamine structure on the adsorption of chlorophenol by modified α-ZrP[2]. In this part, the use of a dimethylhexadecylamine (DHDA) intercalated zirconium phosphate as a potential sorbent for 4-chlorophenol is reported. The interactions between alkylamines, phosphate and 4-chlorophonel are studied by computational methods.

5.4 Previous experimental work

The experimental parts, including the synthesis of α-ZrP, the intercalation of alkylamines and the adsorption of chlorophenol were performed by Dr. Mlambo in our lab[2]. α-ZrP was synthesized using reflux method according to the literature[173]. Intercalation of alkylamines into α-ZrP was also performed following a literature method[133]. The products were studied using XRD, FTIR and UV-vis.

Powder X-ray diffraction measurements were obtained with a Rigaku Miniflex II diffractometer from 2° to 40° (2θ) at a scan rate of 5° per minute using Cu K_{α} radiation (λ=1.5404 Å). The XRD data provided the evidence of the intercalation of alkylamines into the α-ZrP. The XRD data were consistent with different arrangements by amines between the interlayers, with bilayer formation observed for primary amines and the interdigited arrangements with tertiary amines.

5.5 The motivation of calculation work

The experimental work confirmed the intercalation and adsorption of organic molecules into the α-ZrP. It was found that the interdigited DHDA- α-ZrP structure was more effective as an adsorbent for chlorophenol than the bilayer structures with primary amines. The goal of this work is to examine the interactions between 4-chlorophenol and model fragments of selected portions of the modified α-ZrP structures. The interactions between the analyte molecules and α-ZrP layered needs to be understood in order to develop of optimized adsorbents.

Chapter 6 Computational methods to study the adsorption of chlorophenol by intercalated zirconium phosphate

Density functional theory calculations were performed using the B3LYP functional with a 6-311G* basis set using Gaussian 03.[174] Density functional theory is a quantum mechanical method to investigate the electronic structure of many systems, it is among most popular methods to calculate the condensed matter properties.[175] The most widely used method within this theory is B3LYP, which is a hybrid functional in which the exchange energy, in this case from Becke's exchange functional, is combined with the exact energy from Hartree-Fock theory.[176] 6-311G* basis set is a split valence triple zeta plus polarization basis set (6 Gaussians

on core electrons then split 3, 1, 1, Gaussians on valence electrons).[177] The advantage with using the 6-311G* basis set is that it adds the polarization to all atoms, and improves the modeling of core electrons. The calculation includes determination the chain length of alkylamines and chlorophenol, and also the interactions between the phosphate layer, alkylamines and chlorophenol molecules. The energies, that calculated by Gaussian use zero-point energy, because it shows energies at the ground state. The contribution to this internal energy is from the vibration mode, and only the real mode will be considered. [178]

6.1 Intercalation of alkylamines in α-Zirconium phosphate

The characterization of amines intercalated α-ZrP was performed by Dr. Mlambo.[172] X-ray diffraction analysis was used to characterize the structure of synthesized α-ZrP and alkylamine-intercalated α-ZrP. The XRD patterns of α-ZrP, ZrP-BA, ZrP-Octyl, ZrP-HAD, ZrP-DtDA and ZrP-DHDA are shown in Figure 6.1. All the first peaks of intercalated ZrP XRD patterns shifted to lower 2θ, Table 6.1 shows the 2θ value of the first peak (*002* peak), and the corresponding interlayer space. The 00ℓ (ℓ = 2 to 6) basal reflections found in the lower angle region for ZrP-BA, ZrP-Octyl, ZrP-DtDA and ZrP-DHDA are sharp and equally spaced, indicating high range ordering in the c-axis direction. It is also noted that the reflection at 2θ =34° with Miller indices (*020*) in the α-ZrP remains largely unaltered after intercalation of alkylamines suggesting that the intercalation processes occurring in the interlayer region of the α-ZrP do not alter the Zr-O-P framework.

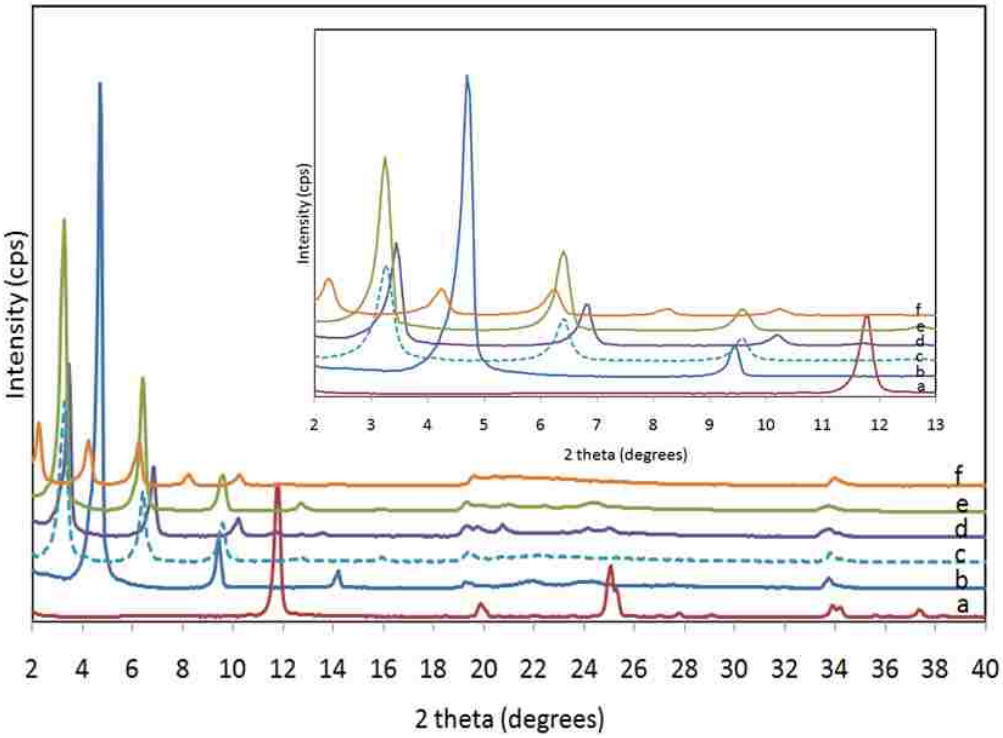

Figure 6.1 Powder X-ray diffraction patterns of ZrP(a), ZrP-BA (b) ZrP-Octyl (c) ZrP-DtDA (d) ZrP-DHDA (e) ZrP-HDA (f). The positions of the (002) peak for each pattern are clearly shown in the insert.[172]

Table 6.1 2Theta values of the first peak (*002*) and interlayer spaces of ZrP and intercalated ZrP

Alkylamine-ZrP	(*002*) peak 2θ value	Interlayer space Å
ZrP	11.7°	7.6
Butylamine (BA)	4.7°	18.6
Octylamine (Octyl)	3.2°	27.6
Hexadecylamine (HAD)	2.1°	43.1
Dimethyltetradecylamine (DtDA)	3.4°	25.6
Dimethylhexadecylamine (DHDA)	3.1°	28.0

The increase in interlayer space due to alkylamine intercalation is calculated by subtracting the zirconium phosphate layer thickness of 6.3 Å [175] from the d-spacing obtained from X-ray diffraction. Then the interlayer space for pristine α-ZrP is 1.3 Å, which is the subtraction of d-spacing 7.6 Å by 6.3 Å, and the interlayer spaces for intercalated ZrP can also be obtained by the same calculation method (shows in Table 7.2). Table 6.2 also shows the length of alkylamine molecules calculated from a B3LYP/6-311G* optimized structure using Gaussian 03.[174] According to the literature,[176;177] the angle of the inclination and the arrangement of amine chains are proposed on the basis of the steric demands of the guest molecules, host layer thickness, and the experimentally found basal spacing and composition of the intercalate. The proposed arrangement was then derived from the analysis of the correlation between interlayer distance and the number of carbon atoms in the alkylamine chain.[144; 175] Table 6.2 shows the proposed arrangement of amine molecules in the ZrP interlayer space. The increase in interlayer spacings for ZrP-BA, ZrP-Octyl, and ZrP-HAD are much larger than calculated chain length, indicating a bilayer arrangement. In the cases of ZrP-DtDA and ZrP –DHDA, the interlayer increases are slightly smaller than the chain length of amines, indicating an interdigitated (or tilted) arrangement.

Table 6.2 Calculated alkylamine chain length and proposed interlayer arrangement of alkylamines in ZrP interlayer space

Alkylamine	Calculated Length (Å)	XRD Observed interlayer Increases (Å)	Arrangement of molecules in the ZrP interlayer space
Butylamine	6.2	11.3	bilayer
Octylamine	11.6	20.9	bilayer
Hexadecylamine	20.7	38.9	bilayer
Dimethyltetradecylamine	21.2	19.5	interdigitated
Dimethylhexadecylamine	22.8	20.2	interdigitated

Figure 6.2 shows the molecule structures of the amines. The difference between DtDA and DHDA versus BA, Octyl and HAD are that the hydrogen atoms attached to nitrogen are replaced by methyl group. The proposed arrangements of the DtDA and DHDA molecules are obviously different than BA, Octyl and HAD. This can be considered as arising due to the different cross sectional areas of the intercalated molecules.

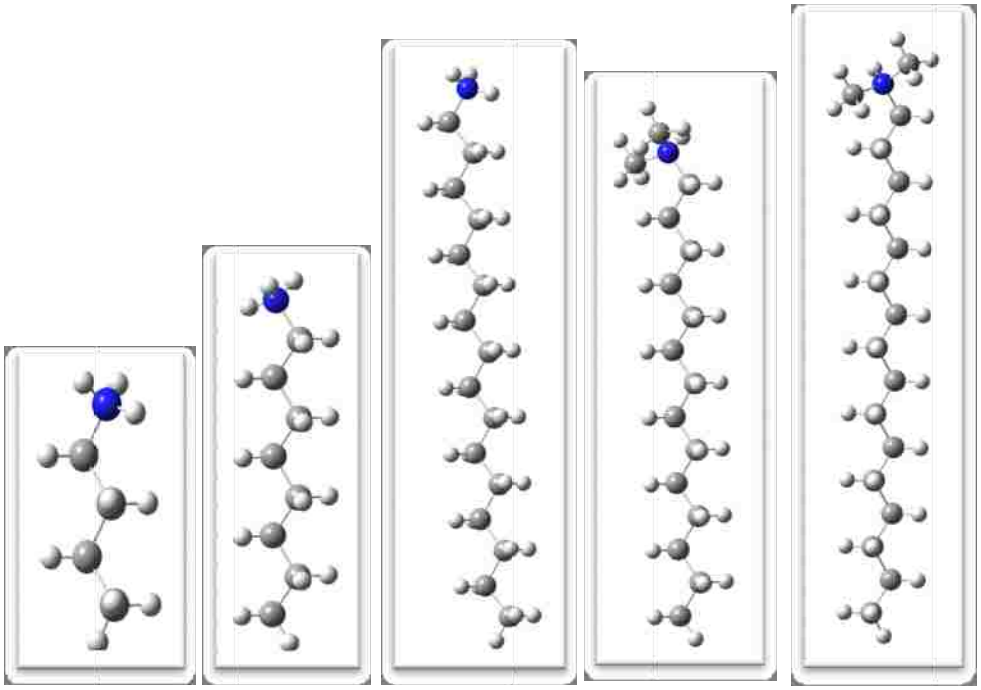

Figure 6.2 The scheme of molecule structure of alkylamines. (: oxygen; : nitrogen; ○: hydrogen)

The cross sectional areas can be calculated using method of Hermann.[178;179] The method considers the molecule as a set of intersecting spheres of carbon, hydrogen, and oxygen, with their radii being equivalent to van der Waals radii. The following values for inter-atomic bond lengths were used: aliphatic C-C, 1.54 Å; C-H, 1.09 Å; C-O (in alcohols), 1.43 Å; and O-H (in alcohols) 0.97 Å.[180;181] The van der Waals radii used were: aliphatic carbon, 1.6 Å; hydrogen, 1.2 Å; oxygen, 1.4 Å and nitrogen, 1.5 Å. The cross section areas are calculated combined the bond length, bond angle and van der Waals radii of atoms in the molecule. In the case of a-ZrP, the cross sectional areas of the intercalated molecules were calculated assuming that the C – N bonds are perpendicular to the host layers. For BA, HAD and Octyl, the cross section areas include only the $–CH_3$ group, and the cross section areas of DtDA, DHDA are the sum of the areas of $–CH_3$ group and N atom. A schematic diagram (Figure 6.3) shows a planar view of a terminal

methyl group and dimethylamino group. The methyl group can be considered as a sphere area rather than individual atoms. The justification for the selection of a 2.0 Å radius sphere for the methyl or methylene group is derived from Pauling's account of experimental measurements on several molecules.[180] Solid curves show a carbon atom in the center (van der Waals radius 1.6 Å) and three tetrahedral hydrogen (van der Waals radius 1.2 Å) located at 1.09 Å from the center of the carbon atom. The dotted curve shows the methyl group as a single sphere with a radius of 2.0 Å. As can be seen, the parts of hydrogen atoms are compensated for by filling the void spaces around the carbon atom. The estimated surface area of the methyl group should, therefore, be 33.2 $Å^2$; this suggests that the total surface area of DtDA and DHDA is 73.5 $Å^2$.

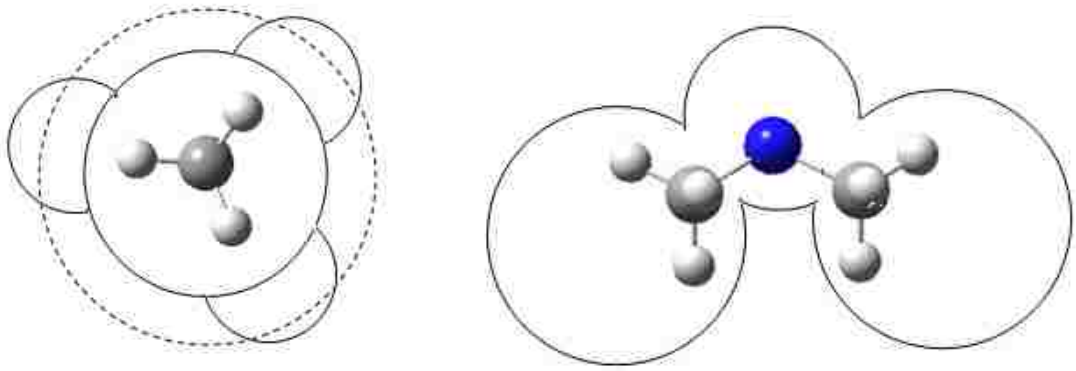

Figure 6.3 Schematic planar view of a terminal methyl group and dimethylamino groups

For ZrP, the free area associated with each P – OH group is 24 $Å^{2(182)}$, that is much smaller than the surface area of DtDA and DHDA. Therefore, not every phosphate between the layers of ZrP-DtDA or ZrP-DHDA, is occupied by the DtDA or DHDA molecules because of the "covering effect" .[136] Figure 6.4 shows the proposed arrangement of BA (a), and DtDA (b) molecules in the intercalate.

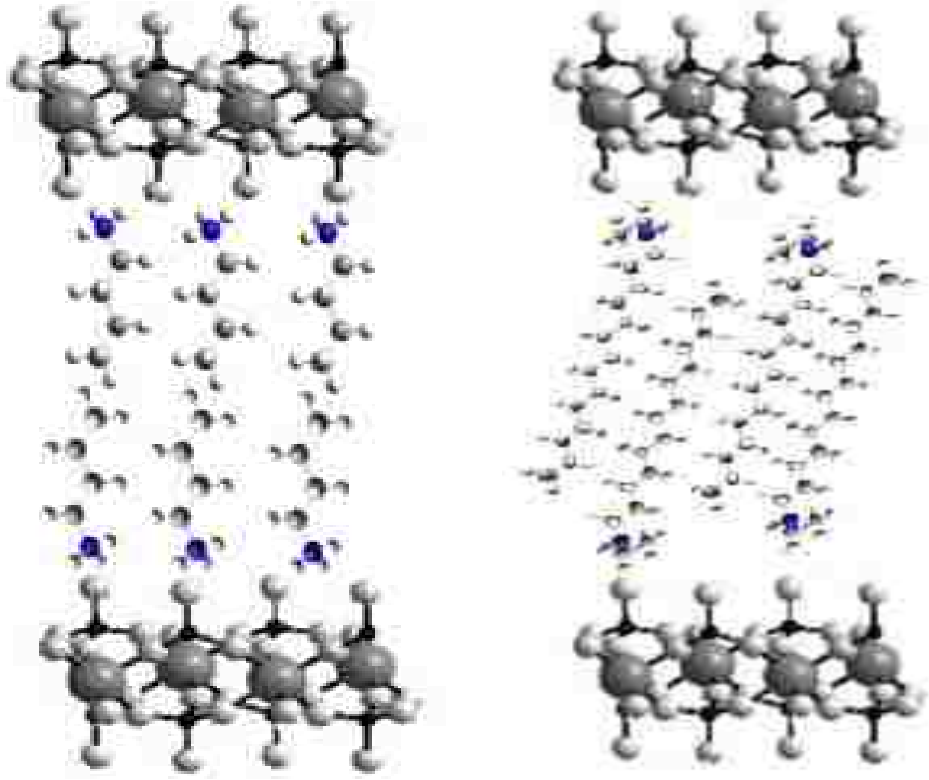

Figure 6.4 Proposed arrangement of BA (a), DtDA(b) molecules in the intercalate

6.2 Adsorption of 4-chlorophenol by intercalated layered α-Zirconium phosphate

6.2.1 X-ray diffraction study of the adsorption of 4-chlorophenol by α-ZrP

Figure 6.5 shows the XRD patterns of pristine ZrP (a), ZrP-DHDA (b) and the product after adsorption of 4-chlorophenol by ZrP-DHDA. The insert part shows the XRD patterns of ZrP-DHDA and the product of 4-chlorophenol intercalated in ZrP-DHDA (Trace c). The interlayer space increases from 2.76 nm to 3.36 nm upon intercalation of 4-chlorophenol. The length of chlorophenol obtained from computation calculations (B3LYP/6-311G*) is 0.63 nm. The increase in the interlayer space (0.6 nm) shown in the insert (trace c) is consistent with

intercalation of 4-chlorophenol oriented perpendicular to the layers. It suggests that 4-chlorophenol and DHDA molecules are co-intercalated in the ZrP interlayer spaces.

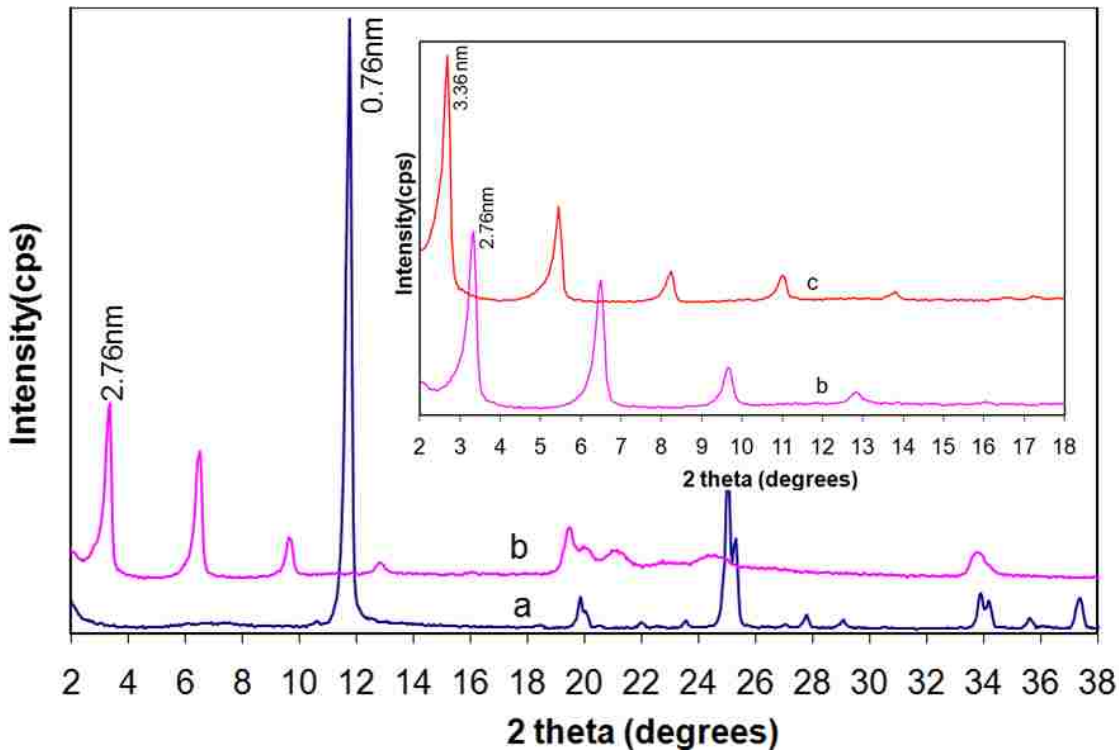

Figure 6.5 X-ray diffraction pattern of α-ZrP (a) ZrP-DHDA (b). Insert shows the X-ray diffraction patterns of ZrP-DHDA (b) and ZrP-DHDA intercalated with 4-chlorophenol (c) in the 2°-20° range

The proposed co-intercalation arrangement of chlorophenol and DHDA in ZrP is also confirmed by infrared spectroscopy. Figure 6.6 shows the ATR-FTIR spectra of ZrP-DHDA and 4-chlorophenol intercalated ZrP-DHDA. The characteristic bands of 4-chlorophenol are observed alongside the absorption bands of the parent material. Absorption bands due to 4-chlorophenol at 1590 cm^{-1} and 1497 cm^{-1} are C=C ring stretching frequency, while the band at 1090 cm^{-1} is C-Cl stretching frequency and the band at 823 cm^{-1} is the out of plane bending mode of the ring C-H vibration.[183;184] Figure 6.6 clearly shows that the infrared bands of the parent material are still

present after the intercalation of 4-chlorophenol. This confirms that the DHDA and 4-chlorophenol are co intercalated.

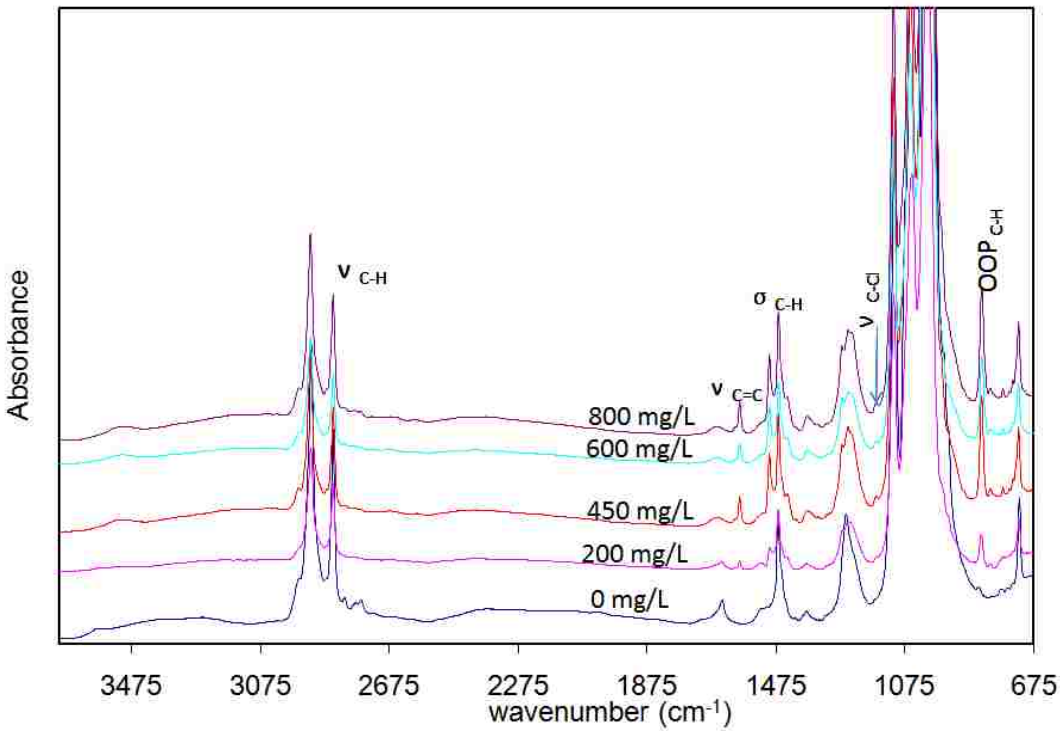

Figure 6.6 ATR-FTIR spectra of phases obtained after adsorption of 4-chlorophenol by 0.1 g of ZrP-DHDA in 30 ml of solution at different 4-chlorophenol concentrations

6.2.2 Computational methods to study the interactions between ZrP, amine and 4-chlorophenol

The XRD and FTIR data are consistent with a co-intercalated structure of 4-chlorophenol adsorbed ZrP-DHDA. In order to better characterize the interaction between ZrP phosphate anions, alkylamine and 4-chlorophenol, computational studies were performed. Figure 6.7 shows a schematic proposed arrangement of alkylamine and 4-chlorophenol molecules at the interlayer of ZrP. The 4-chlorophenol molecule has two electronegative atoms O and Cl, and they can form

ether hydrogen bonding or halogen bonding with positive charged alkylamine ions between layers,[172;185] while the hydrogen atom assigned to the –OH group in 4-chlorophenol could also form hydrogen bonding with phosphate layer in ZrP. The preference of the bonding site with alklyamine and phosphate layer will have lead to the different increasing of the interlayer space of ZrP-alkylamine. The interactions between the three parts (highlighted by the rectangular block in Figure 6.7) were studied by computional methods using DFT method (B3LYP) with the basis set 6-311G*.

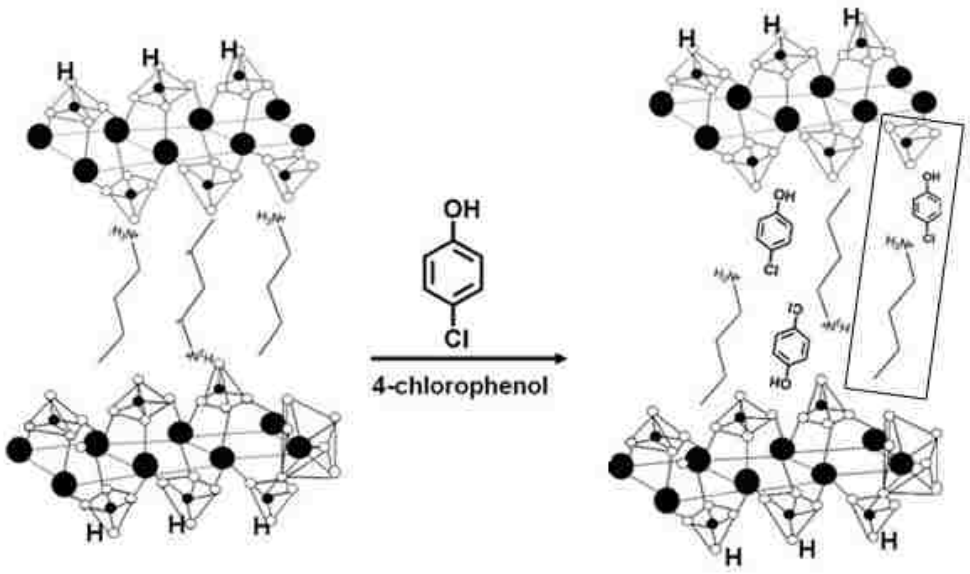

Figure 6.7 Schematic representation of 4-chlorophenol Intercalation into layered ZrP-amine. The rectangular area is the part studied using calculation method

: Zirconium, : Phosphate, : Oxygen.

Models built to analyze the interaction of amines, phosphate ions and chlorophenol molecules

H_3PO_4 (Singlet)

A model of H_3PO_4 (neutral) was built as shown in Figure 6.8, which the parameters of the model were shown in the Table 6.3 at right. The zirconium atoms bonded with oxygen atoms in ZrP were substituted by hydrogen atoms to simplify the calculation.

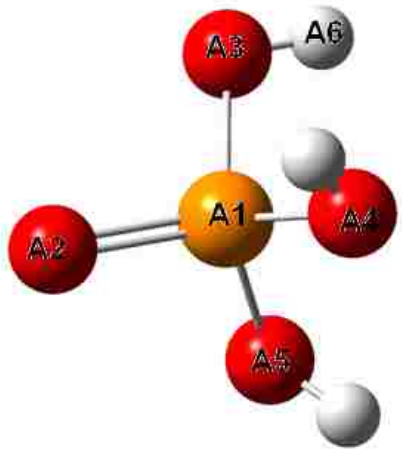

Figure 6.8 Schematic of the phosphate acid model

Table 6.3 The parameters of phosphate acid model

	Bond length/ Å	Bond Angle
A1-A2	1.76	
A1-A3	1.76	
A3-A6	0.96	
A2-A1-A3		109.47°
A3-A1-A4		109.47°
A1-A3-A6		109.50°

NH_3----H_3PO_4

The model of hydrogen bonding between amine and phosphate was built as shown in Figure 6.9. The table 6.4 at the left is the parameters of the model, and the table 6.5 below is the energy changing by the formation of the hydrogen bonding, which the negative energy indicates the more stable state after the formation of hydrogen bonding.

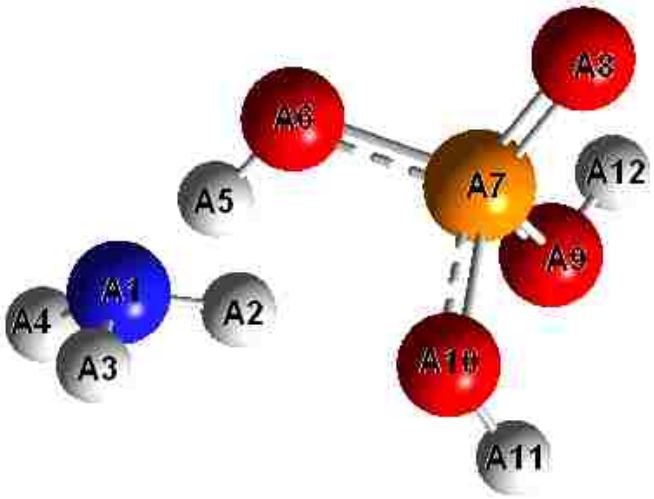

Figure 6.9 Model of hydrogen bonding between amine and phosphate ions

Table 6.4 The parameters of NH_3----H_3PO_4 model

	Bond length/ Å	Bond Angle
A1-A2	1.00	
A1-A3	1.00	
A1-A4	1.00	
A1-A5	1.28	
A5-A6	0.96	
A6-A7	1.60	
A7-A8	1.47	
A7-A9	1.63	
A10-A11	0.96	

A2-A1-A3		109.47°
A5-A6-A7		116.42°
A6-A7-A8		111.99°
A6-A7-A9		106.44°
A6-A7-A10		103.14°
A8-A7-A9		116.19°
A9-A7-A10		98.09°
A7-A9-A12		114.63°

Table 6.5 The formation energy of NH_3----H_3PO_4 model

NH_3	E(RB+HF-LYP) = -56.20	**ΔE= -0.43 A. U. = - 296.82 kcal/mol**
H_3PO_4	E(UB+HF-LYP) = -640.23	
H_3PO_4 - NH_3	E(UB+HF-LYP) = -696.83	

NH_3------ OH-C_6H_4- Cl

The model of hydrogen bonding between amine and chlorophenol molecule is shown in the Figure 6.10, while the Table 6.6 below shows the parameters and the Table 6.7 energy changing after the formation of hydrogen bonding. The hydrogen bonding formation also lowers the total energy.

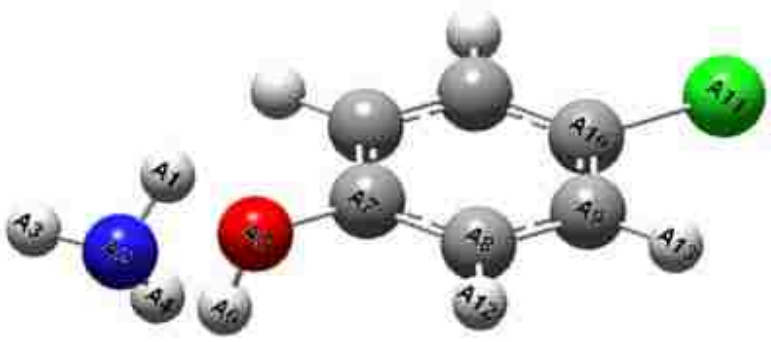

Figure 6.10 Model of hydrogen bonding between amine and chlorophenol

Table 6.6 The parameters of NH_4^+-- OH-C_6H_4- Cl model

	Bond length/ Å	Bond Angle
A1-A2	1.00	
A2-A3	1.00	
A2-A4	1.00	
A1-A5	2.10	
A2-A6	2.03	
A5-A6	0.96	
A5-A7	1.43	
A7-A8	1.39	
A8-A9	1.40	
A9-A10	1.39	
A10-A11	1.81	
A1-A2-A3		110.36°
A6-A5-A7		112.78°
A1-A5-A7		120.34°

Table 6.7 The formation energy of NH_4^+-- OH-C_6H_4- Cl model

NH_3	E(RB+HF-LYP) = -56.20	**ΔE= -0.03 A. U. = - 18.82 kcal/mol**
C_6H_5ClO	E(RB+HF-LYP) = -763.16	
$C_6H_5ClO – NH_3$	E(RB+HF-LYP) = -819.39	

H_3PO_4-----OH-C_6H_4-Cl

Figure 6.11 shows the model of hydrogen bonding between phosphate and a chlorophenol molecule. The Table 6.8 below also shows the parameters of the model and the table 6.9 is the energy changing after the formation of hydorgen bonding.

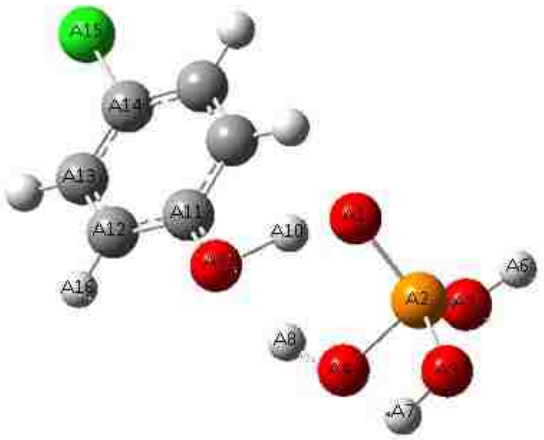

Figure 6.11 Model of hydrogen bonding between phosphate and chlorophenol

Table 6.8 The parameters of H_3PO_4------OH-C_6H_4-Cl model

	Bond length/ Å	Bond Angle
A1-A2	1.69	
A2-A3	1.76	
A2-A4	1.71	
A2-A5	1.79	
A5-A6	1.00	
A3-A7	1.01	
A4-A8	1.02	
A9-A10	1.42	
A1-A10	1.10	
A9-A11	1.34	
A1-A2-A4		98.07°
A2-A1-A10		110.80°
A9-A10-A1		163.78°

Table 6.9 The formation energy of H_3PO_4-----OH-C_6H_4-Cl model

H_3PO_4	E(UB+HF-LYP) = -640.23	**ΔE= -0.13 A. U. = - 81.58 kcal/mol**
C_6H_5ClO	E(RB+HF-LYP) = -763.16	
C_6H_5ClO - H_3PO_4	E(UB+HF-LYP) = -1403.52	

NH_3------Cl-C_6H_4-OH

Figure 6.12 shows the model of halogen bonding between amine and chlorophenol molecule. And the tables 6.10 and 6.11 show the parameters of model and the energy changing after the formation of halogen bonding, which is also negative.

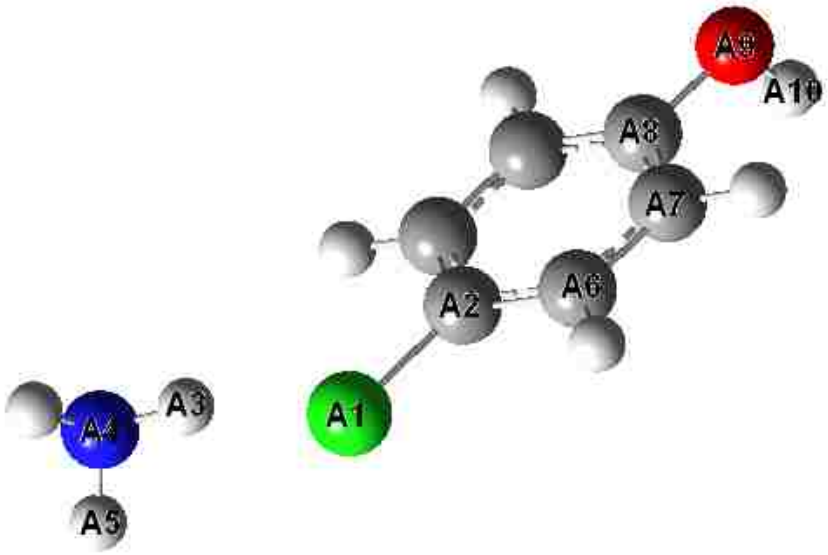

Figure 6.12 Model of halogen bonding between amine and chlorophenol

Table 6.10 The parameters of H_3PO_4-----OH-C_6H_4-Cl model

	Bond length/ Å	Bond Angle
A1-A2	1.76	
A1-A3	2.11	
A3-A4	1.00	
A4-A5	1.00	
A2-A6	1.40	
A6-A7	1.40	
A7-A8	1.40	
A8-A9	1.43	
A9-A10	0.96	
A3-A4-A5		109.47°
A2-A1-A3		130.58°
A1-A2-A6		119.98°

Table 6.11 The formation energy of NH_3---Cl-C_6H_4-OH model

NH_3	E(RB+HF-LYP) = -56.20	**ΔE= -0.04 A. U. = - 25.1 kcal/mol**
C_6H_5ClO	E(RB+HF-LYP) = -763.16	
$C_6H_5OCl – NH_3$	E(RB+HF-LYP) = -819.40	

Table 6.12 is the summary of the energy changings when the formation of the hydrogen bonding or halogen bonding between different molecules. The strongest hydrogen bonding site is between phosphate and amine molecule with the formation energy -296.82 kcal/mol. The second preference one is the hydrogen bonding between phosphate and clorophenol with the formation energy -81.58 kcal/mol. The formation energies give the evidence that the adsorption of the chlorophenol is driven by the formation of hydrogen bonding between phosphate and chlorophenol rather than the interaction between amine and chlorophenol. So the intercalation of alkylamine is for increasing the interlayer space to make it easier for chlorophenol to be adsorpted by α-ZrP. Figure 6.13 is the schematic process of the intercalation of amine and adsorption of chlorophenol into α-ZrP.

Table 6.12 Summary of the hydrogen bonding and halogen bonding formation energies between phosphate, amine and chlorophenol

$H_3PO_4 – NH_3$	**ΔE = -0.43 A. U. = - 296.82 kcal/mol**
$C_6H_5ClO – NH_3$	**ΔE = -0.03 A. U. = - 18.82 kcal/mol**
$C_6H_5ClO – H_3PO_4$	**ΔE = -0.13 A. U. = - 81.58 kcal/mol**
$C_6H_5OCl – NH_3$	**ΔE= -0.04 A. U.= - 25.1 kcal/mol**

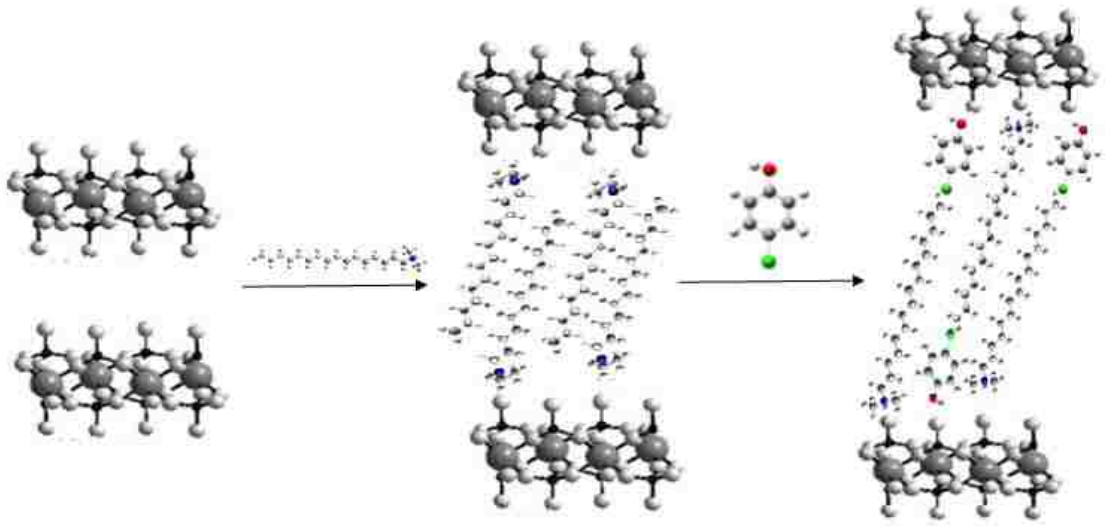

Figure 6.13 Schematic process of the intercalation of alkylamine and the adsorption of chlorophenol by α-ZrP

Chapter 7 Conclusions and potential future directions

α-Zirconium phosphate was synthesized by reflux method, and modified using Butylamine (BA), Octylamine (Octyl), Hexadecylamine (HAD), Dimethyltetradecylamine (DtDA), Dimethylhexadecylamine (DHDA). The combined computational results and XRD data indicate a bilayer arrangement of BA, Octy and HAD, while an interdigitated arrangement of DtDA and DHDA is consistent with the data. The main reason for the different arrangements of amines is because of cross section area, which can be calculated by considering the composition of molecules with the radii be equivalent to van der Waals radii. Therefore, the tertiary amines such as DtDA and DHDA have a larger cross section area (73.5Å) than free area of α-ZrP (24$Å^2$), which leads to the interdigitated arrangement in α-ZrP layers.

Amine intercalated α-ZrP can be effectively used for the removal of 4-chlorophenol from aqueous solutions. And the removal of 4-chlorophenol from water solution is induced by partitioning of the 4-chlorophenol in the ZrP-amine solid, and the chlorophenol was co-intercalated into the ZrP-DHDA interlayer space with the DHDA molecules. The interactions between amines, phosphate and chlorophenol are calculated using density function theory (B3LYP) with a basis set 6-311G*. The formation energies between either of two ions or molecules indicate that the driven force for the adsorption of chlorophenol is the hydrogen bonding between phosphate ion and chlorophenol molecules. And the intercalation of the α-ZrP by alkylamine is to increasing the interlayer space to allow the chlorophenol to get into the interlayer space.

The calculation work provides an explanation of the intercalation process and driving force of the adsorption of chlorophenol by amine intercalated α-ZrP. Future calculation work is needed

to study the adsorption isotherm, kinetics and thermal dynamics by construct two-dimensional structure of ZrP model and other molecules.

REFERENCE LIST

1. Wang, L. J.; Su, S. P.; Chen, D.; Wilkie, C. A. *Polym. Degrad. Stab.,* **2009**, *94*, 770-781.
2. Horrocks A.R. and Price D. *Fire Retardant Materials*. **2001**. England, Woodhead Publishing Limited.
3. Wilkie C.A. and Morgan, A. B. *Fire Retardancy of Polymeric Materials*. **2009**. U.S., CRC Press Taylor & Francis Group.
4. Manzi-Nshuti, C.; Songtipya, P.; Manias, E.; Jimenez-Gasco, M. M.; Hossenlopp, J. M.; Wilkie, C. A. *Polymer* **2009**, 50, 3564-3574.
5. Irvine, D. J.; McCluskey, J. A.; Robinson, I. M. *Polym. Degrad. Stab.,* **2000**, 67, 383-396.
6. Wei, M.; Murphy, D.; Barry, C.; Mead, J. Rubber *Chemistry and Technology*, **2010**, 83, 282-302.
7. Betts, K. *Chemical & Engineering News,* **2010**, 88, 8.
8. Chen, X. L.; Jiao, C. M. *Polym.s Adv. Technol.,* **2011**, 22, 817-821.
9. Wang, L. J.; Xie, X. L.; Su, S. P.; Feng, J. X.; Wilkie, C. A. *Polym. Degrad. Stab.,* **2010**, 95, 572-578.
10. Wang, D. Y.; Wilkie, C. A. . *Polym. Degrad. Stab.,* **2003**, 82, 309-315.
11. Habibi, S.; Rashidi, A.; Shahvaziyan, M.; Bazgir, S. *Asian J. Chem.,* **2010**, 22, 7087-7091.
12. Sun, L.; Boo, W. J.; Liu, J.; Clearfield, A.; Sue, H. J.; Verghese, N. E.; Pham, H. Q.; Bicerano, J. *Macromol. Mater. & Eng.,* **2009**, 294, 103-113.
13. Lu, H. D.; Song, L.; Hu, Y. A. *Polym.s Adv. Technol.,* **2011**, 22, 379-394.
14. Wang, D. Y.; Das, A.; Leuteritz, A.; Boldt, R.; Haussler, L.; Wagenknecht, U.; Heinrich, G. *Polym. Degrad. Stab.,* **2011**, 96, 285-290.
15. Lu, H. D.; Song, L.; Hu, Y. A. *Polym.s Adv. Technol.,* **2011**, 22, 379-394.
16. Becker, C. M.; Gabbardo, A. D.; Wypych, F.; Amico, S. C. *Composites Part A-Applied Science and Manufacturing,* **2011**, 42, 196-202.
17. Zhang, J. G.; Jiang, D. D.; Wilkie, C. A. *Polym. Degrad. Stab.,* **2006**, 91, 298-304.
18. Forano, C. *Environmental remediation involving layered double hydroxides; In Interface Science and Technology Clay Surfaces - Fundamentals and Applications*; Fernando Wypych and Kestur Gundappa Satyanarayana, ed. Elsevier: **2004**; pp 425-458.
19. Nyambo, C.; Wilkie, C. A. *Polym. Degrad. Stab.,* **2009**, 94, 506-512.
20. Zhang, J. G.; Jiang, D. D.; Wilkie, C. A. *Polym. Degrad. Stab.,* **2006**, 91, 358-366.
21. Zhu, J.; Start, P.; Mauritz, K. A.; Wilkie, C. A. *Polym. Degrad. Stab.,* **2002**, 77, 253-258.
22. Giannelis, E. P. *Appl. Organo. Chem.,* **1998**, 12, 675-680.
23. Kojima, Y.; Usuki, A.; Kawasumi, M.; Okada, A.; Kurauchi, T.; Kamigaito, O. *J. Polym. Sci. Part A-Polym. Chem.y,* **1993**, 31, 1755-1758.
24. Vaia, R. A.; Ishii, H.; Giannelis, E. P. *Chem. Mater.,* **1993**, 5, 1694-1696.
25. Schartel, B.; Bartholmai, M.; Knoll, U. *Polym.s Adv. Technol.*, **2006**, 17, 772-777.
26. Chuang, T. H.; Guo, W. J.; Cheng, K. C.; Chen, S. W.; Wang, H. T.; Yen, Y. Y. *J. Polym. Res.-Taiwan* , **2004**, 11, 169-174.
27. Hu, Y.; Tang, Y.; Song, L. *Polym.s Adv. Technol.,* **2006**, 17, 235-245.
28. Zhang, K.; Wang, L. J.; Wu, X. M.; Zhang, G. W.; Xie, X. L. *Plastics Rubber and Composites,* **2008**, 37, 210-213.
29. Lu, H. D.; Song, L.; Hu, Y. A. *Polym. Adv. Technol.,* **2011**, 22, 379-394.

30. Nyambo, C.; Chen, D.; Su, S. P.; Wilkie, C. A. *Polym. Degrad. Stab.,* **2009**, 94, 1298-1306.
31. Nyambo, C.; Wilkie, C. A. *Polym. Degrad. Stab.,* **2009**, 94, 506-512.
32. Costache, M. C.; Heidecker, M. J.; Manias, E.; Camino, G.; Frache, A.; Beyer, G.; Gupta, R. K.; Wilkie, C. A. *Polymer,* **2007**, 48, 6532-6545.
33. Noisong, P.; Danvirutai, C.; Srithanratana, T.; Boonchom, B. *Solid State Sci.,* **2008**, 10, 1598-1604.
34. Sue, H.-J.; Gam, K. T.; Bestaoui, N.; Clearfield, A.; Miyamoto, M.; Miyatake, N. *Acta Mate.,* **2004**, 52, 2239-2250.
35. Boo, W. J.; Sun, L. Y.; Liu, J.; Clearfield, A.; Sue, H. J.; Mullins, M. J.; Pham, H. *Compos. Sci. Technol.,* **2007**, 67, 262-269.
36. Yang, Y.; Liu, C.; Wu, H. *Polym. Test.,* **2009**, 28, 371-377.
37. Zhang, R.; Hu, Y.; Li, B.; Chen, Z.; Fan, W. *J. Mater. Sci.,* **2007**, 42, 5641-5646.
38. Pinnavaia, T. J. *Science,* **1983**, 220, 365-371.
39. McCabe, R. W. *Inorg. Mater.,* **1996**, 295. New York, John Wiley and Sons.
40. Searle, A. B. and Grimshaw R.W. *The chemistry and physics of clays*. **1959**. 45. New York, Inter science publishers.
41. Giannelis, E. P. *Appl. Org. Chem.,* **1998**, 12, 675-680.
42. Krishnamoorti, R.; Giannelis, E. P. *Abstracts of Papers of the American Chemical Society,* **1996**, 212, 33-MSE.
43. Gilman, J. W.; Jackson, C. L.; Morgan, A. B.; Harris, R.; Manias, E.; Giannelis, E. P.; Wuthenow, M.; Hilton, D.; Phillips, S. H. *Chem. Mater.,* **2000**, 12, 1866-1873.
44. Venugopal, B. R.; Rajamathi, M. *J. Colloid Interface Sci.,* **2011**, 355, 396-401.
45. Hibino, T. *Appl. Clay Sci.,* **2010**, 50, 282-287.
46. Ma, Y.; Chen, Y. P.; Xu, L.; Zhai, Z.; Yang, X. Y.; Hou, W. H. *Chinese J. of Inorg. Chem.,* **2010**, 26, 551-559.
47. Saber, O. *Curr. Nanosci.,* **2011**, 7, 134-141.
48. Yazici, O.; Yilmaz, S. *Adv. Appl. Ceram.,* **2010**, 109, 341-345.
49. Hofmeister, W.; Von Platen, H. *GCRY,* **1992**, 3, 3-26.
50. Koch, C. *Hyperfine Interact.,* **1998**, 117, 131-157.
51. Constantino, V. R. L.; Pinnavaia, T. J. *Inorg. Chem.,* **1995**, 34, 883-892.
52. Zhao, S.; Xu, J.; Wei, M.; Song, Y. F. *Green Chem.,* **2011**, 13, 384-389.
53. Bhattacharjee, S.; Dines, T. J.; Anderson, J. A. *J. Catal.,* **2004**, 225, 398-407.
54. Erickson, K. L.; Bostrom, T. E.; Frost, R. L. *Mater. Lett.* **2005**, 59, 226-229.
55. Zammarano, M.; Franceschi, M.; Bellayer, S.; Gilman, J. W.; Meriani, S. *Polymer,* **2005**, 46, 9314-9328.
56. Costache, M. C.; Heidecker, M. J.; Manias, E.; Camino, G.; Frache, A.; Beyer, G.; Gupta, R. K.; Wilkie, C. A. *Polymer,* **2007**, 48, 6532-6545.
57. Prasanna, S. V.; Radha, A. V.; Kamath, P. V.; Kannan, S. *Clays and Clay Miner.,* **2009**, 57, 82-92.
58. Jin, S.; Fallgren, P. H.; Morris, J. M.; Chen, Q. Sci. Technol. *Adv. Mater.,* **2001**, 8, 67-70.
59. Wei, M.; Yuan, Q.; Evans, D. G.; Wang, Z.; Duan, X. *J. Mater. Chem.,* **2005**, 15, 1197-1203.
60. Kandare, E.; Deng, H.; Wang, D.; Hossenlopp, J. M. *Polym. Adv. Technol*., **2006**, 17, 312-319.

61. Kandare, E.; Chigwada, G.; Wang, D.; Wilkie, C. A.; Hossenlopp, J. M. *Polym. Degrad. Stab.,* **2006**, 91, 1209-1218.
62. Kandare, E.; Chigwada, G.; Wang, D.; Wilkie, C. A.; Hossenlopp, J. M. *Polym. Degrad. Stab.,* **2006**, 91, 1781-1790.
63. Levchik, S. V.; Weil, E. D. *J. Fire Sci.,* **2006**, 24, 345-364.
64. Lu, S. Y.; Hamerton, I. *Prog. Polym. Sci.,* **2002**, 27, 1661-1712.
65. Hörold, S. *Polym. Degrad. Stab.,* **1999**, 64, 427-431.
66. Buckingham, M. R.; Lindsay, A. J.; Stevenson, D. E.; Muller, G.; Morel, E.; Costes, B.; Henry, Y. *Polym. Degrad. Stab.* ,**2011**, 54, 311-315.
67. Schmitt, E. Plastics, *Addi. and Comp.,* **2005**, 9, 26-30.
68. Alongi, J.; Frache, A. *Polym. Degrad. Stab.,* **2010**, 95, 1928-1933.
69. Wang, D. Y.; Liu, X. Q.; Wang, J. S.; Wang, Y. Z.; Stec, A. A.; Hull, T. R. *Polym. Degrad. Stab.,* **2009**, 94, 544-549.
70. Wang, M. S.; Pinnavaia, T. J. *Chem. Mater.*, **1994**, 6, 468-474.
71. Leroux, F.; Besse, J. P. *Chem. Mater.*, **2001**, 13, 3507-3515.
72. Mostafa Moujahid, E.; Besse, J. P.; Leroux, F. *J. Mater. Chem*., **2002**, 12, 3324-3330.
73. Ding, P.; Qu, B. *J. Appl. Polym. Sci.,* **2006**, 101, 3758-3766.
74. Costa, F. R.; Abdel-Goad, M.; Wagenknecht, U.; Heinrich, G. *Polymer,* **2005**, 46, 4447-4453.
75. LeBaron, P. C.; Wang, Z.; Pinnavaia, T. J. *Appl. Clay Sci.,* **1999**, 15, 11-29.
76. Pandey, J. K.; Raghunatha Reddy, K.; Pratheep Kumar, A.; Singh, R. P. *Polym. Degrad. Stab.,* **2005**, 88, 234-250.
77. Sinha Ray, S.; Okamoto, M. *Prog. Polym. Sci.,* **2003**, 28, 1539-1641.
78. Vaia, R. A.; Liu, W. *J. Polym .Sci. B Polym. Phys*., **2002**, 40, 1590-1600.
79. Sinha Ray, S.; Okamoto, M. *Prog. Polym. Sci.,* **2003**, 28, 1539-1641.
80. Vaia, R. A.; Liu, W. *J. Polym. Sci. B Polym.Phys*., **2002**, 40, 1590-1600.
81. Gilman, J. W. *Appl. Clay Sci.,* **1999**, 15, 31-49.
82. Gilman, J. W.; Harris, R. H.; Shields, J. R.; Kashiwagi, T.; Morgan, A. B. *Polym. Adv. Technol*. **2006**, 17, 263-271.
83. Lewin, M. *Fire Mater.,* **2003**, 27, 1-7.
84. Lewin, M. *Polym. Adv. Technol.,* **2006**, 17, 758-763.
85. Pavlidou, S.; Papaspyrides, C. D. *Prog. Polym. Sci.,* **2008**, 33, 1119-1198.
86. Babrauskas, V. *Fire Mater*. **1984**, 8, 81-95.
87. Beyer, G. n. Plastics, *Addi.s Comp.,* **2002**, 4, 22-28.
88. Zhuge, J.; Tang, Y.; Gou, J.; Chen, R. H.; Ibeh, C.; Hu, Y. *Polym. Adv. Technol*. **2010**.
89. Lu, H.; Wilkie, C. A. *Polym. Adv. Technol*. **2011**, 22, 14-21.
90. Wei, L. Q.; Ye, S. F.; Tian, Y. J.; Xie, Y. S.; Chen, Y. F. *J. Crys. Growth,* **2009**, 311, 3359-3363.
91. Chippindale, M.; Cowley, R.; Huo, Q.; Jones, H.; Law, D.; Thomas, M.; Xu, R. J.Chem.Soc., *Dalton Trans.,* **1997**, 2639-2644.
92. Wang, L. J.; Xie, X. L.; Su, S. P.; Feng, J. X.; Wilkie, C. A. *Polym. Degrad. Stab.,* **2010**, 95, 572-578.
93. Nyambo, C.; Wang, D.; Wilkie, C. A. *Polym. Adv. Technol.,* **2009**, 20, 332-340.
94. Nyambo, C.; Songtipya, P.; Manias, E.; Jimenez-Gasco, M. M.; Wilkie, C. A. *J. Mater. Chem*., **2008**, 18, 4827-4838.
95. Lu, H. D.; Wilkie, C. A.; Ding, M.; Song, L. *Polym. Degrad. Stab.*, **2011**, 96, 885-891.

96. Wei, L. Q.; Ye, S. F.; Tian, Y. J.; Xie, Y. S.; Chen, Y. F. *J. Crys. Growth,* **2009**, 311, 3359-3363.
97. Schwieger, W.; Altenschildesche, H. M. Z.; Kokotailo, G. T.; Fyfe, C. A. *Zeitschrift fur Anorganische und Allgemeine Chemie,* **1998**, 624, 1712-1717.
98. Marincea, T.; Dumitras, D. G. *Neues Jahrbuch fur Mineralogie-Monatshefte,* **2003**, 127-144.
99. Dick, S.; ner, U.; Wei[beta], A.; Robl, C.; mann, G.; Ohms, G.; Zeiske, T. *Inorg.a Chim. Acta* , **1998**, 269, 47-57.
100. Sakae, T.; Sudo, T. *American Mineralogis,* **1975**, 60, 331-334.
101. Nyambo, C.; Kandare, E.; Wang, D. Y.; Wilkie, C. A. *Polym. Degrad. Stab.*, **2008**, 93, 1656-1663.
102. Myiata, S. *Clays and Clay Miner.,* **1980**, 28, 50-56.
103. Wang, L. J.; Su, S. P.; Chen, D.; Wilkie, C. A. *Polym. Degrad. Stab.*, **2009**, 94, 770-781.
104. Zhu, J.; Morgan, A. B.; Lamelas, F. J.; Wilkie, C. A. *Chem. Mater.,* **2001**, 13, 3774-3780.
105. Jash, P.; Wilkie, C. A. *Polym. Degrad. Stab.*, **2005**, 88, 401-406.
106. Peng, Z.; Kong, L. X. *Polym. Degrad. Stab.,* **2007**, 92, 1061-1071.
107. Lu, H.; Wilkie, C. A.; Ding, M.; Song, L. *Polym. Degrad. Stab.* **2011**, 96, 1219-1224.
108. Lu, H.; Wilkie, C. A.; Ding, M.; Song, L. *Polym. Degrad. Stab.,* **2011**, 96, 885-891.
109. Manzi-Nshuti, C.; Chen, D.; Su, S.; Wilkie, C. A. *Polym. Degrad. Stab.,* **2009**, 94, 1290-1297.
110. Jash, P.; Wilkie, C. A. *Polym. Degrad. Stab.,* **2005**, 88, 401-406.
111. Nyambo, C.; Wang, D.; Wilkie, C. A. *Polym. Adv. Technol*., **2009**, 20, 332-340.
112. Costa, F. R.; Wagenknecht, U.; Heinrich, G. *Polym. Degrad. Stab.,* **2007**, 92, 1813-1823.
113. Kishore, K.; Mohandas, K. *Combust. Flame,* **1981**, 43, 145-153.
114. Wang, L. J.; Su, S. P.; Chen, D.; Wilkie, C. A. *Polym. Degrad. Stab.,* **2009**, 94, 770-781.
115. Kishore, K.; Mohandas, K. *Combust. and Flame,* **1981**, 43, 145-153.
116. Nyambo, C.; Wang, D.; Wilkie, C. A. *Polym. Adv. Technol*., **2009**, 20, 332-340.
117. Wang, L.; Xie, X.; Su, S.; Feng, J.; Wilkie, C. A. *Polym. Degrad. Stab.,* **2010**, 95, 572-578.
118. Marosi, G.; Mbrton, A.; Szqp, A.; Csontos, I.; Keszei, S.; Zimonyi, E.; Toth, A.; Almeras, X.; Le Bras, M. *Polym. Degrad. Stab.,* **2003**, 82, 379-385.
119. Nyambo, C.; Wang, D.; Wilkie, C. A. *Polym.Adv.Technol*., **2009**, 20, 332-340.
120. Zhang, Z.; Lan, B.; Mei, X.; Xu, C. *Sci. China Series B: Chemistry,* **2007**, 50, 392-396.
121. Cao, G.; Hong, H. G.; Mallouk, T. E. *Acc. Chem. Res.*, **1992**, 25, 420-427.
122. Trobajo, C.; Khainakov, S. A.; Espina, A.; Garcia, J. R. *Chem. Mater.*, **2000**, 12, 1787-1790.
123. Clearfield, A.; Smith, G. D. *Inorg. Chem.,* **1969**, 8, 431-436.
124. Troup, J. M.; Clearfield, A. *Inorg. Chem.,* **1977**, 16, 3311-3314.
125. Clearfield, A.; Stynes, J. A. *J. Inorg. Nucl. Chem.*, **1964**, 26, 117-129.
126. Clearfield, A.; Blessing, R. H.; Stynes, J. A. *J. Inorg. Nucl. Chem.*, **1968**, 30, 2249-2258.
127. Alberti, G.; Costantino, U.; Allulli, S.; Tomassini, N. *J. Inorg. Nucl. Chem.*, **1978**, 40, 1113-1117.
128. Boo, W. J.; Sun, L. Y.; Liu, J.; Clearfield, A.; Sue, H. J.; Mullins, M. J.; Pham, H. *Comp. Sci. Technol.,* **2007**, 67, 262-269.
129. Alberti, G.; Casciola, M.; D'Alessandro, E.; Pica, M. *J. Mater. Chem.,* **2004**, 14, 1910-1914.

130. MacLachlan, D. J.; Morgan, K. R. *J. Phys. Chem.,* **1990**, 94, 7656-7661.
131. Hayashi, A.; Nakayama, H.; Tsuhako, M. *Bull. Chem. Soc. of Japan,* **2003**, 76, 2315-2319.
132. Hayashi, A.; Fujimoto, Y.; Ogawa, Y.; Nakayama, H.; Tsuhako, M. *J. Colloid Interface Sci.,* **2005**, 283, 57-63.
133. Clearfield, A. *Inorg. Ion Exchange Mater.,* **1982**. Boca Raton and Florida, CRC Press.
134. Alberti G. and Costantino U. *Intercal. Chem.,* **1982**. New York, Academic Press, Inc.
135. Clearfield, A.; Wang, *Z. J. Chem. Soc., Dalton Trans*., **2002**, 2937-2947.
136. Alberti, G.; Torracca, E. *J. Inorg. Nucl. Chem.,* **1968**, 30, 317-318.
137. Warmuth, W.; Schollhorn, R. *Pro. Intercal. Res.*, **1994**, Kluwer Aacademic Publishing: Dordrecht.
138. Messersmith, P. B.; Giannelis, E. P. *Chem. Mater.,* **1994**, 6, 1719-1725.
139. Burnside, S. D.; Giannelis, E. P. *Chem. Mater.,* **1995**, 7, 1597-1600.
140. Hayashi A.; Nakayama H.; Tsuhako M. *Bull. Chem. Soc. of Japan*, **2003**, 76, 2315.
141. Alberti, G.; Casciola, M.; Costantino, U.; Vivani, R. *Adv. Mater*., **1996,** 8, 291-303.
142. Clearfield, A. *Chem. Rev.,* **1988**, 88, 125-148.
143. Alberti, G.; Costantino, U. *Intercalation Chemistry of Acid Salts of Tetravalent Metals with layered Structure and Related Materials; In Intercalation Chemistry*; Whittingham, S. M., Jackobson, A. J., eds. Academic Press Inc: New York, **1982**; pp 147-180.
144. Clearfield, A.; Tindwa, R. M. *J. Inorg. Nucl. Chem.,* **1979**, 41, 871-878.
145. Troup, J. M.; Clearfield, A. *Inorg. Chem.,* **1977**, 16, 3311-3314.
146. Yamanaka, S.; Horibe, Y.; Tanaka, M. *J. Inorg. Nucl. Chem.,* **1976**, 38, 323-326.
147. MacLachlan, D. J.; Morgan, K. R. *J. Phys. Chem.,* **1992**, 96, 3458-3464.
148. MacLachlan, D. J.; Morgan, K. R. *J. Phys. Chem.,* **1990**, 94, 7656-7661.
149. Bestaoui, N.; Spurr, N. A.; Clearfield, A. *J. Mater. Chem.,* **2006,** 16, 759-764.
150. Xu, J. S.; Tang, Y.; Zhang, H.; Gao, Z. *Chem. J. Chinese Universities-Chinese,* **1997**, 18, 88-92.
151. Marti, A. A.; Colon, J. L. *Inorg. Chem.,* **2010**, 49, 7298-7303.
152. Nakayama, H.; Hayashi, A.; Eguchi, T.; Nakamura, N.; Tsuhako, M. *J. Mater. Chem.,* **2002**, 12, 3093-3099.
153. Benes, L. k.; Melbnovb, K.; Svoboda, J.; Zima, V. t.; Kincl, M. *J. Phys. Chem. of Solids,* **2005**, 68, 803-807.
154. Nakayama, H.; Hayashi, A.; Eguchi, T.; Nakamura, N.; Tsuhako, M. *Solid State Sci.,* **2002**, 4, 1067-1070.
155. Gao, R.; Wang, J. *J. Hazard. Mater.,* **2007**, 145, 398-403.
156. Radhika, M.; Palanivelu, K. *J. Hazard. Mate.,* **2006**, 138, 116-124.
157. Chaliha, S.; Bhattacharyya, K. G. *Chem. Eng. J.,* **2008**, 139, 575-588.
158. Poulopoulos, S. G.; Nikolaki, M.; Karampetsos, D.; Philippopoulos, C. J. *J. Hazard. Mater.,* **2008**, 153, 582-587.
159. Hameed, B. H. *Colloids and Surfaces A: Physicochem. Eng. Aspects,* **2007**, 307, 45-52.
160. Hameed, B. H.; Rahman, A. A. *J. Hazard. Mate.,,* **2008**, 160, 576-581.
161. Wang, S. L.; Tzou, Y. M.; Lu, Y. H.; Sheng, G. *J. Hazard. Mate.,* **2007**, 147, 313-318.
162. Guymont F.J.; Suffet, I. H.; McGuire, M. J. *Activated Carbon Adsorption of Organics drom Aaqueous Phase*; **1984**.Ann Arbor Science: Ann Arbor. MI.
163. Koper, B. O.; Rajagopalan, S.; Winecki, S.; Klabunde, K. J. *Nanoparticle Metal Oxides for Chlorocarbon and Organophosphonate Remediation; In Environmental Applications*

of Nanomaterials : Synthesis, Sorbents and Sensors; Fryxell, G. E., Cao, G., eds. Imperial College Press: London, **2007**; pp 3-22.
164. Seki, Y.; Yurdako, K. *J. Colloid Interface Sci.,* **2005**, 287, 1-5.
165. Goh, K. H.; Lim, T. T.; Dong, Z. *Water Res.,* **2008**, 42, 1343-1368.
166. Hsu, Y. H.; Wang, M. K.; Wang, Y. S.; Pai, C. W. *Appl. Clay Sci.,* **2000**, 16, 147-159.
167. Klumpp, E.; Ortegac, C. C.; Klahrea, P.; Tinoa, F. J.; Yapard, S.; Prtilloc, C.; Stegenc, S.; Queiroloc, F.; Schwuger, M. J. *Colloids Surf. A,* **2004**, 320, 11.
168. Hsu, Y. H.; Wang, M. K.; Wang, Y. S.; Pai, C. W. *Appl. Clay Sci.*, **2000**, 16, 147-159.
169. Mortland, M. M.; Sun, S.; Boyd, S. A. *Clays and Clay Miner.* **1986**, 34, 581-585.
170. Michot, L. J.; Pinnavaia, T. J. *Clays and Clay Miner.,* **1991**, 39, 634-641.
171. Hayashi, A.; Nakayama, H.; Tsuhako, M. *Solid State Sci.,* **2009**, 11, 1007-1015.
172. Mlambo, Darlington. *Detection of quercetin using polymer coated quartz crystal microbalance and the modification of ALPha-zirconium phosphate to develop a sorbent for organic pollutant removal*. **2010**. Chemistry.
173. Clearfield, A.; Kullberg, L.; Oskarsson, A. *J. Phys. Chem.,* **1974**, 78, 1150-1153.
174. Frisch, M. J, Trucks, G. W, Schlegel, H. B, Scuseria, G. E., Robb, M. A, and Cheeseman, J. R. *Gaussian 03*. **2003**.
175. Tanja V., Robert G., *J. Chem. Phys.*, **2002**, 116 (22), 9620–9623.
176. Kim, K., Jordan K., *J. Phys. Chem.*, **1994**, 98 (40), 10089-10094.
177. Wong, M., Gill, P., Nobes, R., Radom, L., *J. Phys. Chem.*, **1988**, 92 (17), 4875-4880.
178. Laidler, J. *The World of Physical Chemistry*. 2001, Oxford University Press. p. 324
179. Clearfield, A.; Costantino, U. *Layered Metal Phosphates and Their Intercalation Chemistry; In Comprehensive Supramolecular Chemistry*; Atwood, J., Davies, J. E. D., Macnicol, D. D., Vogtle, F., eds. Elsevier Science Inc: New York, **1996**; pp 107-150.

180. Menedez, F.; Espina, A.; Trobajo, C.; Rodriguez, *J. Mater. Res. Bull.,* **1990**, 25, 1531.
181. Benes, L. k.; Melbnovb, K.; Svoboda, J.; Zima, V. t.; Kincl, M. *J. Phys. Chem. Solids.* **2005**, 68, 803-807.
182. Valvani, S. C.; Yalkowsky, S. H.; Amidon, G. L. *J. Phys. Chem.,* **1976**, 80, 829-835.
183. Hermann, R. B. *J. Phys. Chem.,* **1972**, 76, 2754-2759.
184. Pauling L. "*The Nature of the Chemical Bond"*. **1960**. 260-262. N.Y., Cornell University Press.
185. Sutton, L. E. *"Table of interatomic Distance"*. **1965**. London, Chemical society.
186. Troup, J. M.; Clearfield, A. *Inorg. Chem.,* **1977**, 16, 3311-3314.
187. Bardakci, B. *J. Arts and Sci. Say,* **2007**, 7, 13-19.
188. Zierkiewicz, W.; Michalska, D.; Zeegers-Huyskens, T. *J. Phys. Chem. A,* **2000**, *104*, 11685-11692.
189. Riley, K. E.; Murray, J. S.; Politzer, P.; Concha, M. C.; Hobza, P. *J. Chem. Theory and Comput.,* **2008**, *5*, 155-163.

APPENDIX

Model: H_3PO_4 (Singlet)

Frequencies

183.233

225.133

292.556

346.972

382.268

384.206

414.89

757.12

857.748

883.857

1048.15

1073.3

1104.99

1227.13

3518.79

3540.5

3540.89

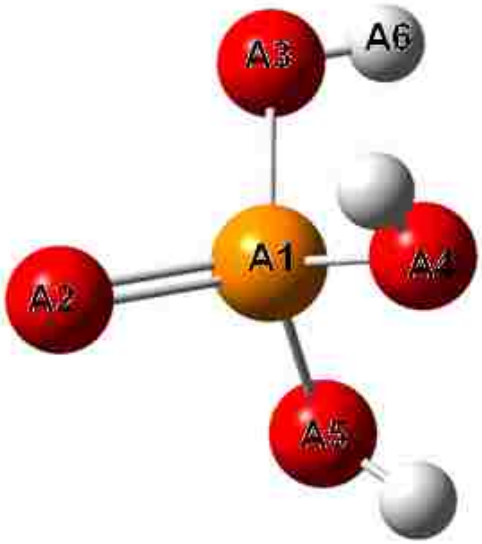

	Bond length/ Å	Bond Angle
A1-A2	1.76	
A1-A3	1.76	
A3-A6	0.96	
A2-A1-A3		109.47°
A3-A1-A4		109.47°
A1-A3-A6		109.50°

NH_3----H_3PO_4

Frequencies

43.023
101.25
167.431
221.56
245.95
310.46
342.366
357.402
385.147
407.176
448.156
465.933
518.042
578.341
604.75
712.133
792.543
931.876
991.32
1047.45
1113.1
1233.343
1414.43
1594.76
1678.731
1784.35
1789.71
3043.43
3412.25
3455.91
3457.76
3483.13
3543.33

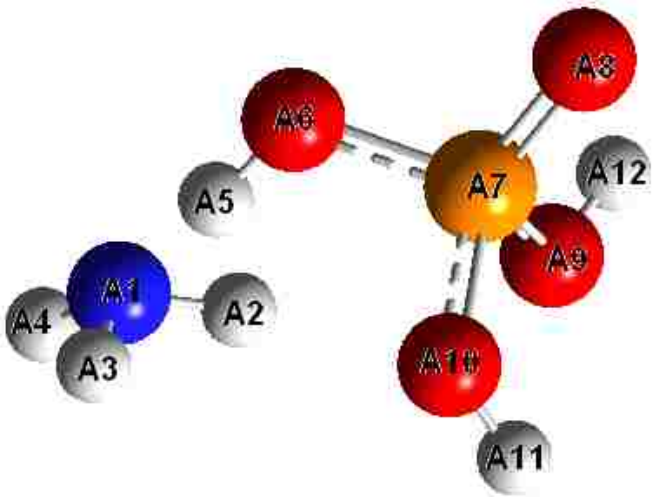

	Bond length/ Å	Bond Angle
A1-A2	1.00	
A1-A3	1.00	
A1-A4	1.00	
A1-A5	1.28	
A5-A6	0.96	
A6-A7	1.60	
A7-A8	1.47	
A7-A9	1.63	
A10-A11	0.96	
A2-A1-A3		109.47°
A5-A6-A7		116.42°
A6-A7-A8		111.99°
A6-A7-A9		106.44°
A6-A7-A10		103.14°
A8-A7-A9		116.19°
A9-A7-A10		98.09°
A7-A9-A12		114.63°

NH_3------ $OH\text{-}C_6H_4\text{-}Cl$

Frequencies

32.2047
46.5655
48.1236
129.046
157.603
247.626
317.006
367.548
401.209
439.751
449.95
450.662
509.18
574.257
650.851
667.262
760.413
825.932
867.036
886.319
1027.5
1030.67
1055.5
1108.74
1146.53
1193.52
1229.32
1265.1
1317.94
1360.75
1438.86
1494.79
1539.57
1612.85
1618.61
1640.06
1685.08
2098.02
3223.11
3225.38
3345.13

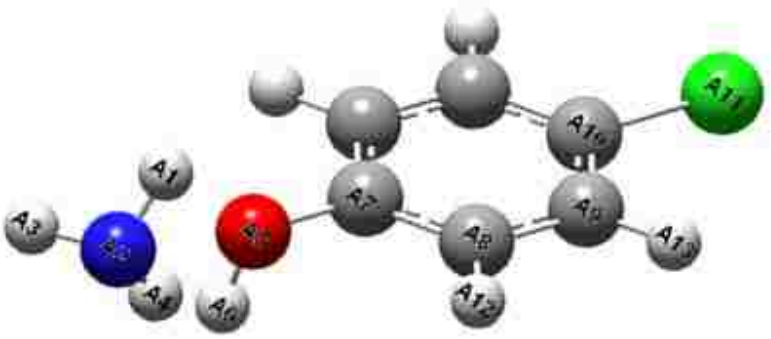

	Bond length/ Å	Bond Angle
A1-A2	1.00	
A2-A3	1.00	
A2-A4	1.00	
A1-A5	2.10	
A2-A6	2.03	
A5-A6	0.96	
A5-A7	1.43	
A7-A8	1.39	
A8-A9	1.40	
A9-A10	1.39	
A10-A11	1.81	
A1-A2-A3		110.36°
A6-A5-A7		112.78°
A1-A5-A7		120.34°

3247.08
3350.13
3433.76
3437.81
3534.99

H_3PO_4-----OH-C_6H_4-Cl

Frequencies

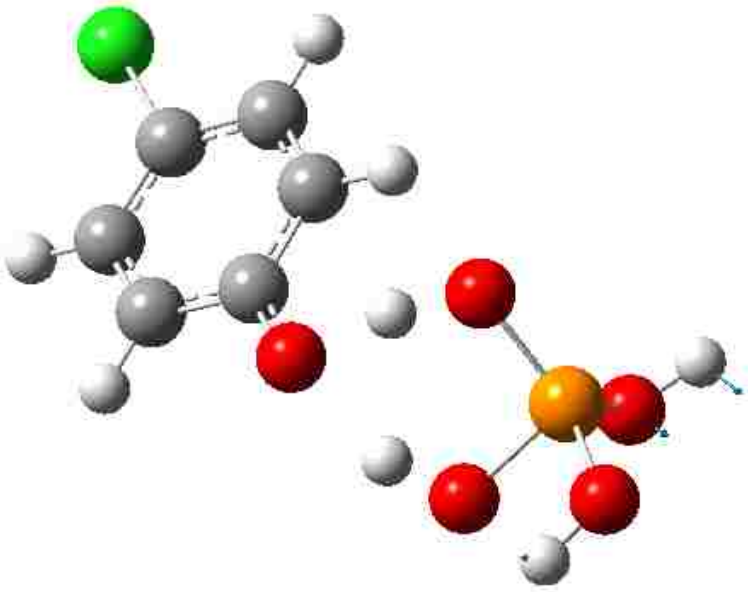

30.43
39.19
58.05
80.13
112.12
138.82
201.49
209.19
231.38
291.23
330.00
339.97
373.02
381.12
431.56
454.79
460.33
533.75
539.31
547.54
610.57
636.96
665.87
703.11
756.34
784.61
835.44
841.32
848.49

859.67
904.22
994.94
1025.4
1034.02
1050.77
1088.9
1115.93
1136.95
1186.09
1218.81
1285.89
1316.01
1334.81
1371.97
1444.32
1534.16
1576.59
1587.01
1623.42
2009.49
3010.68
3201.59
3226.52
3259.21
3272.91
3395.45
3506.65

	Bond length/ Å	Bond Angle	
A1-A2	1.69		
A2-A3	1.76		
A2-A4	1.71		
A2-A5	1.79		
A5-A6	1.00		
A3-A7	1.01		
A4-A8	1.02		
A9-A10	1.42		
A1-A10	1.10		
A9-A11	1.34		
A1-A2-A4		98.07	
A2-A1-A10		110.80	
A9-A10-A1		163.78	

NH_3------Cl-C_6H_4-OH

Frequencies

45.49
87.90
110.12
190.00
241.65
259.71
321.73
333.21
343.34
365.81
410.69
417.45
448.47
527.51
617.70
664.84
742.64
833.59
845.00
881.71
1004.45
1019.00
1038.27
1087.06
1134.28
1184.44
1230.10
1323.32
1347.79
1379.15
1468.98
1541.86
1543.00
1609.98
1611.12
1617.44
1636.06
1780.55
1787.16
2891.62

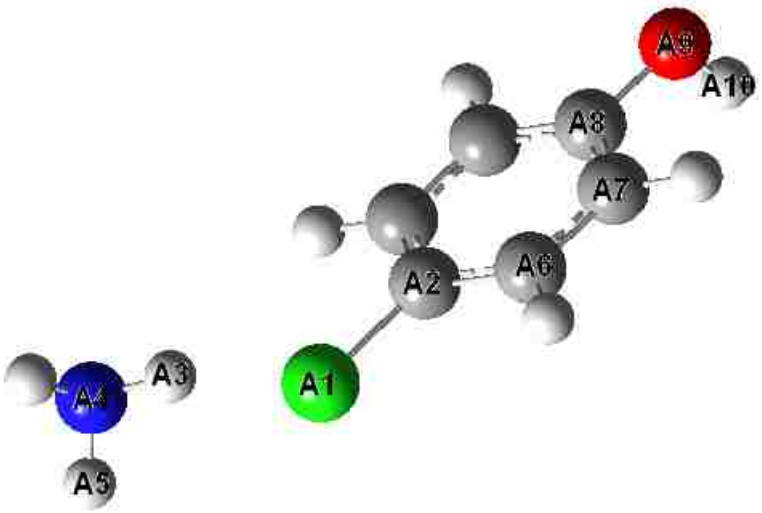

	Bond length/ Å	Bond Angle
A1-A2	1.76	
A1-A3	2.11	
A3-A4	1.00	
A4-A5	1.00	
A2-A6	1.40	
A6-A7	1.40	
A7-A8	1.40	
A8-A9	1.43	
A9-A10	0.96	
A3-A4-A5		109.47°
A2-A1-A3		130.58°
A1-A2-A6		119.98°

3205.78
3231.76
3238.15
3248.20
3330.02
3407.28
3408.50
3527.87